Ca' Foscari
University
of Venice

Master's Degree programme in
Science and Technology of Bio and Nanomaterials

Supervisors

Prof. Elisa Moretti
Dr. Tofik Ahmed Shifa

Graduand

MHD AMMAR ALBOUCHI
875550

Academic year

2021/2022

Abstract

The need for energy has increased as the world's population has grown, impacting items we use every day such as domestic appliances, portable electronics, cars, aircraft vehicles, and industrial machinery. Energy production that is both economical and environmentally friendly is in urgent need to be developed by today's technological society. To meet our growing needs this thesis is focused on Water splitting reaction. Mainly the Oxygen evolution reaction (OER) due to its crucial role in energy conversion and storage, especially in water electrolysis. Utilizing transition metal-based electrocatalysts because of their inherently excellent activities towards the oxygen evolution reaction (OER), they are attracting increasing attention in the field of renewable energy research. Significant efforts have been made to date to enhance the performance of these catalysts. Herein, we present an optimization procedure for an electrochemical cobalt (II) oxide catalyst and developing a heterostructure by adding sulfur through hydrothermal reaction, producing cobalt sulfides (CoSx) of various proportions. The manufactured heterostructures exhibited a synergistic activity increase in electrocatalysis under a strong alkaline media of (1.0 M KOH) then a slight decrease in activity as we progressed in concentrations, hinting to the presence of an optimal concentrations, the samples showed a Tafel slope (mV dec-1) of and an overpotential of (mV).

.

INDEX

7. References

1. General introduction

1.1 Background:

With technological advancements and an ever-increasing population in this booming globe, worldwide energy consumption is anticipated to climb by a factor of two, from 15 TW/year today to 27 TW/year by 2050, and 43 TW/year by 2100 if current trends continue[1], **Figure 1**. Fossil fuels currently provide the primary energy supply, accounting for 85 percent of total world energy consumption[2]. The most serious technological difficulties that mankind faces are the impending depletion of fossil fuels and related environmental issues such as pollution and greenhouse gas emissions because of their use. As a result, it is critical to investigate alternate energy sources in order to address the energy crisis and climate change.

Hydrogen has been increasingly essential source of energy in the last two decades, due to its inherent capability as an energy carrier where it can deliver or store a tremendous amount of energy. Together with its bountiful supply as a renewable energy source and it's cleanliness and non-toxic features, all but make hydrogen a preferred source of energy. The technologies that now dominate hydrogen production include natural gas reforming, coal and petroleum coke gasification, and heavy oil gasification and reforming. Despite the fact that water electrolysis has been around for over 200 years, it still accounts for a small portion of total hydrogen production (4 percent of the worldwide hydrogen production).[3][4][5][6]

When compared to other available technologies, water electrolysis produces exceptionally pure hydrogen (> 99.9%), which is excellent for some high-value-added industries like electronic component manufacturing[7].

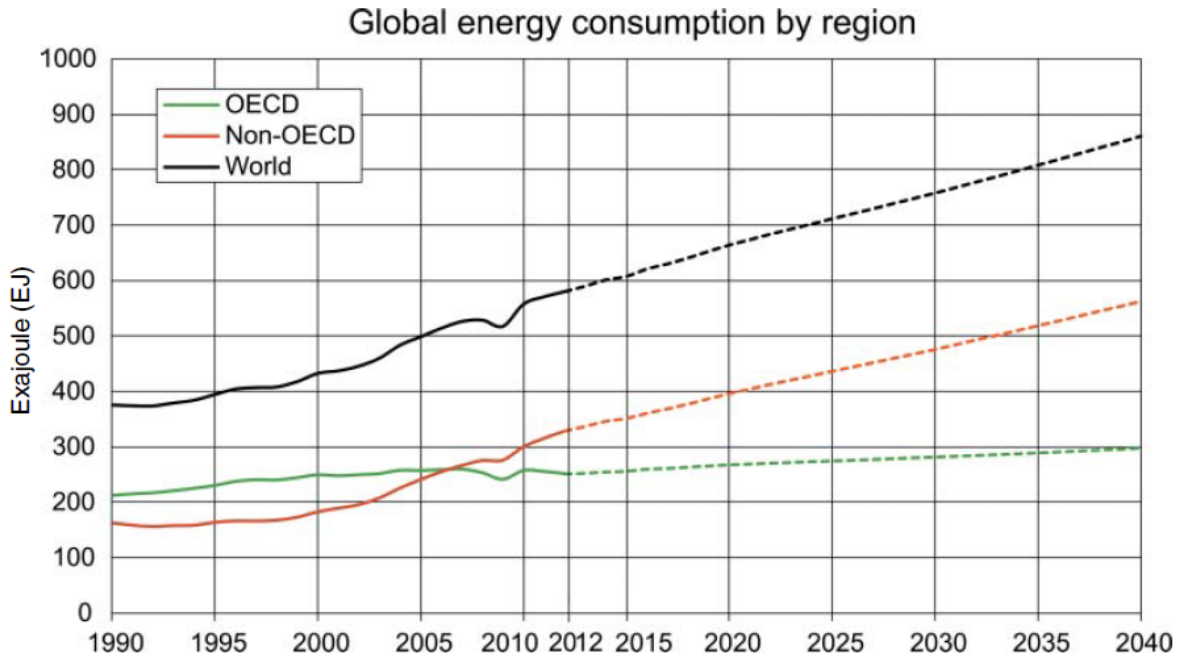

Figure 1: Global energy consumption from 1990 until 2012 and correspondent forecast until 2040. Source: The authors with data from (EIA 2016). OECD (Organization for Economic Cooperation and Development**)** countries including USA and Europe, non-OECD countries including Russia, China, Brazil and India. [8]

1.2 Future energy, Water Splitting & H2 Economy:

Hydrogen (H2) is currently used in a variety of critical industrial activities. Ammonia, fertilizers, oil refineries, and petrochemicals are just a handful of the industries that use more than 25 million tons of hydrogen each year. Nature established the first green photosynthesis process in plants 3.2 billion years ago to harness solar-driven chemistry for long-term H2 generation.[9]

Scientists have directed their efforts to producing H2 as an undisputed future energy source, motivated by the natural approach for producing environmentally friendly fuel and its realization as an appealing alternative to the intermittency of solar/wind energy. It is one of the most efficient and clean sources of energy, with a mass energy density of 120-140 MJ/kg and a 100 percent efficiency that is three to four times higher than standard fossil fuels' equivalent energy capacity. However, over 90% of H2 is currently created using a steam reforming process (SRP) from fossil fuels at high temperatures (700-1100 °C), which is releasing a large amount of CO2 and other undesired gases into the atmosphere, contributing to global warming and other environmental challenges.

As a result, addressing these issues for a safe and sustainable future while utilizing renewable energy resources (sun, water, wind, and biomass) for ecologically friendly H2 generation is critical. Water is one of the cleanest and most abundant sources of hydrogen accessible on the globe among renewable energy options. [10][11]

1.3 Hydrogen production:

A concise rundown of key existing and emerging hydrogen generation systems will be discussed here starting with the following areas that will be looked at: **Figure 2.**

i) The creation of hydrogen using fuel processing technology and its main two pathways.
ii) Water and biomass as an alternate sources of hydrogen production.

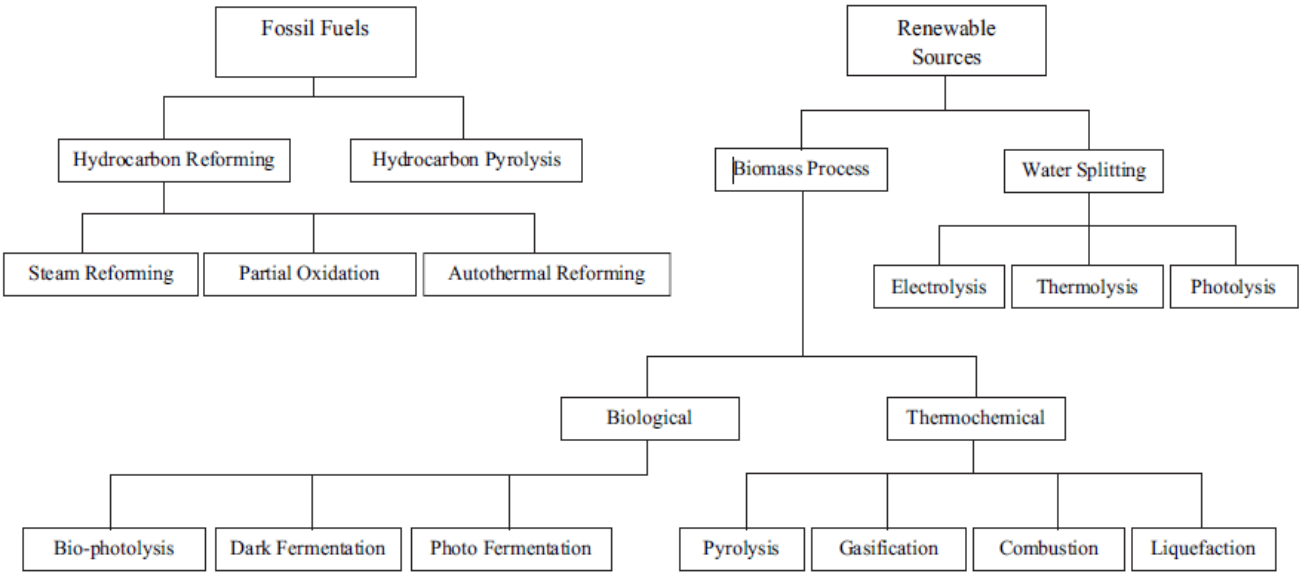

Figure 2: Hydrogen production methods.[12]

1.3.1 Fuel processing:

Technologies for processing fuel turn a hydrogen-containing substance, like gasoline, ammonia, or methanol, into a hydrogen-rich stream. The most popular way of producing hydrogen now used in industry is fuel processing of methane. The majority of hydrocarbon fuels contain at least a small quantity of sulfur, which taints the catalyst used in fuel processing.[13][14]

1.3.1.1 Hydrocarbon reforming:

Steam reforming, partial oxidation (POX), and autothermal reforming (ATR) are the main methods for producing hydrogen from hydrocarbon fuels. The benefits and drawbacks of each of these techniques are listed in the **Table 1**. A gas stream largely made up of hydrogen, carbon monoxide, and carbon dioxide is created during the reforming process. An external heat source is necessary for endothermic steam reformation of hydrocarbons. In contrast to POX and ATR, steam reforming does not require oxygen, operates at a lower temperature, and generates reformate with a high H2/CO ratio (3:1), which is advantageous for the synthesis of hydrogen. It does, however, produce the most emissions of the three processes. [14][15]

By partially oxidizing (combusting) the hydrocarbon with oxygen, partial oxidation turns hydrocarbons into hydrogen. The combustion is "managed," which produces the heat. It has

less methane slip, is more sulfur tolerant than the other processes, and does not require a catalyst to operate. The H2/CO ratio (1:1 to 2:1) is preferred for the feeds of hydrocarbon synthesis reactors like Fischer-Tropsch during the process, which takes place at high temperatures with some soot generation. Autothermal reforming generates heat through partial oxidation and increases hydrogen generation through steam reforming, creating a thermally neutral reaction. When compared to POX reforming, autothermal reforming typically operates at a lower pressure and has a smaller methane slip. POX is exothermic, and ATR contains POX, therefore the reactor does not require an external heat source for these procedures. However, they need an expensive and complicated oxygen source, or the reactor or the separation unit with just pure oxygen where Nitrogen is used to dilute product gas.

Typically, steam reforming is a recommended industrial method for producing hydrogen. [14][15]

Technology	Advantages	Disadvantages
Steam reforming	• Most extensive industrial experience • Oxygen not required • Lowest process temperature Best H2/CO ratio for H2 production	• Highest air emissions
Autothermal reforming	• Lower process temperature than POX • Low methane slip	• Limited commercial experience • Requires air or oxygen
Partial oxidation	• Decreased desulfurization requirement • No catalyst required • Low methane slip	• Low H2/CO ratio • Very high processing temperatures • Soot formation/handling adds process complexity

Table 1: Comparison of reforming technologies (adapted from [17][18][19])

1.3.1.2 Pyrolysis:

Another method for creating hydrogen is pyrolysis, in which the hydrocarbon is broken down into hydrogen and carbon without the presence of water or oxygen.[20] Any organic material can undergo pyrolysis, which produces hydrocarbons, carbon nanotubes, and carbon spheres.[17][18]

There is no need for secondary reactors (WGS, PrOx, etc.) because neither water or air are present, which prevents carbon oxides (such CO or CO2) from forming. As a result, this method significantly reduces emissions. Although considerable CO2 and CO emissions will be created if air or water is present, for instance if the materials have not yet been dried. Fuel flexibility, relative simplicity and compactness, clean carbon by-product, and a decrease in CO2 and CO emissions are some of the benefits of this method. [17][18][13]

The possibility of fouling from the carbon generated is one of the difficulties with this technology, however proponents assert that this may be mitigated by proper design. Pyrolysis may play a big role in the future due to its potential for decreased CO and CO2 emissions and its ability to be operated in a way that recovers a sizeable portion of the solid carbon that is easily sequestered. [17][18][13]

1.3.1.3 Plasma Reforming:

Although the fundamental reforming reactions in plasma reforming are identical to those in conventional reforming, energy and free radicals are supplied for the reforming reaction by a plasma that is commonly produced with electricity or heat [23][20][21]. H, OH, and O radicals are produced along with electrons when water or steam is added to the fuel, which creates the conditions for both reductive and oxidative processes. Plasma reforming, according to proponents, eliminates numerous drawbacks of conventional methods, including cost and catalyst degradation, size and weight constraints, slow response, and restrictions on hydrogen production from heavy hydrocarbons[12][22]. They can be set up to function at lower temperatures than classical reforming as well [12][22]. The procedure is very sulfur tolerant when catalysts are not utilized to aid in reforming. The electrical requirements and significant electrode degradation at high pressures are the two main drawbacks that have been reported. Technologies for plasma reforming have been created to aid in partial oxidation.

Steam reforming, partial oxidation (POX), and autothermal reforming (ATR), with POX and ATR making up the majority of the reactors [27]. Plasma reformation can be broadly divided into two categories: thermal and non-thermal [27].

In thermal plasma the use of a high electric discharge (>1 kW) is necessary for reformation. The heating up of the neutral species and the electrons to extremely high temperatures consume a lot of energy (5000–10,000 K). where in order to prevent the electrodes' metals from vaporizing at these high temperatures, even more electricity is needed to cool them. This technology faces considerable challenges in terms of power consumption reduction. While in non-thermal plasmas only the electron temperatures (>5000 K) are elevated; the bulk species temperature does not considerably rise. Few hundred watts of power are needed because only the electrons are directly stimulated. [23][28][27][26]

1.3.1.4 Aqueous phase reforming:

Aqueous phase reformation (APR) is being developed to transform oxygenated hydrocarbons or carbohydrates into hydrogen[29]. These reactors commonly operate at 220–270 °C temperatures and 25–30 MPa pressures. Supported Group VIII catalysts have been the subject of the majority of study to far, with catalysts containing Pt having the maximum activity. Nickel-based catalysts have been studied despite having lesser activity because of nickel's low price [30]. The benefits of APR reactors include eliminating the requirement to evaporate feedstock and water, which eliminates a system component. They also enable the processing of fuels like glucose that cannot be vaporized without first degrading them.

APR takes place at low temperatures, allowing WGS to boost the hydrogen yield while reducing CO. As a result, numerous reactors are eliminated as the reforming and WGS take place in a single phase. The proponents of this technique assert that it is better suited for effectively and selectively converting biomass feedstocks to hydrogen. For glucose and glycols, aqueous feed values of 10–60% were recorded[31]. Methanation, which is

thermodynamically advantageous, as well as Fischer Tropsch products like propane, butane, and hexane should be avoided[32]. With a feed made up of 60% glucose in water, Rozmiarek [31] reported an aqueous phase reformer-based process that reached >55 percent efficiency. However, during long-term experiments (200 days on stream), the catalyst was not stable [31].

Finally, these reactors often have a considerable footprint due to the moderate space time yields. Microreactor technology, however, may help to enhance this. There is a lot of room for improvement in terms of catalyst activity and durability.

1.3.1.5 Ammonia reforming:

Ammonia reforming has mostly been presented as a fuel cell application for portable electricity[33]. Due to its application in the creation of fertilizer, it is a cheap fuel with a vast distribution network that includes thousands of miles of pipeline. The energy density of pure ammonia is 8.9 kWh/kg, which is more than that of methanol (6.2 kWh/kg), but lower than that of diesel or JP-8 (13.2 kWh/kg) [106]. Ammonia's strong stench makes leak detection easy, lowering some of the risk, as proponents swiftly point out [34]. Since exposure of ammonia to the acidic proton-exchange membrane (PEM) electrolyte results in a severe and irreversible loss in performance, PEM fuel cells need ammonia levels to be lowered below ppb levels to ensure long life Since ammonia will accumulate in the electrolyte, the losses add up. However, ammonia can be supplied straight into a solid-oxide fuel cell (SOFC) without having to undergo any reforming [34]. Endothermic ammonia cracking is viewed as the opposite of the synthesis reaction. Approximately 400-600 °C and 250 atm are needed for ammonia production in the industrial setting.

Iron oxide, molybdenum, ruthenium, and nickel are typical catalysts used in both the production and breaking of ammonia. In contrast to ammonia synthesis, ammonia cracking prefers low pressures and operates at temperatures of about 800-900°C[34]. The high temperatures can be achieved by either carrying a second fuel, such as propane or butane, which is then burned, or by burning some of the hydrogen created when ammonia cracks.

1.3.2 Non-reforming hydrogen production:

Other than reforming, there are numerous other ways to create hydrogen. The creation of hydrogen from water is also discussed, along with a brief overview of some of the biomass-based methods. A very quick overview of chemical hydrides will also be given, despite the fact that they are often thought of as hydrogen storage materials.

1.3.2.1 Hydrogen from biomass:

Biomass is the most likely sustainable organic fuel to replace petroleum in the near future. As a primary energy source among renewable resources, it is only surpassed by hydropower [35]. Animal wastes, municipal solid wastes, crop residues, short-rotation woody crops, agricultural wastes, sawdust, aquatic plants, short-rotation herbaceous species (such as switch grass), waste paper, corn, and a variety of other materials are all sources of biomass [30][31]. The following biomass processes are now used to generate hydrogen: gasification, pyrolysis, conversion to liquid fuels through supercritical extraction, liquefaction, hydrolysis, etc.,

followed in certain cases by reformation, and biological hydrogen synthesis[37][21]. Here is a brief explanation of gasification and biological hydrogen production.

1.3.2.1.1 Biomass gasification:

Gasification is a fairly developed commercial technology that is frequently utilized with biomass and coal in many processes. It is a form of pyrolysis and, as such, relies on the partial oxidation of the materials into a gas mixture known as a producer gas, which is composed of hydrogen, methane, carbon monoxide, carbon dioxide, and nitrogen [38]. Since pyrolysis and steam reforming have already been discussed, only a cursory analysis of the key distinctions is done here. Since moisture in the biomass must also be evaporated, the gasification process often has low thermal efficiency [39]. It can be done in a fixed bed or fluidized bed reactor and with or without a catalyst, with the fluidized bed reactor often producing superior performance[40]. A syngas stream (H2 to CO ratio of 2:1) is created when steam and/or oxygen are added to the gasification process. This stream can be sent to a Fischer-Tropsch reactor to produce higher hydrocarbons or to a water gas shift system (WGS) to produce hydrogen[40],[21]. High hydrogen yields have been achieved by reforming dry biomass with superheated steam (900 °C).

1.3.2.1.2 Biological hydrogen:

Research on bio-hydrogen has grown significantly over the past few years as a result of greater focus on sustainable development and waste reduction [36][37]. The primary bioprocess technologies used to produce bio-hydrogen include photolysis, also known as direct photolysis, which produces hydrogen from water using green algae or cyanobacteria, dark-fermentation, which produces hydrogen during the acidogenic phase of anaerobic digestion of organic material, and photo-fermentation processes. hydrogen production by water-gas shift and two-stage dark/fermentative processes [36][37]. The discovery and functional characterization of only a tiny portion of naturally occurring microorganisms should be recognized. The properties of the existing organisms are also being improved.

Water for photolysis processes and biomass for fermentative processes serve as the feedstocks for biological hydrogen production. A Brief description with their advantages and limitations will be presented here.

1.3.2.1.2.1 Direct photolysis:

Solar energy is used during photosynthesis to change carbon dioxide and water into sugars and oxygen. For some species, extra solar energy is "vented" by producing hydrogen directly from water through photolysis. Scientists are attempting to modify algae and bacteria so that the majority of the solar energy is directed toward the generation of hydrogen, with just enough directed toward the production of carbohydrates to sustain life. There are two methods for directly photolyzing water. It can first produce oxygen and hydrogen ions by using the photosynthetic skills of green algae. Two photosystems, where the process takes place, are found along the thylakoid membrane **Figure 3**.

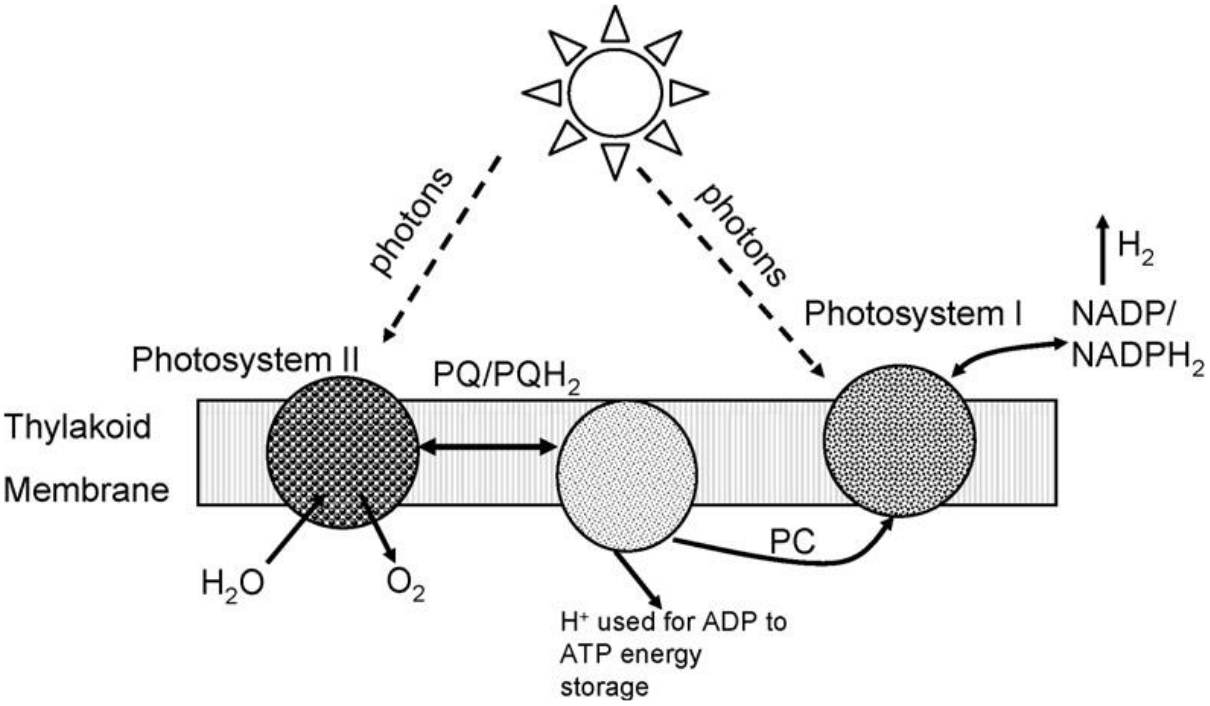

Figure 3: Direct photolysis process

Utilizing solar energy, water is split into oxygen as the initial step. The Plastiquinone (PQH_2) molecule is where the hydrogen in this process is bonded. The accumulated energy from the PQH_2 is transferred from the PQH_2 to the cytochrome B6F, which then transmits the energy to the plastocyanin (PC). The photosystem II receives the recycled PQ. Photosystem I, which is utilized to transfer the chemical energy from PC to Ferredoxin (FD), absorbs additional sun radiation. The NADP is changed to $NADPH_2$ using the FD. Carbohydrates are created from CO_2 by the $NADPH_2$ via the Benson-Bass-Ham-Calvin Cycle. However, some species vent the extra electrons by employing a hydrogenase enzyme, which turns the hydrogen ions in the FD into hydrogen gas under anaerobic conditions or when too much energy is acquired in the process[43]. The main feed for this technology is water, which has the benefit of being both affordable and widely accessible.

At the moment, this process requires a huge surface area to gather enough light. Regrettably, these microbes not only produce hydrogen when it is combined with oxygen, oxygen is produced which causes it to stop producing hydrogen[44]. as a result, work is being done to either find or develop less oxygen sensitive materials. Separate the hydrogen and oxygen cycles in organisms, and/or alter the photosynthesis (oxygen generation) ratio to oxygen consumption during respiration to avoid oxygen increase. Sulfate is added to the solution, which is reported to reduce oxygen generation and sensitivity but also suppress the mechanisms that produce hydrogen. Significant safety and separation difficulties arise as a result of the co-production of oxygen and hydrogen in a mixed gas. When compared to the prior usage of 5 percent, recent revolutionary research has significantly boosted light utilization efficiency by up to 15 percent.

Efficiency for photosynthetic to biomass can reach up to 2 percent on coral reefs, although it typically hovers around 0.2 percent worldwide. This results in a theoretical maximum

photosynthetic hydrogen generation efficiency of around 1%. By modifying organisms to better harness sun energy, proponents of photolytic hydrogen synthesis assert that 10–13 percent can be achieved. The effectiveness of light hydrogen in 2007 is only 0.5%, albeit [45], Continually producing hydrogen under aerobic conditions is another difficult task. By 2013, the U.S. DOE hopes to reach 10 minutes of continuous operation (the current state is 1 second). Although there is a lot of potential in this technology, there are also many difficulties.

1.3.2.1.2.2 Dark fermentation:

As the name implies, dark fermentation uses mostly anaerobic bacteria on substrates rich in carbohydrates while also using some algae[39][41]. The biomass employed in fermentative processes must be biodegradable, widely accessible, reasonably priced, and have a high carbohydrate content[47]. The best sugars are those that are pure, simple, and easily biodegradable, such lactose and glucose, but these are less common and/or more expensive.

The routes depend on the kind of bacteria being employed. Theoretically, the standard fermentative process can produce up to 4 moles of hydrogen for every mole of glucose. At this time, fermentation processes yield 2.4 to 3.2 moles of hydrogen per mole of glucose [44].With the aim of increasing hydrogen generation to a theoretical maximum of 12 moles hydrogen per mole glucose, it may be able to alter the fermentative route through molecular engineering. A mixture of hydrogen, carbon dioxide, methane, carbon monoxide, and some hydrogen sulfide are present in the gas that is created [46]. In order to obtain high pure hydrogen, a separation stage is necessary. The partial pressure of hydrogen plays a role in dark fermentation processes; as the pressure rises, less hydrogen is produced [47]. Removing the hydrogen as it is produced is the apparent answer to this constraint. The production of acetic, butyric, and other organic acids during fermentation is a more serious issue. By directing the metabolic route toward the creation of organic chemicals, these acids can reduce hydrogen output. Additionally, the system becomes more expensive and sophisticated due to the subsequent wastewater treatment required for their manufacture. To increase hydrogen generation and streamline the process, this channel must either be deleted, or it must be utilized.

1.3.2.1.2.3 Photo-fermentative processes:

Purple non-sulfur bacteria have a nitrogenase enzyme that can be used in photo-fermentative processes, commonly known as photosynthetic bacterial hydrogen production, to produce hydrogen. Light energy is captured during this process by light-harvesting pigments such chlorophylls, carotenoids, and phycobilins, which then transmit it to membrane reaction centres like to those found in photolytic organisms (algae). Water is transformed by sunlight into protons, electrons, and O_2 The nitrogen and ATP are combined with the nitrogenase catalyst to produce ammonia, hydrogen, and ADP. Cyanobacteria divide nitrogen fixation and oxygen synthesis either geographically or temporally because oxygen inhibits the nitrogenase. Through the uptake hydrogenase enzyme, bacteria in nature use the hydrogen by-product to power other energy-demanding processes. In order to restrict this enzyme, researchers are working to genetically alter bacteria. While other reduced compounds may be employed, the process is carried out under nitrogen-deficient circumstances predominantly employing infrared light energy[46][48]. Reduced organic acids are preferred. These bacteria can be used in a number of settings, including batch operations, continuous cultures, and

immobilization in carrageenan, agar gel, porous glass, activated glass, or polyurethane foam, which is advantageous since oxygen does not block the process [46][48]. The lack of readily available organic acids, the nitrogenase enzyme's slowness, the process's high energy demand, and hydrogen re-oxidation are the drawbacks [46][48].The right balance of carbon to nitrogen nutrients must be maintained in order to boost nitrogenase activity and lower energy needs. To lessen the nitrogenase's sensitivity to high quantities of nitrogen nutrients, enzyme engineering techniques are being developed. Microengineering is also being used to stop hydrogen re-oxidation by making the bacteria's hydrogenase enzymes inactive. The nitrogenase produces hydrogen, which is recycled by the hydrogenase enzymes to stimulate cell growth. Finally, photosynthetic organisms are not effective sun collectors, only capturing an average energy flow of 100–200 W/m2 during the day and night. About 1.9 percent is the current efficiency.

1.3.2.1.2.4 Microbial electrolysis cells:

Biodegradable materials are directly converted into hydrogen by electrohydrogenesis in microbial-aided electrolysis cells, also known as bio-electrochemically assisted microbial reactors (BEAMR)[49]. A modified microbial fuel cell is the MEC **Figure 4**. Exoelectrogens (special microorganisms) in a microbial fuel cell break down (oxidize) organic matter and transfer electrons to the anode. After passing through an external load and arriving at the cathode, the electrons mix with the protons and oxygen to produce water. No oxygen is present at the cathode while a MEC functions, therefore an external voltage is provided to the cell rather than being produced by it. Since acetate substrate breakdown is not spontaneous under typical conditions, additional energy is required [49]. At the cathode, hydrogen is created. In neutral pH (pH 7), the predicted potential for hydrogen production is 0.61 V, VCat vs. Ag/AgCl[50]. Exoelectrogens produce anodes with potentials around Van = 0.5 V. As a result, 0.11 V [50] is the minimum applied potential (Vapp = Van VCat). Due to electrode overpotentials and ohmic resistance, the actual applied voltage for acetate is >0.3 V [50].

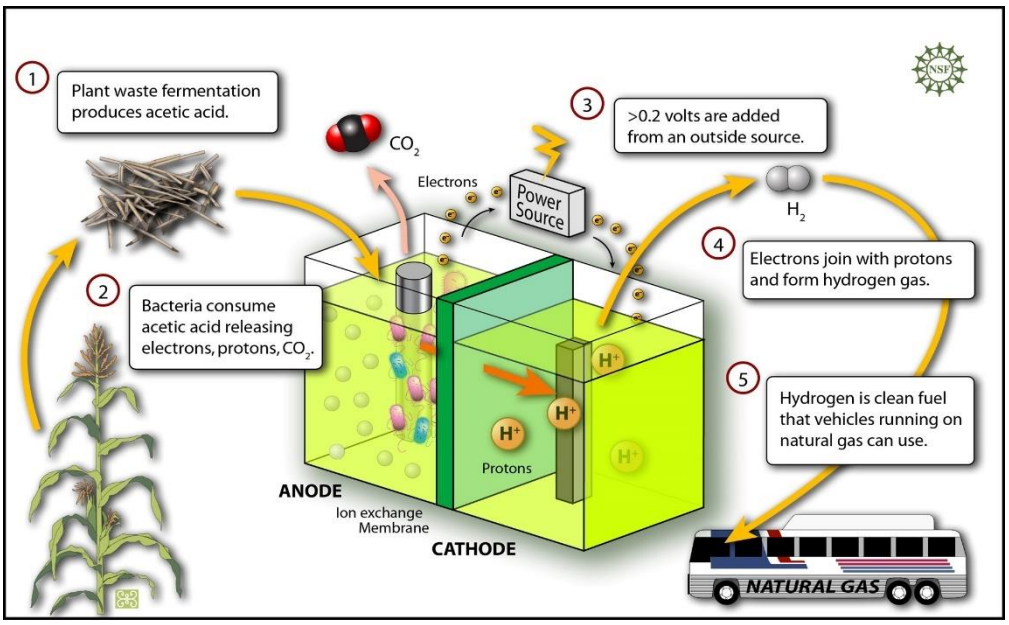

Figure 4: Microbial electrolysis cell [51]

1.3.2.1.2.5 Multi-stage integrated process:

To maximize the hydrogen production from the feed, a multi-stage process has been put in place[48] The procedure originally had two stages: dark fermentation and then photo fermentation [48], but three or even four stages have since been suggested in various arrangements. In this procedure, the biomass material is initially added to a reactor for dark fermentation, where the bacteria break down the feedstock to produce hydrogen and an effluent that is rich in organic acids. This removes the difficulty of sourcing organic acids for the photo-fermentative process because the effluent contains organic acids. The sunlight is initially filtered through a direct photolysis reactor, which predominantly employs visible light but does not use infrared light because the photo-fermentative process largely requires that wavelength. In the fourth stage, microbial electrolysis cells are used to produce hydrogen rather than electricity. The same organic acids are used in this cell, but light is not necessary. It can therefore function at night or during other periods of low light. Prior to sending the first stage's effluent to the second stage, some dilution and neutralization are needed to get the pH of the effluent to 7, as ammonia inhibits the second stage[48].

1.3.2.1.2.6 Water-gas-shift

The WGS reaction is the oxidation of CO to CO_2 using H_2O and H_2 production is a by-product following the equation:

$$\mathbf{CO + H_2O \rightleftharpoons CO_2 + H_2}.$$

It was brought to light that some Rhodospirillacae photoheterotrophic bacteria may thrive in the dark by simply consuming CO[46], but enzymes are used as the catalyst here rather than metal. Thermodynamics promote a high CO to CO_2 and H_2 conversion since it takes place at low temperatures and pressures [46]. Compared to other biological processes, its conversion rate is actually quite high, but it does need a CO supply and complete darkness [46].

1.3.2.2 Hydrogen from water:

Water splitting to produce hydrogen and oxygen has been extensively studied; in fact, its commercial applications date back to the 1890s Three categories can be used to classify water splitting: Thermolysis, Photoelectrolysis, and Electrolysis

1.3.2.2.1.4 Thermochemical water splitting:

Heat alone is utilized to break down water into hydrogen and oxygen in thermochemical water splitting, commonly known as thermolysis[13]. These procedures are thought to be capable of achieving close to 50% overall efficiency. Water begins to break down at a temperature of 2500°C, however materials that can withstand this temperature as well as sustainable heat sources are difficult to come by[13]. In order to lower the temperatures, chemical reagents have been suggested. From the 1960s through the early 1980s, this field of study attracted a lot of attention. But until recently, virtually all R&D was abandoned after the mid-1980s. In the literature, more than 300 water splitting cycles are mentioned. Although every method has drastically lowered the operating temperature from 2500°C, they all often call for higher pressures. There are five requirements that must be fulfilled while choosing the process. (1) The ΔG of each reaction must be close to zero at the temperatures taken into account. The most crucial factor is this one. (2) There should be a minimization of the chemical steps required to acquire hydrogen from primary thermolysis reagents. (3) Each

phase in the process must have quick reaction times as well as rates that are consistent with those of the previous steps. (4) There cannot be any chemical by-products from the reaction, and any separation of the reaction products must be inexpensive and energy efficient. (5) Intermediate by-products need to be manageable. The Ispra-Mark and UT-3 processes, as well as the sulfuric acid decomposition process, are among the processes that currently meet the five criteria. However, they are still not cost and efficiency competitive with other hydrogen generation technologies, which is the main focus of research in those processes [52].These procedures also call for substantial stocks of extremely dangerous corrosive compounds. New materials are required as a result of corrosion and high temperatures, pressures, and temperatures. The hybrid sulfur Ispra-Mark process, for example, calls for ineffective electrochemical stages that need to be improved[52].

Scaling up the processes is thought to help this technology overcome one of its main problems by improving thermal efficiency [52]. Additionally, lower costs for producing hydrogen can result from a greater comprehension of the connection between capital expenses, thermodynamic losses, and process thermal efficiency [52]. It is thought that an effective two reaction procedure would make this technology practicable because all present processes utilize four reactions or more [52]. In order to improve materials, reduce costs, and boost efficiency[53].

1.3.2.2.2 Photoelectrolysis:

Using semiconductor materials similar to those used in photovoltaics, photoelectrolysis uses sunlight to directly split water into hydrogen and oxygen. A p-n junction is created in photovoltaics by joining two doped semiconductor materials of the p- and n-types. When the charges in the p and n-type of material rearrange, a persistent electric field is created at the junction. An electron is liberated, and a hole is created at the junction when a photon with energy larger than the bandgap of the semiconductor material is absorbed there.

An electric current will be produced if an external load is also connected because the hole and electron are compelled to move in opposing directions due to the presence of an electric field [43][54].

When a photocathode, a p-type material with excess holes, or a photoanode, an n-type material with excess electrons, are submerged in an aqueous electrolyte, this type of situation occurs in photoelectrolysis, but instead of producing an electric current, water is split into hydrogen and oxygen **Figure 4** [54].

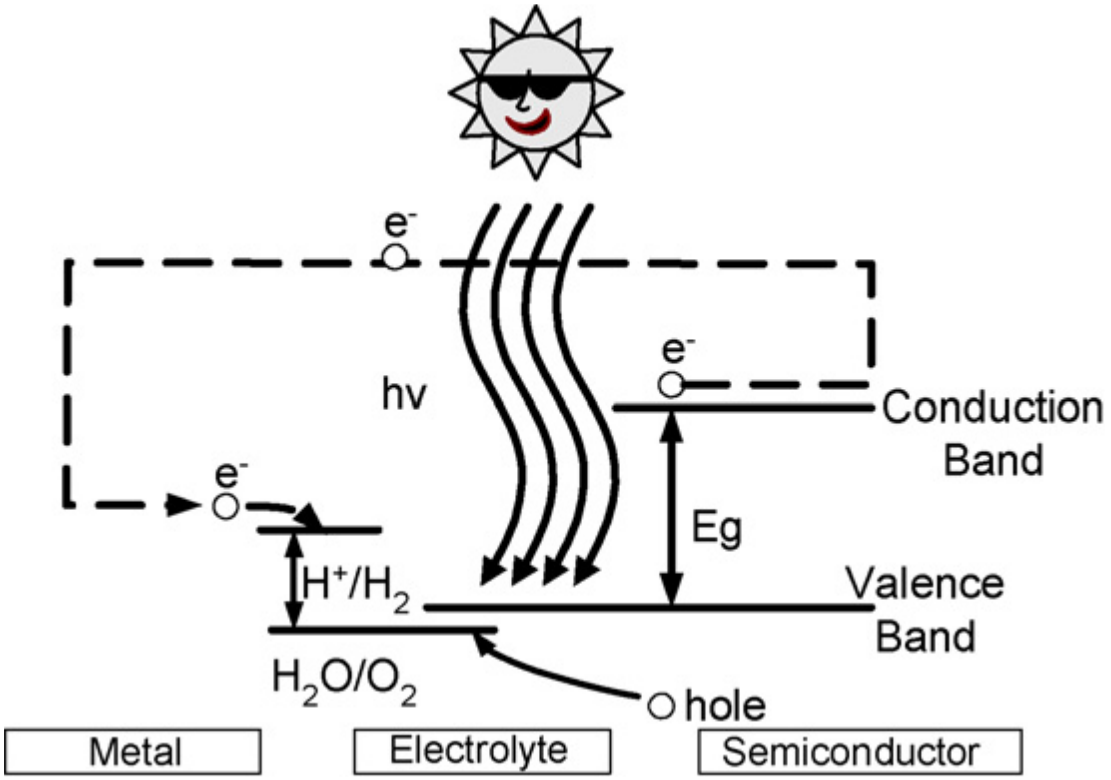

Figure 4: Energetic diagram of n-type semiconductor photoelectrochemical cells [13]

For a photoanode-based system, the procedure can be summed up as follows: (1) An electron-hole pair is formed when a photon that has more energy than the bandgap reaches the anode. (2) While the electrons move through the rear of the anode, which is electrically coupled to the cathode, the holes breakdown water at the front surface of the anode to generate hydrogen ions and gaseous oxygen. (3) After passing through the electrolyte, the hydrogen ions at the cathode interact with the electrons to produce hydrogen gas.(4) For processing and storage, the oxygen and hydrogen gasses are separated, for instance using a semi-permeable membrane [54].

Thin-film WO3, Fe2O3, and TiO2, as well as n-GaAs, n-GaN, CdS, and ZnS for the photoanode, and CIGS/Pt, p-InP/Pt, and p-SiC/Pt for the photocathodes, have all been explored for usage in photoelectrodes [55]. The system's performance is determined by the materials used to make the semiconductor substrate and photoelectrodes. The efficiency of hydrogen production is typically constrained by flaws in the crystalline structure, photoelectrode bulk and surface properties, material resistance to corrosion from aqueous electrolytes, and capability to drive water decomposition reactions [54].

The energetics of the electrochemical reaction must be in harmony with the solar radiation spectrum, which is a non-trivial problem, in order to enhance the efficiency of this process, a mismatch between the solar radiation and the materials can result in photo-generated holes that can cause surface oxidations and either form a blocking layer on the semiconductor surface or cause the electrode to corrode through dissolution.[56]

The efficiency of utilizing photons to split water into hydrogen is currently poor in photoelectrodes used in PEC that are stable in aqueous solutions. More than 16 percent solar energy to hydrogen is the desired efficiency. This includes three features of the material system required for effective conversion: (1) The band gap should be within the range necessary to achieve the energetics for electrolysis while yet allowing maximal solar spectrum absorption. This is between 1.6 and 2.0 eV for a single photoelectrode cell and between 1.6 and 2.0 eV/0.8 to 1.2 eV for top- and bottom-stacked tandem cells, (2) straddle the redox potentials of the H2 and O2 half reactions with their respective conduction and valence band edges, (3) have a high quantum yield (>80 percent) over their absorption band to provide the efficiency required for a practical device. Since the material or device needs to have the right energy to split water, the efficiency is directly related to the semiconductor band gap (Eg), or the energy difference between the bottom of the conduction band and the top of the valence band, as well as the band edge alignments. The band edges, which must cross the redox potential of water with enough room to account for inherent energy losses, are what determine the energetics. The development of affordable, long-lasting catalysts with suitable band edge and Eg locations is necessary. The photoelectrodes must be "current matched" in order to operate in tandem with the best efficiency achievable. The system's efficiency may be improved by adding surface improvements such as electron transfer catalysts. These improvements can reduce the surface overpotentials in relation to the water and speed up reaction kinetics, reducing the system's electric losses. To comprehend the underlying mechanisms and find suitable candidate surface catalysts for these systems [56] [60][61]fundamental research is being conducted.

Metal complexes suspended in solution can be used as photochemical catalysts in addition to semiconductor photoelectrolysis devices [59]. These so-called dyes provide a voltage boost for water cleavage by visible light. Nanoparticles made of ZnO, Nb2O5, and TiO2 have often been employed [62]. The N3 dye and the Black dye are two of the most promising dyes. The 2,20-bipyridyl-4,40-dicarboxylic acid in L stands for the N3 dye, cis-RuL2(NCS)2 [62]. (Tri)cyanto)-2,20200-terpyridyl-4,40400-tricarboxylate) Ru(II) is the black dye. These systems have the potential for high efficiency and the utilization of inexpensive materials as advantages [62]. The limited light absorption and subpar time stability of these devices are being addressed in current research.

1.3.2.2.1 Electrolysis:

In its most basic form, water splitting involves an electrical current flowing through two electrodes to split the liquid water into hydrogen and oxygen gases. System efficiency for commercial low temperature electrolyzers range from 56 to 73 percent (70.1 to 53.4 kWh/kg H_2 at 1 atm and 25 ^oC)[43]. To measure such efficiencies using the simple equation of water electrolyses reaction

$H_2O_{(liquid)}$ + 237.2 kJ/mole electricity + 48.6 kJ/mole heat → H_2 + ½ O_2

The electrolysis system efficiency can be calculated as the heating value of the hydrogn produced divided by the electricity used as follows: where HHV is higher heating value and LHV is lower heating value. [60]

$$Electrical\ efficiency_{(HHV)} = \frac{HHV\ of\ H_2\ produced}{Electricity\ used}$$

$$Electrical\ efficiency_{(LHV)} = \frac{LHV\ of\ H_2\ produced}{Electricity\ used}$$

In essence, hydrogen is created as a by-product as electrical energy is converted, and oxygen is a valuable by-product of this process. Alkaline-based electrolysis technology is the most widely used, but proton exchange membrane (PEM) and solid oxide electrolysis cells (SOEC) units are growing in popularity[61]. The least developed of the technologies, SOEC electrolyzers are the most electrically efficient. Corrosion in the SOEC due to high temperature hydrogen could lead to electrodes poisoning that could ultimately lead to loss of hermeticity within the SOEC Stack, sealing of the SOEC stacks on the other hand and their subjection to the hydrogen high temperatures as well as the sealing material local defects will cause long term issues within the cell like temperature increase and higher degradation rates and heat cycling where the changes of heating temperatures from room to operating ones which causes thermal stress inside the cell due to mismatched coefficients of thermal expansion of the cell (CTE) eventually reducing the service life and shortens the application fields of SOEC in general are problems with SOEC technology.[62][63][64] PEM electrolyzers are more effective than alkaline, do not experience SOEC's corrosion and seal problems, but they are more expensive. The most advanced and economically efficient systems are alkaline ones.

As a result of their lowest efficiency, they use the most electricity. High-pressure electrolyzers (pressures > 1000 ppsig) are now being developed, in addition to producing high purity hydrogen [65]. The removal of pricey hydrogen compressors is a benefit of high-pressure operation. At the moment, producing hydrogen using electrolysis is more expensive than doing it through large-scale fuel processing methods. Additionally, generating electricity for electrolysis using non-renewable energy actually produces more emissions than natural gas reforming [66]. It should be emphasized, nevertheless, that on-site electrolysis production may be less expensive if the hydrogen must be transported in cylinders or tankers. To solve these shortcomings, a variety of strategies have been put forth. These include high temperature electrolysis, off-peak hydrogen production using surplus power from existing generators, and the use of renewable energy sources like solar, wind, and hydro to generate electricity[66]. The cost of using renewable energy for electrolysis has been the subject of numerous studies, all of which have come to the same conclusion that as natural gas prices rise, renewable energy will become economically competitive at both centralized production facilities and distributed generation points, especially if carbon dioxide and other pollutants are taken into consideration [67].

1.3.2.2.1.1 Alkaline electrolyzers:

The standard components of an alkaline electrolyzer are electrodes, a microporous separator, and an aqueous alkaline electrolyte with a concentration of around 30% KOH or NaOH [43]. The most typical cathode material in alkaline electrolyzers is nickel with a catalytic coating, such as platinum. Metals covered with metal oxides, such as manganese, tungsten, ruthenium, nickel or copper are utilized as the anode. Despite not being consumed in the reaction, the liquid electrolyte must be replaced over time due to system losses, particularly during hydrogen recovery. Water is introduced into an alkaline cell's cathode, where it breaks down into hydrogen and OH. Through the electrolytic substance, the OH flows to the anode, where

O2 is created. The alkaline solution still contains hydrogen. After that, the hydrogen and water are separated in a gas-liquid separations unit not connected to the electrolyser. Based on the lower heating value of hydrogen and the average current density of 100–300 mA cm2, alkaline electrolyzers typically attain efficiencies of 50–60%[43].

The overall reactions at the anode and cathode are:
Anode:

$4\ OH \rightarrow O_2 + 2\ H_2O$

Cathode:

$2\ H_2O + 2\ e \rightarrow H_2 + 2\ OH^-$

Overall:

$H_2O \rightarrow H_2 + 12\ O_2$ DH = -288 kJ mol^-1

1.3.2.2.1.2 Proton exchange membrane electrolyzer:

The most recent developments in PEM fuel cell technology are built upon by PEM electrolyzers. Pt black, iridium, ruthenium, and rhodium are frequently used as electrode catalysts in PEM-based electrolyzers, and a Nafion membrane also serves as a gas separator in addition to separating the electrodes[43]. Water is added to PEM electrolyzers at the anode, where it splits into protons and oxygen. When the protons reach the cathode through the membrane, they unite once more to form hydrogen. Along with the unreacted water, the O_2 gas is left behind.

A separations unit is not required. After a gas/liquid separation unit, remaining water may be removed using a dryer, depending on the purity requirements. Due to the low ionic resistance of PEM electrolyzers, large currents of >1600 mA cm2 can be attained while yet maintaining high efficiencies of 55–70% [43]. The anode's and cathode's reactions are as follows:

Anode:

$2\ H_2O \rightarrow O_2 + 4H + 4\ e^-$

Cathode:

$4\ H^+ + 4\ e^- \rightarrow 2\ H_2$

Overall is the same as for alkaline electrolyzers:

$H_2O \rightarrow H_2 + ½\ O_2$ DH = -288 kJ mol^-1

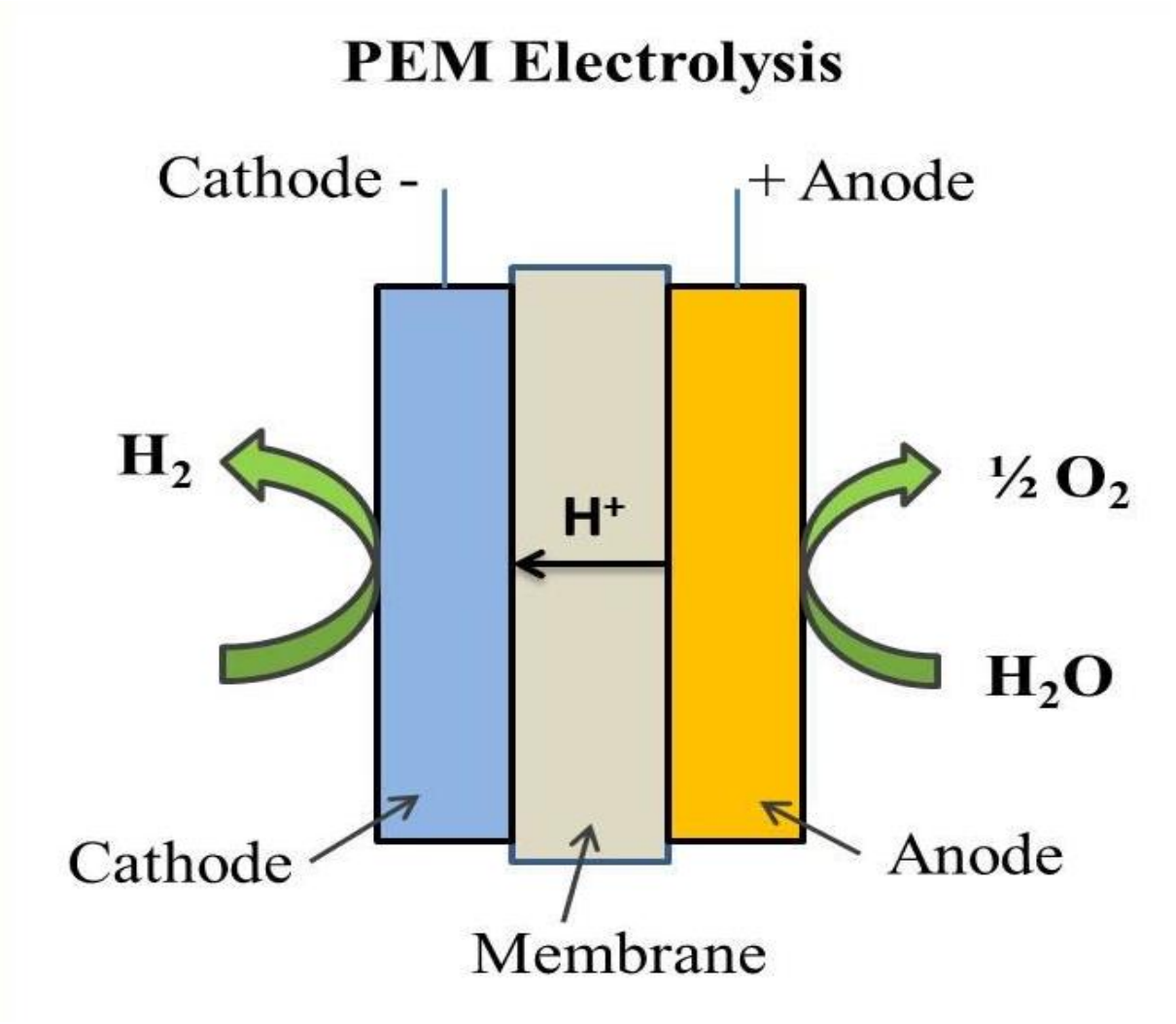

Figure: A Schematic illustration of PEM water electrolysis. [67]

1.3.2.2.1.3 Solid oxide electrolysis cells:

In essence, solid oxide fuel cells that operate in reverse are solid oxide electrolysis cells (SOEC). These devices use thermal energy instead of all of the electrical energy needed to divide water[68]. The lower anode and cathode overpotentials, which result in power loss in electrolysis, boost the electrolyzer efficiency at higher temperatures[68]. For instance, a temperature rise from 375 to 1050 K reduces the total amount of thermal and electrical energy used by over 35% [68][69]. In that an oxygen ion passes through the electrolyte while leaving the hydrogen in the unreacted steam stream, an SOEC functions similarly to an alkaline system. The use of a solid electrolyte that, unlike KOH for alkaline systems, is non-corrosive and does not encounter any liquid and flow distribution problems is another benefit for high temperature electrolysis with a solid oxide based electrolyzer[68]. Of course, in addition to a heat source, high temperature operation calls for the employment of expensive materials and fabrication techniques [70]. The materials share concerns with seals with those being researched for solid oxide fuel cells (SOFC), Yttria-stabilized zirconia (YSZ) electrolyte, nickel-containing YSZ anode, and metal doped lanthanum metal oxides [68], [70].

The efficiency of high temperature electrolysis depends on both the temperature and the heat source. With efficiencies of between 85% and 90% recorded, the efficiency as a function of electrical input alone can be very high. The efficiency, however, may suffer greatly when the

thermal source is included. For instance, SOEC may be able to attain up to 60% efficiency when using modern high temperature nuclear reactors. Solar energy is being developed and may create the high temperature source with higher efficiency than traditional combustion or nuclear energy [71]. Co-generation of electricity and hydrogen has been suggested using an SOEC and SOFC combination[72]. A SOFC and SOEC are manifolded into one stack in this hybrid system and fed the same fuel, such as natural gas. The SOEC then generates hydrogen, and the SOFC generates power. Efficiencies of up to 69% have been shown for proof-of-concept short stacks [72].Coking which affects the anode weakens electrochemical catalytic oxidation and causes the surface to become inactive is considered a significant problem in addition to the other difficulties SOEC is facing, and it is still only utilized at a rate of about 40%.[73]

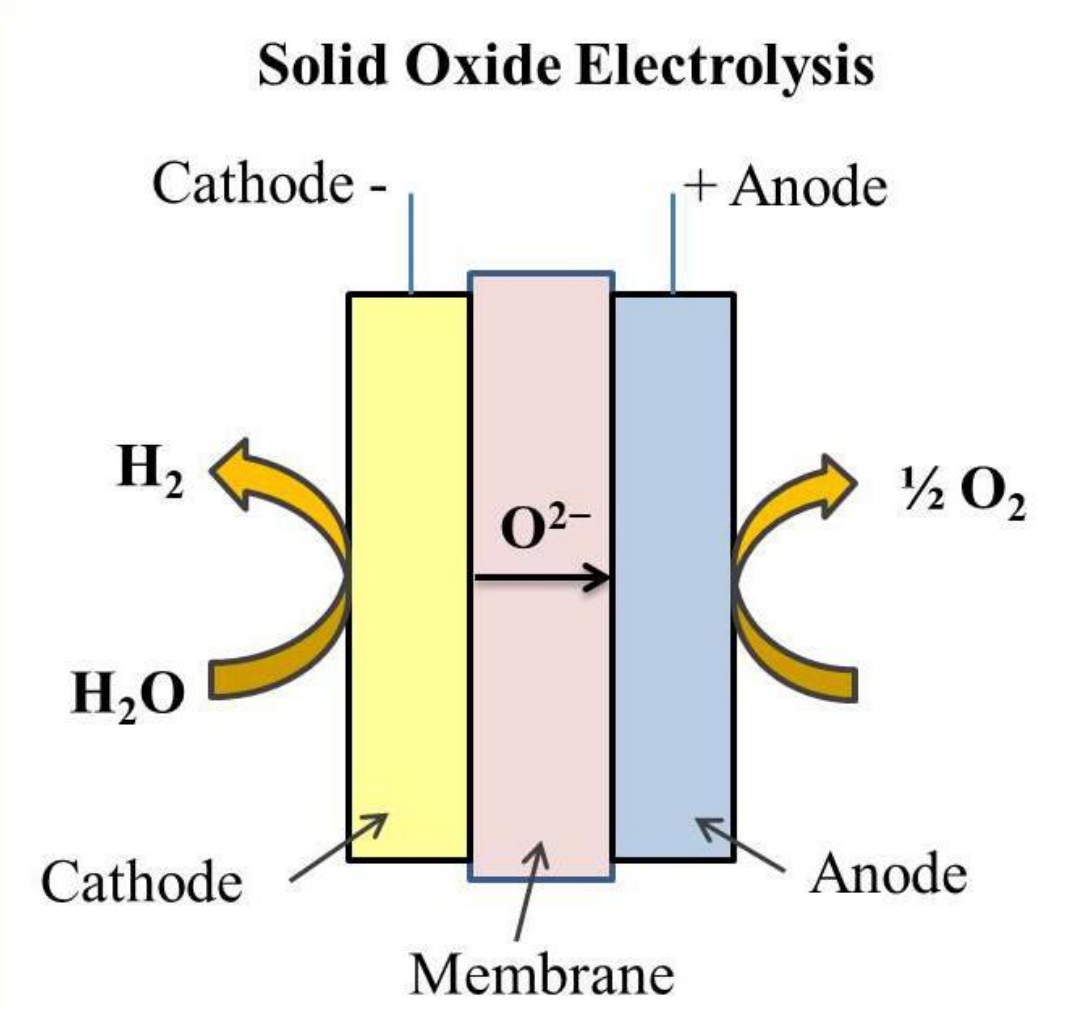

Figure: A Schematic illustration of Solid Oxide electrolysis. [67]

1.3.3 Hydrogen usage advantages and characteristics:

The following are some of the benefits of using hydrogen as a fuel in fuel cells:

• strong electrochemical reactivity,

• high theoretical energy density,

• infinite availability (as long as you can break down the water), and

• its environmentally friendly combustion product (H2O).

The principal disadvantages on the other hand of using pure hydrogen in fuel cells include its low density under normal conditions, the difficulty of storage, and the risk of explosion.[74]

1.4 Diverse Integrated Systems and Water Splitting:

Water electrolysis is traditionally carried out in a two-electrode system, with oxygen evolution reaction (OER) and hydrogen evolution reaction (HER) occurring at the anode and cathode, respectively, as indicated in the diagram. [10]

$2\ H_2O\ (l) \rightarrow 4\ e^- + 4\ H^+\ (aq) + O_2\ (g)$ (Oxidation reaction at anode, OER)

$4\ e^- + 4\ H^+\ (aq) \rightarrow 2\ H_2\ (g)$ (Reduction reaction at cathode, HER)

Both the OER and the HER are high-energy, high-thermodynamic-demanding processes in which the entire water splitting can be accomplished by providing at least 1.23 V versus RHE thermodynamic potential. It can be done electrochemically (electrocatalysis) or photochemically to give a sufficient amount of energy (photocatalysis). Semiconducting materials that replicate natural photosystem are employed as light harvesters and energy converters in photocatalysis. Excitation of electrons from the valence band of photocatalysts to the conduction band generates electron-hole pairs (excitons) after irradiation. Solar-fuel devices, which include photovoltaic materials (PV), proton exchange membranes (PEM), oxidation and reduction catalysts, are used to produce H_2 in this energy conversion scheme.[13]

However, it can be classified as a wireless or wired arrangement architecturally **Figure 5**. Semiconducting materials (photovoltaic cells) are directly exposed to sunlight in a wireless configuration[10], causing electrons and holes to be trapped towards their respective/opposite poles for oxidation and reduction activities at the catalyst-electrolyte interface. The electrodes are externally connected with conducting wire and inwardly separated by PEM in the wired form. Following the trapping of sunlight, water is oxidized at the hole, and electrons are transported to the cathode via an external circuit to complete the cycle. The created hydrogen can be stored from the appropriate electrodes in both configurations while directly harvesting the sunlight[10]. Despite the fact that these are desired ways with their own set of benefits and chemistry, they are not the subject of this dissertation. As a result, we'll concentrate on the electrochemical water splitting module, its electrode chemistry, and future prospects.

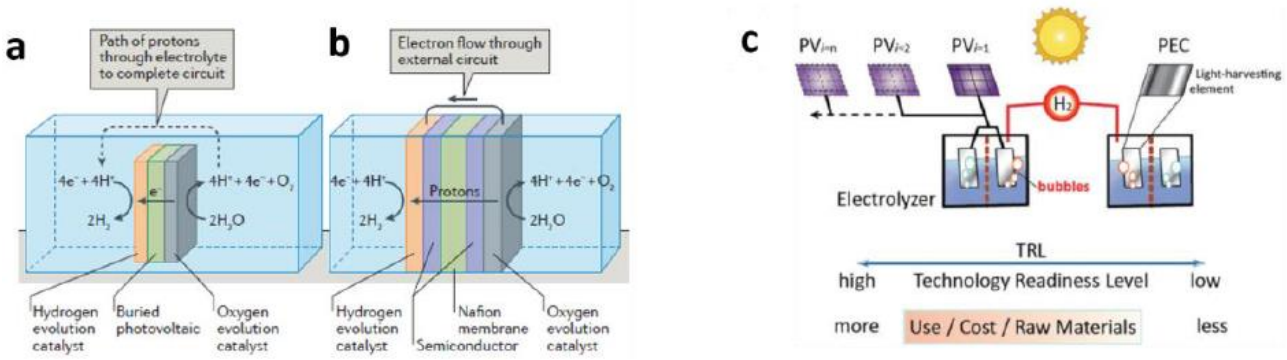

Figure 5: Schematic illustration of various water splitting modules (a) wireless configuration for photocatalytic water splitting assembled with PV cell in-between the electrodes (b) wired configuration for photocatalytic water splitting assembled with semiconductors-based materials as light harvester (c) PV-cell electrolysis (left) and comparison with photocatalytic water splitting (right).[10]

1.5 Electrochemical Water Splitting Module:

Water can be heterogeneously split at the surface of electrodes electrochemically by generating potential across the electrodes that is greater than the thermodynamic potential (1.23V). At the anode, electrons, protons (H^+), and molecular oxygen are created during the oxidation of water. These protons and electrons travel from the anode to the cathode via the electrolyte and external circuit, respectively, to complete the cycle and release molecular H_2.[10]

Commercially accessible electrolyzers are divided into two categories: alkaline electrolyzers and proton exchange membrane (PEM) electrolyzers. The latter is more efficient, with the ability to achieve current densities of 1000-2000 mA/cm2 while employing extremely costly electrode materials. Alkaline-based electrolyzers, on the other hand, use transition metal-based electrode materials (Ni-based spinel family and perovskite) and yield a lower current density (20-30 mA/cm2) than alkaline-based electrolyzers. Both of these electrolyzers operate in highly alkaline environments (high pH).

Solid oxide-based electrolyzers have also been introduced to work at high temperatures with high efficiency, in addition to these two electrolyzers. However, the cost of hydrogen produced through water electrolysis is currently around 2-3 times that of hydrogen produced from the steam reforming process, due to the necessity for high input potential under ambient circumstances and the overall inefficiency of the water splitting process.

As a result, PV-cell electrolysis is a more advanced form of the water splitting process, in which the PV-cell generates energy by gathering sunlight[75]. In comparison to typical electrolyzers and basic photocatalysis, the solar-driven electrochemical water splitting process is the leading and burning area of research, with a cheap cost and high technology readiness level[75]. However, it may be understood scientifically by first developing highly efficient PV materials with high photon to electron conversion efficiency (PEC) that can be stored in batteries and used to power a competent electrolyzer for overall water splitting with

high conversion efficiency[76]. Integration of these two modules (electrolyzer and PV) in a single assembly with suitable H_2 gas storage is an important step toward electrochemical solar-driven technology for long-term hydrogen production. Although technical challenges, social perception, political impact, and research opportunities are all crucial in establishing such an independent energy production grid, the technical hurdles, societal perception, political impact, and research opportunity are all equally important. The current market penetration of PV cells, as well as the continual decline in their cost, is a promising sign for this technology. However, improving the catalytic efficiency of electrolyzers is also critical in order to energetically accelerate the difficult redox reaction of the water splitting process at low cost while maintaining high conversion efficiency. To solve the challenges with electrolyzers and the poor activity of the earth's abundant materials, many models have been created to increase the efficiency of water conversion. For example, the newly introduced models in this respect are[77]: **Figure 6**

i) total water splitting process
ii) decoupled water splitting process
iii) hybrid water splitting method
iv) tandem water splitting approach

In general, utilizing a basic or acidic media improves the kinetics of the OER and HER processes. However, creating an independent/separate compartment for the various redox reactions complicates the electrode setup. As a result, developing catalysts that are bifunctional in nature and effective throughout a large pH range, or at the very least can catalyze both OER and HER at neutral pH, is a top priority **Figure 6a**. The use of such bifunctional catalysts is beneficial not only in terms of simplifying electrode architecture, but also in terms of lowering the overall cost of the water splitting process. Among the two half-cell responses, however, Because the OER process is kinetically sluggish, it cannot meet the number of electrons required for proton reduction on the counter electrode. To overcome this issue, a novel model called as decoupled water electrolysis was developed, which includes a specific separation of the OER and HER compartments as well as a redox mediator (RDM) **Figure 6b.**

The purpose of RDM is to stop the mixing of H2/O2 (reversible reaction) while also partially preventing the creation of oxygen species by oxidizing itself in a solution rather than using the traditional OER method. RDM transfers electrons to the external circuit during oxidation and then reduces on the same electrode with OER. This reduces the risk of reversible reactions while also compensating for the electron shortage caused by OER's slow kinetics. Similarly, for efficient electrolyzers, the demand for high input potential for OER is a significant obstacle that must be solved.

Furthermore, the molecular O_2 created during the oxidation process is not considered a water splitting process result. In this regard, the hybrid water electrolysis concept provides an alternative route, in which biomass-derived small compounds/intermediates with high thermodynamic favourability, such as urea, thiourea, and HMF-derived molecules, are used in electrolyzers with low overpotential oxidation compared to OER **Figure 6c**.

As a result, the simple oxidation of organic moieties at the anode may not only reduce the total overpotential for water splitting, but also yield valuable organic products. In addition, it can inhibit H2/O2 mixing and improve proton reduction selectivity at the cathode in the presence of other organic species.

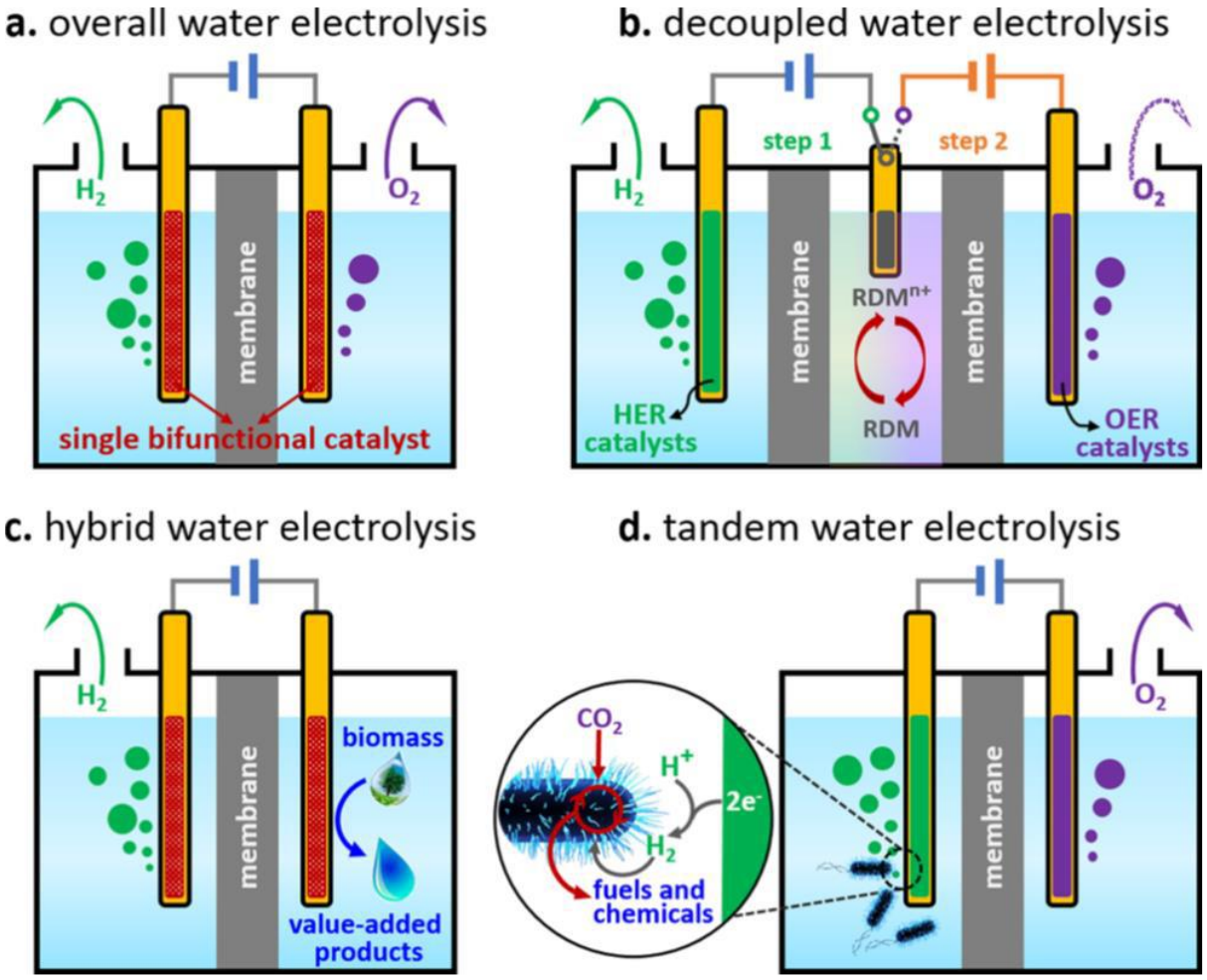

Figure 6: Schematic illustration of various electrochemical water splitting modules (a) overall water splitting catalysis using bifunctional electrode materials (b) decoupled water splitting scheme with redox mediator (RDM) (c) hybrid water splitting scheme with catalysis of biomass (d) tandem water splitting scheme for the direct utilization of H2 with consumption of CO2.[77]

The cost-effective storage and transportation of H2 once water has been divided is the next major hurdle. To overcome this problem, a novel alternative approach called as 'tandem water splitting,' which is similar to natural photosystem II, has been developed. The liberated H2 can be used directly to reduce CO2 on the cathode using biological catalysts (enzymes) to produce value-added products in this conversion process (CH4 and NH3 etc.). It has been deemed a promising strategy for the perfect use of H2, consumption of CO2 gas, and

generation of value-added chemicals/fuels by water electrolysis if implemented on a big scale **Figure 6d**.

Considering the benefits of all electrolyzers and various water splitting modules, the entire water splitting process utilizing bifunctional electrode material is of essential relevance and considerably more developed. Efforts have been made in recent decades to better understand the nature of electrocatalysts, electrode chemistry, and mechanism in order to improve the efficiency of electrolyzers, as well as to raise interest in and achieve technology readiness for solar-assisted water splitting pathways.

1.6 Thermodynamics and Chemistry of Electro-assisted Water Splitting:

The overall water electrolysis reaction can be written as below:

$$\mathbf{H_2O\ (\mathit{l}) \longrightarrow H_2\ (\mathit{g}) + 1/2\ O_2\ (\mathit{g})} \qquad 1.1$$

It can be done in an electrochemical cell with 2/3 electrodes set up as the working electrode and a counter one as an experiment. The electrodes are submerged in an electrolyte and electrically connected to a potential source (Potentiosat). Potentiostate's job is to control and provide the potential across the electrodes.[10] Under certain conditions, the electrolysis process recognizes a set of thermodynamic parameters such as cell potential, electrons transported, and enthalpy change (heat transferred).

At ambient temperatures, water splitting, like many other reactions, is an endothermic process (STP). The quantity of released energy (enthalpy change, Hws) during electrolysis is equal to the heat of formation (enthalpy of formation, -Hf) of 1 mole of water, according to the equation 1.1. The Highest quantity of heat (H_{HH}) created by burning 1 mole of H2 is equal to this absolute amount of energy (286 kj/mol or 2.96 eV).[78]

However, the minimum required potential (equilibrium potential) for the reversible electrolysis is 1.23 V, which depends upon the Gibb's free energy of any reaction as below:

$$\mathbf{\Delta G = nFEo} \qquad 1.2$$

G represents the Gibbs free energy change, n represents the number of electrons (2e- for 1 mole of H2O), F represents the Faraday constant (96485 C/mol), and Eo represents the cell potential. G for water splitting has been experimentally proved to be +237.38 kJ/mol (water) or 2.46 eV. The total amount of energy necessary for water splitting at 298 K can be written as: Taking the absolute value of cell/equilibrium potential (1.23 V) and adding the entropy factor, the total amount of energy required for water splitting at 298 K can be written as:

$$\mathbf{\Delta Hws = \Delta H^{o}HH = -\Delta H^{o}f = \Delta Gws + T\Delta S^{o}ws} \qquad 1.3$$

The final term denotes the change in entropy at STP, which is 49 kj/mol, implying that this much energy will be obtained from the environment (electrolyte), which can also be regarded input energy for the water splitting process. As a result, the maximum quantity of needed potential can be expressed as:

$$\mathbf{\Delta H^{o}HH = V^{o}HH = 2FEo = 1.48\ V} \qquad 1.4$$

At STP, in the applied potential range of 1.23-1.48 V, the above equation implies that water electrolysis is an endothermic process. The system will cool down or run isothermally if fed with a constant source of heat under ideal conditions (excluding all ohmic resistance/loss processes) at a potential of ≤ 1.48 V. Equations 1.1 and 1.2 also show how the input/applied potential may decrease as the temperature rises.

The above discussion demonstrates that water electrolysis is non-spontaneous in nature due to the positive Gibb's free energy change. A potential difference of at least 1.23 V between the electrodes should be provided to make the reaction go downhill. The potential range can be widened by increasing or reducing the temperature or modifying the reaction circumstances.

1.7 Electrodes Chemistry:

The standard electrode potential required to derive the half-cell reactions taking place at the cathode and anode can be expressed by Nernst equation.

1.7.1 Reaction at Cathode:

$$2\,H^+ + 2\,e^- \longrightarrow H_2 \quad E^o = 0.0\ V \text{ vs RHE} \qquad 1.5$$

$$E = E^o + \frac{0.059}{2 * \log[H^+]2}$$

By applying the logarithmic formula, we can write it as:

$$E = E^o + 0.059 * \log[H^+] = 0.0 + 0.059 * pH \qquad 1.6$$

1.7.2 Reaction at Anode:

$$2\,H_2O \longrightarrow 2\,H^+ + O_2 + 4\,e^- \quad E = 1.23\ V \text{ vs RHE} \qquad 1.7$$

$$E = E^o + \frac{0.059}{4 * \log[H^+]4}$$

$$E = E^o + 0.059 * \log[H^+] = 1.23 + 0.059 * pH \qquad 1.8$$

To carry out the water splitting reaction, a potential difference of 1.23 V is necessary, as shown in the equations above. However, due to ohmic resistance and other loss processes at the electrode-electrolyte interface, we must offer a potential greater than 1.23V in practice, which is referred to as the overpotential.

As a result, the ultimate cell potential is as follows:

$$E_{applied} = 1.23 + \eta_{cathode} + \eta_{anode} + iR \qquad 1.9$$

It's also worth mentioning that the applied cell potential is strongly influenced by the reaction medium's pH **Figure 7b**. Although the pH factor cancels out in the overall water splitting process, it is critical for measuring the potential with potentiostate for half-cell reactions. As a

result, we normally measure/normalize the potential against the 'Reversible Hydrogen Electrode' to eliminate the pH component, allowing us to directly measure the redox potential for the Faradaic reaction (Equation 1.9). By altering the pH of the reaction medium, the range of the applied potential decreases/increases systematically, as shown in **Figure 7**.The slope of the curve (potential versus pH) over the entire pH range corresponds to a jump of 59 mV in the applied cell potential when the pH is increased by one degree. [11]

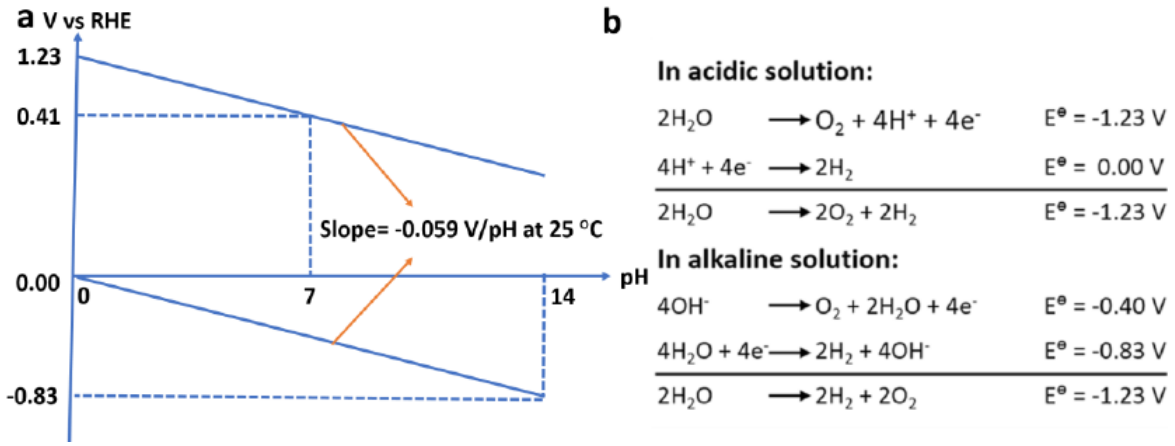

Figure 7: Schematic illustration of pH dependent cell potential for water splitting (a) pH vs potential graph with a slope of 0.059 V (b) water splitting reaction in acidic and basic medium and their corresponding cell potentials.

1.8 Figure of Merits and Water Splitting Catalysis:

A suitable cell with standard electrode set up (reference electrode, counter electrode, and working electrode), conducting electrolyte, and potential controller can be used to electrochemically split water. The potential is adjusted across the working electrode in a three-electrode system, either for reduction or oxidation, and the potential range is determined by the thermodynamics of the reaction. For the redox reaction, two electrodes, the cathode and anode, are used in the total water splitting process. In a half-cell reaction, however, only the working electrode is decorated with desirable catalytic materials and their catalytic potential is tested through various studies. Overpotential, Tafel slope, stability test, turnover frequency (TOF), Faradaic efficiency, Butler-Volmer Equation, and electrochemical active surface area are among the parameters examined in depth.

1.8.1 Butler-Volmer Equation:

An electrochemical reaction involves the exchange of electrons between an electrode that conducts electricity and an electrolyte that conducts ions. A reaction-dependent activation barrier regulates the pace of electron flow through this boundary phase. The rate of the electrochemical reaction is additionally determined by the reaction mechanism. The applied

voltage can affect the kinetics of electrochemical reactions because the activation barrier (electron energy at the Fermi level) is dependent on the cell's potential. The well-known Butler-Volmer equation relates current to the activation overpotential and the rate of electrochemical processes. [79][80]

$$\mathbf{j = j_o \left\{ e^{\left(\frac{-\alpha\eta F}{RT}\right)} - e^{\left(\frac{(1-\alpha)\eta F}{RT}\right)} \right\}}$$

where η is the activation overpotential, j_0 is the exchange current density and α is the transfer coefficient. The activation overpotential of an electrochemical reaction is the difference between the applied potential (E) and the equilibrium cell potential (E_0).

The exchange of electrons is a component of an electrochemical reaction. This has to do with the discrepancy between the metal's Fermi energy and the electron's free energy in the redox system (electrolyte). These two levels of energy are equal when the metal and the electrolyte surrounding it are in equilibrium, and the resulting current density is referred to as exchange current density. The potential of the metal electrodes changes in relation to the electrolytes when a potential difference is introduced to the cell. The interaction between the excess charge on the metal and the ions on the electrolyte mainly determines the size of the activation overpotential and later the rate of the electrochemical reaction.[79][80]

For tiny (5 mV) overpotentials, the Butler-Volmer equation can be fitted to a linear relation, and there are two limiting examples that can be discovered.

$$\mathbf{j = j_o \left(\frac{-\alpha\eta F}{RT}\right)}$$

while for high overpotentials (> 200 mV) the Butler-Volmer equation is well described by the Tafel equation:

$$\mathbf{\eta = k\{ln(j_o) - ln(j)\}}$$

Where $\mathbf{k = \left(-\frac{RT}{\alpha F}\right)}$ and is defined as the Tafel slope.

The field of electrocatalysis investigates the activation barrier and ways to speed up electrochemical reactions. The electron structure of a metal's atoms, which in turn controls the adsorption behaviour of the species on its surface, closely correlates with the metal's electrocatalytic activity. A high value of exchange current density is a characteristic of a good

electrocatalyst. The so-called "volcano plot" connects the exchange current density to the bond energy between the metal and the adsorbed species (such as hydrogen). [79][80] **Figure 8**

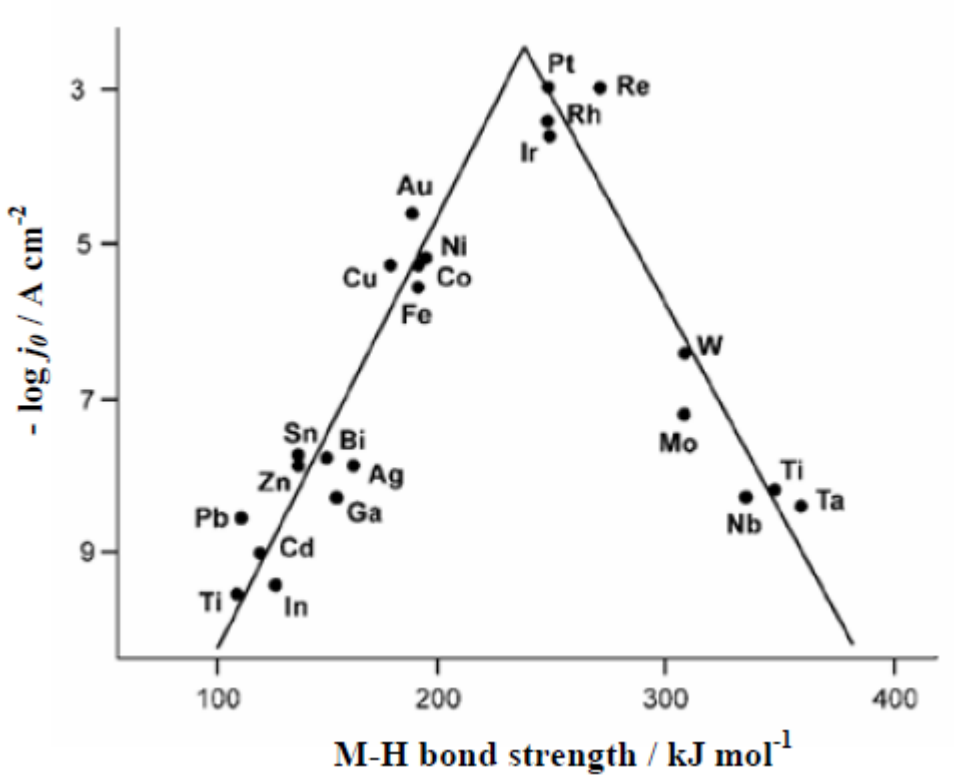

Figure 8: Volcano plot for the hydrogen evolution reaction (HER) (Adapted from [81])

Pt-group metals can obtain the highest exchange current densities (j_0), while transition metals including Cu, Au, Ag, Fe, Ni, and Cu have intermediate values. The electrochemical reaction rate is determined by the choice of the appropriate electrode material.

To further elaborate, we consider a Chlor-alkali membrane cell with a cathode equation of:

$2\,H\,O + 2\,e^- \rightarrow H_2 + 2\,OH^-$

And at the anode:

$2\,Cl^- \rightarrow Cl + 2e^-$

The occurrence of a side reaction that produces oxygen at the anode is one of the most significant issues with chlorine generation. where Equation 1.11 that shows a typical reversible potential for the electrochemical oxidation of water is lower than that for chlorine standard potential, making it thermodynamically advantageous:

$$2\,Cl^- \rightarrow \quad Cl_2 + 2\,e^- \qquad (E^0 = -1.36\ V) \qquad 1.10$$

$$2\,H_2O \rightarrow 4\,H^+ + O_2 + 2\,e^- \qquad (E^0 = -1.23\ V) \qquad 1.11$$

Low exchange current densities are achieved for noble metals due to the kinetics and reaction mechanism of the oxygen evolution reaction, whereas the exchange current densities for the chlorine evolution process are often higher. In this approach, at moderate and high current densities, the chlorine evolution process predominates. [79][80][82] High chloride concentrations should be retained at the anode surface, and the pH should be kept in the ideal range of 2 to 5, in order to reduce the formation of oxygen. In order to ensure that chloride ions are evenly distributed throughout the surface of the electrode, saturated brine solutions are often delivered to the anode compartment. Strong electrical conductivity, electrochemical stability against oxidation and chemical attack by NaCl, HCl, Cl2, HOCl, ClO3 - and O2, and high electrocatalytic activity for the chlorine reaction are the primary requirements for the anode material (high exchange current density). The cathode material must demonstrate strong electrocatalytic activity for hydrogen evolution, good stability under open circuit conditions, and excellent corrosion resistance in concentrated alkaline solutions. [79][80][82]

1.8.2 Overpotential (η):

Overpotential is one of the most important criteria to consider when evaluating the efficiency and inherent capability of an electrocatalyst for a difficult catalysis reaction. Each electrochemical reaction has an equilibrium potential (EP), with overpotential being the additional potential required to drive an electrochemical process spontaneously from its (EP). 1.23 V versus RHE is the (EP) for water splitting, which is the minimum necessary potential to divide one mole of water under typical conditions.[83]

To start an electrochemical reaction, the applied voltage should be equal to the EP. In practice, however, kinetic barriers and different ohmic losses destroy the ideal environment around the electrodes, increasing the requirement for input potential, which is referred to as overpotential.[84]

Overpotential can have a variety of causes, including activation overpotential, concentration overpotential, and resistance overpotential, among others. The activation overpotential of a catalyst is a natural feature that can be minimized by using active catalytic materials. Under certain operational conditions, concentration overpotential arises during the electrolysis process. The overpotential is caused by a decline in concentration at the electrode after the electrolysis process begins, most likely due to limited diffusion and non-homogeneous ion distribution.

However, stirring the reaction media can help control it to some extent. Similarly, resistance at the system's interfaces contributes to the overpotential, also known as junction resistance. By measuring the iR adjusted data, it can be abolished. Furthermore, the creation of bubbles on the surface of electrodes, as well as their inappropriate detachment, may contribute to the overpotential.

The final operating potential is represented by Equation 4.9, which varies depending on the materials/reaction. Low overpotential indicates that the electrocatalyst and reaction circumstances are adequate for initiating electrolysis near the equilibrium potential. Furthermore, the amount of current density obtained beyond the onset potential is an essential characteristic to consider when evaluating the consistent performance of electrode materials throughout a restricted potential range. In general, the literature compares electrocatalysts using an overpotential required to reach a current density of 10 mAcm-2. This comparison is only valid if all of the catalysts are subjected to the same environment, including the pH of the electrolyte and the temperature around the electrodes. [11]

1.8.3 Tafel slope:

The essential restrictions in any electrochemical process are voltage and current. Changing the potential window, according to Nocera et al., basically corresponds to tuning the driving force of the electrode-electrolyte system.[85] Tafel slope analysis is the most extensively used parameter to explore the kinetics and mechanistic aspects of electrochemical processes in this regard. The relationship between current and applied potential in multi-step reactions like OER/HER is given by the following equation (Equation 1.12):

$$\mathbf{i = io}\, e^{\left(\frac{\alpha F \eta}{RT}\right)} \qquad 1.12$$

where αa: equilibrium/transfer coefficient, η: overpotential, io: exchange current density, which shows the rate of reaction at an equilibrium potential. In logarithmic form, we can write this equation as:

$$\mathbf{\ln i = \ln io + \frac{\alpha F \eta}{RT}} \qquad 1.13$$

By taking natural log:

$$\mathbf{2.303 \log i = 2.303 \log io + 2.303 \frac{\alpha F \eta}{RT}} \qquad 1.14$$

Dividing by 2.303

$$\mathbf{\log i = \log io + 2.303 \frac{\alpha F \eta}{RT}} \qquad 1.15$$

The above equation can be rearranged as below:

$$\mathbf{\eta = a + b \log io} \qquad 1.16$$

This expression is known as Tafel equation, where ‘a’ is constant and ‘b’ is Tafel slope (2.303αF/RT). It can also be written as below:

$$\mathbf{b} = \frac{\delta\eta}{\delta\log(\mathbf{i})} = 2.303\ \frac{\mathbf{RT}}{\alpha\mathbf{aF}} \qquad 1.17$$

Tafel slope is the rate of change of current with respect to overpotential during an electrochemical reaction, as calculated by (equation 1.17). If we take a current density (j) from the steady-state polarization curve and plot log j against the overpotential. The Tafel slope value is the well-balanced representative of an electrode process, and it is obtained by fitting log j versus linearly. It gives details on the reaction mechanism, rate-determining step, and overall kinetics of the electrochemical process. Smaller Tafel slope values, in general, indicate a kinetically quick electrode process (fast charge transfer), and vice versa. Because Tafel slope might change by picking higher and lower potential regions for the same rate-determining step[86], it is more beneficial to compute it in the onset potential region. The intricacies of the relationship between the Tafel slope and a potential mechanism/rate-determining step for both HER and OER are described below:

The absorbed hydrogen (H) as an intermediate on the electrode surface takes part in the reaction pathways in the typical HER process, which is a two-electron transfer process in a single Volmer-Heyrovsky or Volmer-Tafel mechanism. The pH level of the electrolytes is crucial to the HER process. The HER operates in acid solution in accordance with the following steps:

(i) Proton discharging to form an adsorbed hydrogen atom:

$$\mathbf{H} + \mathbf{e}^- \rightarrow \mathbf{H}* \text{ (Volmer reaction)}$$

Depending on the surface of the electrodes, the following two alternate procedures can then be used to create molecular H2.

(ii) The quick coupling of two adsorbed hydrogen atoms to generate a hydrogen molecule:

$$\mathbf{H}* + \mathbf{H}* \rightarrow \mathbf{H_2} \text{ (Tafel reaction)}$$

(iii) Combination of one adsorbed hydrogen atom with a proton to generate a hydrogen molecule:

$$\mathbf{H}* + \mathbf{H}+ \rightarrow \mathbf{H_2} \text{ (Heyrovsky reaction)}$$

Due to the low concentration of H+ in an alkaline environment, molecular H2O participates in the Volmer and Heyrovsky reactions:

$$\mathbf{H_2O} + \mathbf{e}^- \rightarrow \mathbf{H}* + \mathbf{OH}^- \text{ (Volmer reaction)}$$

$$\mathbf{H}* + \mathbf{H_2O} \rightarrow \mathbf{H_2} + \mathbf{OH}^- \text{ (Heyrovsky reaction)}$$

The HER catalyst's free energy of hydrogen adsorption (abbreviated as ΔGH) is an important characteristic. [87], [88]A too-negative value may slow down the execution of future Tafel or Heyrovsky stages. The negative value of ΔGH signifies a beneficial combination of H with the

electrode's surface and the Volmer step. The overall process is inefficient when ΔGH is positive because weaker interactions between protons and the electrode surface result.

It is a more complex reaction on the anode of the OER process, with four electron transfers and more surface-adsorbed intermediates. It is also a pH-dependent process (in an alkaline or acidic environment), with the alkaline OER receiving the majority of research attention in the following pathways[89]:

$$OH^- + * \rightarrow OH_{ads} + e^-$$

$$OH_{ads} + OH^- \rightarrow O_{ads} + H_2O + e^-$$

The ''*" means active site of the catalyst and ''ads" means the adsorption on the catalyst. There are different routes that can lead to the formation of molecular O2:

(i) The combination of two Oads intermediates to form O2:

$$O_{ads} + O_{ads} \rightarrow O_2$$

ii) O_{ads} coupling with OH− to form OOH_{ads} and subsequent combination with OH^- to form O_2:

$$O_{ads} + OH^- \rightarrow OOH_{ads} + e^-$$

$$OOH_{ads} + OH^- \rightarrow O_2 + H_2O + e^-$$

However, it's worth noting that the kinetics of the OER process can be hampered by solution resistance (Rs) and charge transfer resistance (Rct). Specifically, when the Rs value exceeds 6 Ω and the catalyst has a high current density (Jmax greater than 100 mAcm-2). [90] Electrochemical impedance spectroscopy (EIS) can thus be used to determine the real kinetics of a catalytic reaction. In addition to the overpotential noticed on the cyclic voltammogram, at least 100 mV of extra overpotential must be collected for this reason. As a result, the 1/Rct delivers accurate equilibrium (exchange) current density at various high overpotentials to show the kinetics of the whole electrode process over a wide potential range, minimizing the experimental mistakes generally associated with the Tafel slope estimated from CV.[90]

1.8.4 Electrochemical active surface area ECSA:

In order to determine the electrochemical active surface area, the electrochemical double-layer capacitance (C_{dl}) is measured. By measuring the capacitance of the double layer at the solid-liquid interface using CV, the C_{dl} may be effectively assessed. Without using the faradaic processes, CV is carried out inside a specific possible frame.[91] First, a range of sweep speeds (10–200 mV s-1) are used to the CV tests, and typically 5–10 successive points are chosen. The obtained CV curves may diverge from the rectangle as scanning speed increases. It is necessary to select an appropriate scanning speed in order to guarantee the linear connection of the final data. Next, a scan rate vs. the variations in current density (ΔJ=Ja−Jc) at overpotential (the midpoint of the applied potential range) is to be shown.

When the slope is twice the Cdl, linear regression can be used to fit the shown lines and estimate C_{dl}. The large C_{dl} exhibits significantly higher current density and more exposed surface reactive sites. Hence C_{dl} is given by the following equation: $\mathbf{i_c = v\, C_{dl}}$, where (*j*) is the non-faradic current density and (ν) is the scan rate and thus a plot of i_c as a function of v yields a straight line with a slope equal to C_{dl}.

1.8.5 stability:

One of the most critical factors for OER catalysts is long-term stability. In general, there are two different types of evaluation techniques: the CV and the chronoamperometry (current-time curve) or Chronopotentiometry test (potential-time curve). Potential cycles for CV tests often match those in the LSV range. By contrasting the Polarization curves before and after the continuous CV cycles, the stability is assessed (normally 500-10000 cycles). It indicates strong durability if the Polarization curves almost perfectly overlap with the initial one or if the overpotential only slightly rises by less than 10% from the original values. When a potential or current density is applied, a chronoamperometry or chronopotentiometry test is performed. Chronopotentiometry testing is more common among researchers and often involves current densities of 10 mA cm-2; however, more recent industrial applications have used criteria for evaluating stability based on current densities of 50, 100, 500, 800, and 1000 mA cm-2. Typically, a standard for comparison is 10 hours or even longer.[92], [93] In addition, the observed i-t curves will display in a typical serrate shape together with the O2 bubbles from accumulation to release. Although the negative effects of O2 bubbles can be partially mitigated by stirring, the generated O2 bubbles not only cover the catalytic sites for oxygen production but also have the potential to cause the electrode materials to detach from the electrode surface during the process of bubble release. More intriguingly, during the OER process from oxygen creation to release, the anode material is inexorably oxidized and slightly stretched. [92], [94]

1.9 Electrode and electrolyte:

Due to their various structural characteristics, conductivities, levels of wettability, and accessibility of the catalyst to an electrolyte, the working electrodes and substrates are crucial in determining performance and have a significant impact on the reaction rate. The two types of electrode supports are flat surface electrode and 3D electrode, depending on the structure and level of electrolyte movement.[95]

The 3D substrates, such as carbon cloth/paper (CC and CP) and Ni foam, allow multiple pathways for electrolyte penetration from all sides of the catalyst and involve all the material in the catalytic reaction. In contrast, the flat surface electrodes, such as glassy carbon (GC), Cu/Ti foil, and indium doped tin oxide (ITO) substrate, only allow single-way electrolyte penetration that limits the catalysis to the catalyst's surface.[96]

Each of these electrode substrates has its own benefits and drawbacks. For instance, the GC electrode is simple to use and frequently used in literature but only allows for a small loading of catalyst (1 mg cm-2)[97]. Additionally, the GC electrode needs a binder to stabilize the catalysts, which has a negative impact on wettability and causes unavoidable powder

agglomeration. Additionally, these binders raise resistance, inhibit active sites, and stop ion diffusion.[98]

As a result, many research teams work to grow catalyst directly on conductive substrates like Ni foam, CC, and CP in an effort to do away with nonconductive binders. This also creates a strong electrical connection between the catalyst and current collector. Importantly, 3D textures from graphene or Ni foam results in higher gas diffusivity, easier electrolyte penetration, and improved catalysis. However, the surface of the substrate can be modified for better connection to prevent the catalyst from peeling off as a result of mismatched growth and inadequate stability when it is directly fabricated on a supporting substrate. Furthermore, it can be challenging to manage the bulk loading of active elements during direct growth, which could make it impossible to compare performance. The performance of the electrode material is greatly influenced by various electrolytes, such as acid or alkaline. While OER electrocatalysis in neutral electrolytes is challenging and performs at very low levels in acidic solutions, it is more advantageous in alkaline solutions. The majority of current research focuses on developing OER electrocatalysts that are stable in alkaline environments, such as carbon-based materials, transition metal oxides or oxyhydroxides, hybrids, and complicated ternary systems (spinel and perovskites).[99]

1.10 Alkaline medium OER catalyst synthetic methods:

Due to the basic and economic significance of the electrolysis of water, the oxygen evolution reaction (OER) has historically been one of the most significant processes in the field of electrochemistry. Since they have the lowest overpotential for the OER at useful current densities, various noble metals and their oxides, such as Ru, Ir, RuO2, and IrO2, are currently acknowledged to be the finest OER electrocatalysts in aqueous acidic and alkaline solutions.[100] However, due to their scarcity and expensive price, their vast commercial uses are severely constrained. As a result, some scientists work to create ternary metal oxides based on Ru or Ir that perform as well as noble metals in terms of lowering OER overpotential while using less of the noble metals. Commercial electrolyzers, on the other hand, work in highly conductive media, which can be either acidic or alkaline. Sadly, RuOx, IrOx, and their composites only show significant stability in acidic solutions; they are unstable in alkaline media as a result of the formation of an unstable film.[101][102] As a result, the search for low-cost electrocatalysts that can effectively conduct OER with a minimal overpotential is ongoing. As a result, great effort has gone into designing, synthesizing, and characterizing alternative OER electrocatalysts based on first-row transition metal compounds (TMC) that are inexpensive, extremely active, and long-lastingly stable under oxidizing conditions, making the overall water splitting more practically feasible. [103], [104]

In actuality, we shouldn't just concentrate on creating the most effective catalysts. Additionally, because these exceptional catalysts are almost entirely synthesized with unsupported structure, such as nanoparticles, developing catalyst assembly and subsequent activation processes, as well as examining the evolution of the structure and OER performance for the integrated electrode in commercial Alkaline electrolysis cell (AEC) during long-term service, are crucial to determining whether the newly developed catalytic materials have the potential to replace the existing commercial electrodes. In genuine industrial service, they must come together with their supports to form an integrated electrode. Once built as integrated electrodes for use in commercial AEC, it is difficult to

fully use the inherent performance of the original catalysts without frequently experiencing activity and stability loss. In the meantime, because OER occurs on surfaces (or more precisely, within ultrathin films), a well-thought-out electrode architecture can significantly boost activity in electrochemical performance. Therefore, the design of 3D electrodes/supports with easy charge/electrolyte/bubble migration and increased catalyst loading contributions to the catalytic activity are extensively researched in order to produce effective means of further increasing electrocatalytic reactions at the three phase border.[105][106]

The majority of in situ Electrochemical activation (ECA) strategies have been used as an effective activation method for the integrated electrodes to improve OER performance[107]. Upon ECA treatment which includes the subjection of the entire volume of liquid held within the cell to the action of the electric field rather than just the intimate vicinity of the anode and the cathode, the electrode surfaces are changed from bulk phase, which can adjust local electrical structures, produce more active species, increase surface area, and improve OER performances.[108][109] The electrocatalysis methods for splitting water can be coupled with the atomic, electrical structures using this method. In situ electrochemical activation offers greater benefits over conventional chemical treatment, including ease of use, a comfortable environment, flexible control, high efficiency, and flexibility.[110]

1.10.1 Catalysts for OER:

1.10.1.1 Noble metals and their oxides as OER catalysts:

The most researched catalysts are noble metals and their oxides because of their outstanding OER performance. It has been demonstrated through experimentation that materials made of iridium (Ir) and ruthenium (Ru) are more active toward OER than those made of platinum (Pt) and palladium (Pd) (Pt Pd Ir Ru).[97] Thus, Ir and Ru-based catalysts are the main subject of research. Ir and Ru are still regarded as the most advanced OER electrocatalysts due to their exceptional stability, low overpotential, and Tafel slope.[111] While the ordered uniform structure of the metallic lattice is considerably changed by the arrangement of two or more atoms of various sizes, alloying noble metals together can produce a synergetic effect. This strategy has demonstrated prospective outcomes for enhancing the noble metals' electrocatalytic activity for a variety of electrochemical processes, including OER.[112]

Due to their excellent electrocatalytic activity toward OER in alkaline solution, iridium oxide (IrO_2) and ruthenium oxide (RuO_2) catalysts are frequently regarded as benchmark electrocatalysts for oxide reduction reactions (OER).[113] As previously mentioned, RuO_2 is unstable at high anodic potential and will degrade (dissolve) during OER. In contrast, IrO_2 is a more stable catalyst than RuO_2, however it is less effective for OER. By using the co-precipitation approach in an ethanol medium, Ru-Ir based oxides with a large surface area have been created in order to further enhance the activity and stability of RuO_2 and IrO_2.[114] It was discovered that $Ru_{0.9}Ir_{0.1}O_2$ exhibits activity similar to that of RuO_2, critically with a notable improvement in stability.[99]

1.10.1.2 First-row transition metal compounds as OER catalysts:

Noble metals and their oxides are well-known OER electrocatalysts with high activity, but they are expensive and scarce, as was previously indicated. Therefore, a lot of work has gone

into creating OER catalysts that are affordable and made from elements that are abundant on Earth. The most extensively researched noble metal free OER catalysts are those used in first row TMC, specifically Co, Fe, and Ni-based catalysts. The OER performance of the metal oxides, (oxy) hydroxides, phosphates, phosphides, sulfides, selenides, and nitrides are some of the compounds that is considered to be among the best. It is noteworthy that current research indicates that the surface oxides and (oxy) hydroxides species produced during the electrochemical oxidation process are probably the key active sites of the metal phosphides, sulfides, and selenides for OER. In light of this, OER electrocatalysis has focused on the synthetic and structural tailoring of metal oxides, (oxy) hydroxides, toward increased activity and stability.[115]–[123]

1.10.1.3 Fe-Based transition metal compounds as OER catalysts:

In comparison to precious metals and even other transition metals, iron offers a number of advantages. First off, iron is significantly more affordable than other metals frequently utilized to create water-splitting electrocatalysts because it is the second most common metal in the Earth's crust. Second, iron is a fundamental component of many biological processes and is comparatively less hazardous than other metals. Thirdly, it is recognized that iron-based catalysts efficiently mediate some significant biological processes in nature. Additionally, iron has various valence states and has emerged as a prominent OER material. Fe-based OER electrocatalysts have not received as much research attention as other transition metals like Co and Ni, particularly for pure Fe (oxy)hydroxides. Fe is often particularly well known to be introduced into Ni-/Co-based OER catalysts as a dopant or impurity, significantly enhancing their OER performances. It's interesting to note that some recent research suggested Fe is the active site and that Ni or Co (oxy)hydroxide largely serves as an electrically conducting, chemically stable, and high-surface area host. [124]–[127]

1.10.1.4 Ni-Based transition metal compounds as OER catalysts:

Due to its earth-abundant nature and theoretically high catalytic activity, Ni-based OER catalysts are currently generating more and more interest in the academic community. These catalysts typically consist of Ni-based hydroxides and oxides, as well as Ni-based hydroxides. Due to its comparatively high stability and advantageous activity, nickel is often utilized in industrial electrocatalytic electrolysis units in strongly alkaline electrolytes as the promising electrode material. The most popular conductive substrate for the creation of three-dimensional (3D) catalysts is nickel foam (NF), which has a long-range organized porous structure that not only exposes more reaction active sites but also speeds up quick ion and electron movement.[128]–[130]

1.10.1.5 In situ electrochemical activation based OER catalysts:

The in situ ECA approach, which is a novel electrochemical tuning access to improve catalytic performances in a simple, mild, environmentally friendly, and controllable manner, has been used most frequently for OER in alkaline conditions. Cui's group was the first to investigate the possibility of creating transition metal oxides (TMOs) from sulfides, such as Co, Ni, and Fe (TMS). After being transferred to TMS, the electrodeposited TMOs on the carbon fiber cloth were then returned to the TMOs in situ (referred as ECT-TMOs). In contrast to conventional electrodeposited TMO nanosheets, ECT-TMOs developed pores and were made up of tiny grains with a lower degree of crystallinity.[131]

Increased current densities, lower onset potentials, and greater ECSA are proof that such small grains produced more flaws and surface catalytic sites for OER. Additionally, under the same electrochemical settings, the improved OER activities of binary, ternary, or quaternary ECT-TMOs may also be seen. The increased oxidation state of metals under anodic potentials, which can facilitate the multi-electron transfer in water oxidation, is one explanation for the enhanced OER capabilities. High OER performance is further aided by the low-crystalline, porous nanostructures that contain a large number of flaws and surface sites. Researchers have progressively found that produced lattice distortion upon in situ ECA might effectively promote water splitting by increasing intrinsic activity.[132]–[134]

A new pre-treatment method for electrocatalysts is made possible by this tuning strategy, which is considerably different from the conventional chemical treatment that is always carried out in harsh, contaminated environments. Peer workers were significantly inspired by these efforts to examine more transition metal compounds that were readily available under electrochemical activation and to get a deeper understanding of the activation mechanism.

Shifa et al. showed that doping of Ni_5P_4 with Sn would results in a greater catalytic activity on OER in alkaline media, proving that in-situ generated metal oxides would increase the activity of the electrode In addition to the metal phosphide, with an achieved overpotential of 173 mV vs RHE and a Tafel slope of approximately 46 mV dec^{-1}.[135]

1.10.1.6 Co-based transition metal compounds as OER catalysts:

Co-based TMC have become a suitable candidate for studying OER in an alkaline media due to their affordability, thermal stability, abundance of reserves, and environmental friendliness. As a result, efforts have been made to aggressively investigate the synthesis, fine structural optimization, and knowledge of the structure-property connections in the OER of cobalt-based catalysts. These cobalt-based TMC OER catalysts can generally be divided into phosphides, oxides/(oxy) hydroxides, and sulfides.[136]–[138]

Recently, there has been a lot of interest in co-based catalysts for HER, OER, and general water splitting, and a timely assessment will offer helpful direction for future study. Here, current developments in Co-based water splitting catalysts are discussed **Figure 7**. The first phase is an introduction to co-based catalysts for water splitting, followed by a discussion of the catalytic processes of co-based catalysts in water splitting, including the production of intermediates in HER/OER and rate-limiting steps. Finally, the difficulties facing the development of Co-based catalysts are examined, along with their perspectives and the roles played by the active sites and intrinsic activity of Co-based catalysts.

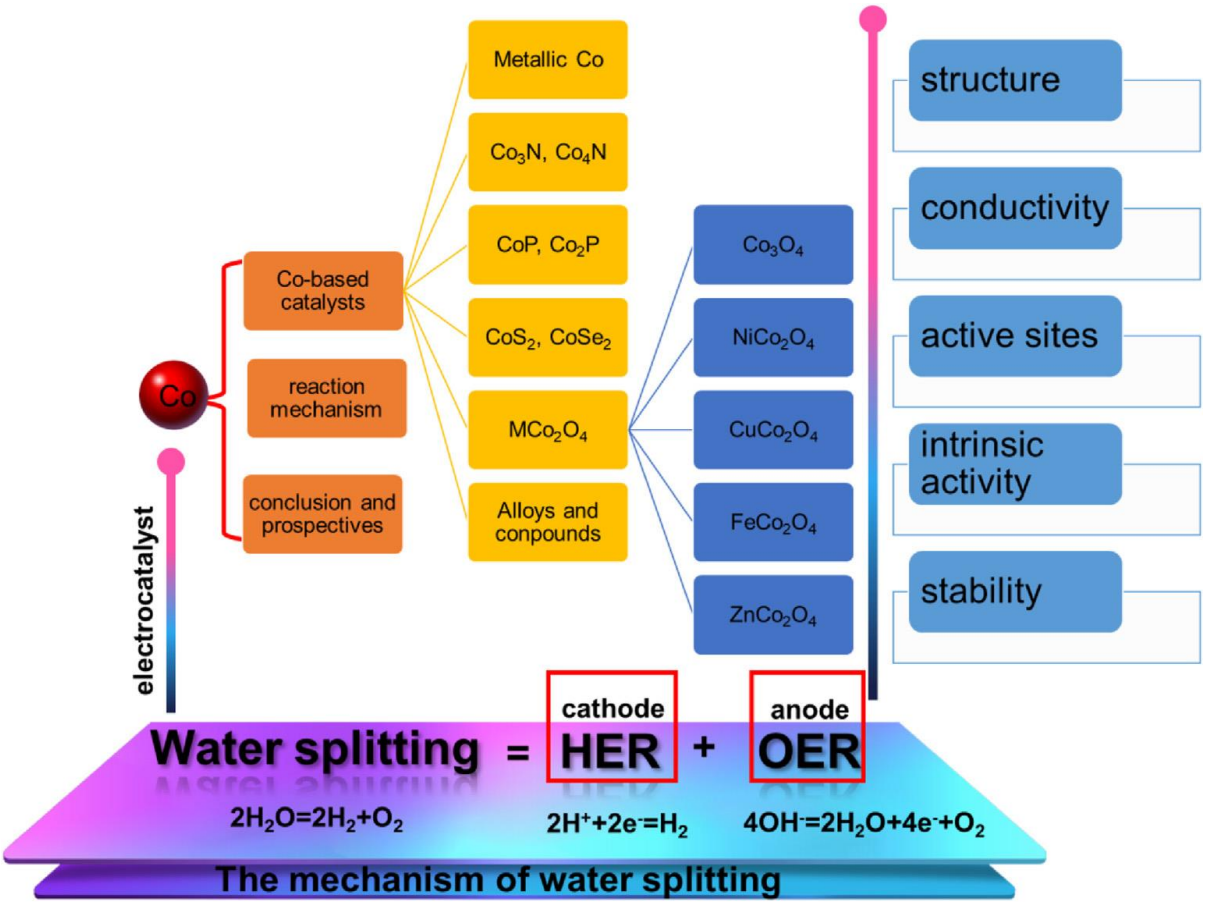

Figure 7: Outline of Co-based catalysts. Schematic summarizing the application of Co-based electrocatalysts to water splitting showing the structure, conductivity, active sites, intrinsic activity, and stability of the different types of Co-based catalysts. [139]

1.10.1.6.1 Metallic cobalt:

Due to its excellent HER/OER properties and high conductivity, metallic cobalt (Co) has gained interest. However, owing of the thick passivating oxide coating on the Co surface, the pure Co catalyst needs a significant overpotential to create H2/O2. A conductive substrate can be coupled with in order to improve the HER/OER characteristics. Co-embedded N-rich CNTs were created by Zhou et al. using two thermal processes, including the production of CoCl2$6H2O on graphitic carbon nitride (C3N4) and pyrolysis at 700 C. Co NPs@N-CNT exhibits strong HER activity at all pH levels.[140][141]

Co-based catalysts have made some progress, although it is challenging to regulate the size of the Co nanoparticles. The electrocatalytic capabilities can be improved by shrinking the particle size to the nanoscale or even atomic scale due to more exposed active sites and effective material usage. Overcoming aggregation during fabrication and electrochemical reactions is the main challenge for stability on the nanoscale or atomic scale. The loading of metal species on supporting materials, the encapsulation of metal clusters on cavities, and the electrical interaction of the metals with the substrates have all been investigated as spatially constrained approaches.[142][143]

By adsorbing Co2 on melamine-formaldehyde resin and then annealing it at 800C, Pereira et al., for instance, were able to create Co nanoparticles on N-doped graphitic carbon. Co nanoparticle aggregation cannot be prevented without the spatially constrained approach, and the resulting Co product has a huge diameter of 40 nm. Another method to evenly distribute Co nanoparticles in N-doped graphene layers has been put forth by Guo et al. The Co nanoparticles had restricted graphene layers and a mean diameter of 11.1 nm. At a current density of 10 mA/cm2, the materials exhibit a modest overpotential of 350 mV in OER and 220 mV in HER. [144][145]

A further reduction in size, from the nanoscale to the atomic scale, can increase atom usage and even reach 100%. The site isolation effect causes the surface selectivity to rise when a single atom is isolated separately. Recently, the procedure of creating single atom electrocatalysts has been investigated using zeolitic imidazolate frameworks (ZIF), a subclass of metaleorganic frameworks (MOF) with a high concentration of nitrogen in the organic ligands.[146]–[148]

The Co phase also affects the characteristics, as Yan et al. have shown, in addition to the impacts of nanoparticle size. The core-shell structure of Co@NC has been constructed, and it has been suggested that hcp Co@NC has a larger electron injection from the Co core to the NC shell than face centered cubic (fcc) Co@NC. This can enrich the NC surface charge for the reaction of water or OH and intermediates.[149]

1.10.1.6.2 Co3N and Co4N:

Materials based on cobalt nitride have garnered a lot of interest due to their metallic conductivity, dispersed d-band electrical structure, and great corrosion resistance. In general, cobalt nitride-based catalysts outperform oxides or metals in terms of catalytic performance. Kand et al. created 3D mesoporous Co3N@amorphous N-doped carbon nanotubes (Co3N@ANeC NCs) with a carefully managed open-framework structure. More active sites, more ion transport space, and high conductivity are all provided by the Co3N@ANeC NCs, which have porous structures wrapped in conductive N-doped carbon layers. Due to its increased conductivity and intrinsic activity, Co3N@AN-C NCs exhibit a lower overpotential than Co3O4 (which has a significant overpotential of 335 mV at 10 mA/cm2 and Tafel slope of 97.1 mV/dec for OER).[150][151]

Pure cobalt nitrides exhibit good HER/OER properties, but they still need to improve their catalytic activity if they want to compete with noble metal electrocatalysts. It is possible to adjust the dband center of cobalt (Co) in cobalt nitride (Co4N) to promote hydrogen desorption for enhanced HER/OER activity by doping Co4N with transition metals (nickel [Ni], vanadium [V], molybdenum [Mo], tungsten [W], etc.). Ni is added to CoN to create NiCoN, which has exceptional HER properties such low overpotentials of 48 and 149 mV at 10 and 100 mA/cm2, respectively.[152][153]

Because of potential synergistic effects, creating heterostructures with additional substances is another method to increase the HER/OER activity in addition to elemental doping. Because there are more borders between the two new phases for the transition of H2O/OH species, Zhao et al. have demonstrated that phase conversion of Co4N to CoSx results in the creation of additional active sites. In order to create well-defined nitride-based heterostructures of

Co3O4eCo4Non carbon cloth, Liu et al. developed an in-situ plasma nitridation method. They also demonstrated that electron transfer from Co3O4 to Co4N has synergistic effects. As a result, the hybrid Co3O4eCo4N possesses good HER characteristics, including a Tafel slope of 57.8 mV/dec and an overpotential of 90 mV at a current density of 10 mA/cm2.[152][154]

1.10.1.6.3 CoP, Co2P:

Composites made of cobalt phosphide have generated interest because of their inherent electrical structure, affordable price, desirable catalytic activity, and chemical stability. Cobalt phosphide-based catalysts have undergone substantial improvement since Popczun et al. initially reported multiface cobalt phosphide (CoP) nanoparticles with good hydrogen evolution reaction (HER) activity and stability in acid conditions in 2004. Cobalt phosphide has potential HER/OER properties; however, it still has to develop in terms of its electrocatalytic capabilities. The appropriate surface shape and nanostructure are crucial for the active areas. Because they have more exposed active sites, a bigger specific surface area, and shorter mass/charge transport channels than their solid counterparts, hollow spheres, nanotubes, nanocages, nanoboxes, and nanosheets are currently receiving more research interest.[155]–[157]

Other workable methods to alter the electron density close to the metal atom centers' Fermi levels and lower the energy of the hydrogen bonding include heteroatom doping and alloying. In general, metal doping provides certain benefits in terms of chemical stability and tunable electron structure. For instance, the electrical conductivity of the 3D flower-like bimetallic phosphide (NiCoP) with ruthenium (Ru) doping results in HER and OER activity of 44 mA at 10 mA/cm2 and 216 mV at 20 mA/cm2, respectively. When Co2P is doped with chromium (Cr), this results in a highly polarized electron distribution and potent electron interactions that can lower the Co d-band center and lower the energy of the H bond. Additionally, high-valence Cr can behave as active sites for the adsorption of water. [158]–[160]

Despite recent improvements in electrocatalyst activity, the water electrolysis cell still has low practical current densities and limited hydrogen generation. A high current density can be produced through relationship design with the right structure. Bifunctional porous CoP foam on Ni foam has been created by Li et al. with an overpotential of 290 mV in HER and 380 mV in OER at a high current density of 1000 mA/cm2, stabilizing at this value for 4000 h.[161]

1.10.1.6.4 CoS2 and CoSe2:

Unsaturated transition metal sites, natural abundance, excellent electrical conductivity, and favourable OH adsorption are all characteristics of cobalt disulfide (CoS2) and cobalt selenide (CoSe2). However, because to the limited exposed active sites and self-aggregation during operation, CoS2 and CoSe2 as catalysts in HER and OER often result in poor activity. Morphological engineering can be used to increase the exposed active sites on CoS2 and CoSe2 to increase the number of active sites. To boost the HER and OER activities, Lan et al. created the hollow shape to enhance the active sites on urchin-like CoSe2. In HER and OER, Yao et al. large surface area, 3D dandelion-flower-like CoS2 produced low overpotentials of 28 mV at 10 mA/cm2 and 200 mV at 20 mA/cm2, respectively. Another technique to reduce

aggregation and improve charge transfer is to combine CoS2 and CoSe2 with conductive materials like graphene, CNTs, and carbon black. CoS2 nanoparticle embedded graphene (CoS2/G) was created by Tong et al. Electrostatically, Co2 binds to graphene oxide, and when this mixture is combined with sulfuric acid and thiourea, it forms cobalt disulfide nanoparticle embedded graphene (CoS2/G), which is then heated to 500°C for annealing. NeCoS2/G has improved catalytic activity with low overpotentials of 109 mV in HER and 260 mV in OER at a current density of 10 mA/cm2 due to more exposed active sites and better conductivity.[162][163]

The hydrogen adsorption energy or intermediate adsorption energy can be reduced by elemental doping or the creation of a hybrid structure to further improve the kinetics in electrocatalytic reactions and increase the intrinsic activity of CoS2 and CoSe. For instance, adding Fe atoms to CoSe2 speeds up the production of H2 and enhances the adsorption-desorption of intermediates.[164]

1.10.1.6.5 Co3O4:

Cobalt tetraoxide (Co3O4) normally contains two kinds of Co ions, Co^{2+} in tetrahedral sites and Co^{3+} in octahedral sites (Co^{2+} Co_2^{3+} O4). It makes little difference whether Co3O4 has a conventional or inverse spinel structure; either way, it is a promising catalyst with high stability, cheap cost, and good activity. However, because Co3O4 in bulk has a low conductivity and a limited number of active sites, attempts have been undertaken to build nanostructures or combine them with conductive carbon materials to increase the activity. Co3O4 nanorod arrays, Co3O4 core-shell structures, porous Co3O4 nanowires, Co3O4 nanoflowers, and hollow Co3O4 have all recently been created using various techniques. The HER/OER activity is increased by the combination of conductive materials such graphene, carbon nanotubes (CNTs), carbon black, and metal-organic framework (MOF) structures.[165]–[168]

The size of the Co3O4 grain, the electrical structure, the valence states of the ions, and the number of vacancies are other parameters that affect water splitting performance. A smaller grain size lowers the activation energy in the charge transfer and ion diffusion, according to research by Hao et al. on the impact of grain size on the electrochemical characteristics of Co3O4. Catalyst downsizing to subnanometric clusters or single atoms has been shown to be a successful method for enhancing catalytic characteristics. Through a thermally induced phase segregation procedure and subsequent O2 plasma treatment, Yan et al. have created CoOx clusters with an average size of 1.3 nm uniformly scattered on the rutile titanium dioxide (TiO2) substrate.[169][170]

1.10.1.6.6 Alloys and compounds:

Co-based materials have unique physical, chemical, and electrical features that make them ideal electrocatalysts for overall water splitting, although single catalysts are often constrained by their low activity, conductivity, and stability. By combining the benefits of each component, hybrid architectures and alloying can increase the water splitting activity. Wang et al. designed 3D pomegranate-like NiCoFe nano-assemblies by adjusting the Ni/Co/Fe atomic ratios, and several pomegranate-like assemblies as well as numerous holes have been found. As a result of the addition of Fe to the NiCo matrix, a distinctive pomegranate-like structure with a flexible electrical structure and plenty of oxygen vacancies

can be formed. Excellent OER properties of NiCoFe include a low overpotential of 313 mV at 10 mA/cm2 and a Tafel slope of 51.9 mV/dec.[171]–[173] Hybrid CoeMoeP/Co nanowires have been created by Hoa et al. as bifunctional electrodes, and they need a cell voltage of 1.495 V to accomplish 10 mA/cm2. In OER and HER, respectively, Li et alCoeFeeP .'s nano frame immobilized on N and P co-doped CNTs (CoFeP NFs/NPCNTs) demonstrated low overpotentials of 278 mV and 132 mV at a current density of 10 mA/cm2.[171]–[175]

High-entropy alloys (HEAs) with five or more metal components are desirable not only for their hybrid structure but also for their high entropy and deformed lattice, which allow for the control of surface electrical characteristics and catalytic activity. Although the synthesis of nanoscale HEAs is not simple, compared to bulk HEAs, nanostructured HEAs have a greater surface area and more active sites to increase the catalytic capabilities and materials utilization. Recently, carbothermal shock synthesis, dealloying techniques, and sputtering deposition have all been used to create nanostructured HEAs with tunable compositions. By using carbothermal shock synthesis, Hu et al. have suggested a generic method to enable up to 8 elements in HEA nanoparticles on carbon nanofibers (CNFs). In order to create HEAs with customized size, composition, and phase, the metal salt precursor MClxHy (M 1/4 Fe, Co, Ni, Cu, Pt, Pd, Au, etc.) is combined in a solution, loaded onto CNFs, and heated to 2000 K by flash heating (105 K/s). AlNiCuMoCoFe nanoporous HEAs with a ligament size of 2e3 nm have been created by Qiu et al. AlNiCuMoCoFe with a lower Pt loading level showed better HER activity than the Pt/C catalyst thanks to the mixing effect and porous structure.[176]–[178]

The primary goal of the dealloying procedure is to create porous structures using wet etching. Al96Ni1Co1Ir1X1 (X: Mo, Nb, V, etc.) was utilized by Jin et al. as the precursor to dealloy the alloy chemically in an alkaline solution and remove the Al to create nanoscale pores and alloy ligaments. The AlNiCoIrMo alloy has significant HER and OER activities, and the AlNiCoIrMo electrode-based cell exhibits good catalytic characteristics, outperforming commercial Pt/CeIrO2 catalysts with a 1.505 V at 10 mA/cm2 value. By dealloying in (NH4)2SO4 solution, Liu et al. have created free-standing nanoporous NiMnFeMo alloy belts. In order to achieve more effective HER, the NiMnFeMo surface exhibits a more moderate hydrogen bonding energy, as evidenced by the low overpotentials of 67 mV at 100 mA/cm2 and 290 mV at 1000 mA/cm2. Another method for depositing nanoparticles or thin films on a flat surface is sputtering deposition. Using a Pt50Fe11Co10Ni11Cu10Ag8 HEAs as an example, high purity and fine grain Pt, Fe, Co, Ni, and Ag are combined in accordance with the molar ratio, and then pressed under 2500 psi to create a multi-element alloy target. Ar plasma sputters the metal atoms in the target, depositing them as HEA nanoparticles on the substrate.[179]–[181]

1.11 Role and motive behind catalysts:

When it comes to these previously mentioned factors and tests are inextricably tied to the electrode's material composition. The most effective screening method for discovering novel catalysts is based on theoretical calculations and simulations using density functional theory (DFT). Understanding the process of catalytic water splitting requires DFT calculations, which are crucial in guiding experimental. It can be used to forecast the reactions' thermodynamics, kinetics, and mechanism.[182] It calculates the free energy of intermediate ion adsorption and desorption in particular. It is known that an ideal catalyst binds neither too

forcefully nor too weakly, as according to the Sabatier principle that states that the interaction between a catalyst and a substrate should be just right, as a very strong interaction will cause the product to fail to dissociate and on the other hand a very weak interaction will cause the molecules to fail to bind to the catalyst and no reaction will occur. Catalysis at the nanoscale, on the other hand, has gained unique physical and chemical features with the advancement of nanoscience and technology. In bulk metals, valence electrons form continuous bands. The migration of electrons in a particular direction is confined when the bulk material is reduced to the nanoscale scale in that direction. Nanostructured materials have substantially larger total exposed surface areas and a variety of surface patterns than bulk metals, and electronic confinement effects within the nanomaterial can cause significant changes in the electronic structure. This opens the door to fine-tuning the catalytic process. In this way, nanotechnology could be a useful tool for controlling the surface structure and electrical characteristics of innovative materials in a quantitative and practical manner. The goal is to generate nanomaterials with different sizes, morphologies, numbers of active sites, and conductivities.

1.11.1 Role of nanostructure in catalysis:

The "Holy Grail" of catalytic chemistry—and a large portion of chemistry overall—has long been the customization of catalysts and catalytic processes. The fundamental steps of catalytic reactions, including reactant adsorption, intermediate diffusion, and product desorption, all require electron transfer between the catalyst surface and the reactive species, according to catalysis research conducted over the past century. Thus, it is possible to directly regulate catalytic features such as the activation energy barrier, which governs the reactivity and choice of reaction pathways, as well as product selectivity, by adjusting the spatial and energy distribution of valence electrons at the catalyst surface.[183][184] Frontier molecular orbital theory has the potential to explain important phases of surface catalytic processes. The hypothesis suggests that the symmetry and spin state of the reactant molecular or atomic orbitals, as well as matching the energy levels of the reactants to those of the catalyst surface, are directly related to the strength of the reactant adsorption and bonding on catalyst surfaces. Researchers have long attempted to improve catalytic performance by modifying the surface structure and electronic state of a catalyst surface by adding additives to the core catalytic components. Since the establishment of surface science in the middle of the previous century, researchers have discovered that even different faces of the same crystal may have dramatically varied distributions of valence electrons because of their various atomic arrangements and interactions. This distinction may result in differences in the molecule adsorption and reactivity on certain crystal faces.[185] Invoking a hypothesis known as the "d-band center," Norskov and colleagues stress that the density of d band valence electrons around the Fermi level is a significant factor impacting catalytic processes. This theory is based on a substantial body of experimental and theoretical results.[186]

Meanwhile, the distinct physical and chemical characteristics of nanoparticles (NPs), which the growth of nanoscience has brought about, have garnered considerable interest in a variety of sectors, including catalysis. Metals in bulk have continuous bands formed by valence electrons. The travel of electrons in a particular direction is constrained when the bulk material is decreased in this direction to the nanoscale scale. NPs have far more total exposed surface areas and different combinations of surface structures than bulk metals, and electronic confinement effects within NPs may significantly alter the electronic structure. [187] This

expands the potential for catalytic process adjustment. In this sense, nanotechnology may offer a practical method for controlling the surface structure and electrical characteristics of supporting nanocatalysts without modifying their chemical makeup. Therefore, it is hoped that adsorption and catalytic processes can be made more efficient by consistently changing the size of catalysts that are nanoscale in size. Since the beginning of catalytic research, studies of ultrafine particles and single-site catalysts, for example, have revealed size effects in nanoparticles. Catalytic activity have long been shown to frequently increase with smaller catalyst particle sizes. However, it was previously believed that a reduction in particle size merely results in an increase in the fraction of catalytically active surface species, as well as an increase in surface defects; these factors were typically regarded to be the primary sources of the size effect.[188][189] However, the growth of nanoscience has raised awareness of the fact that catalytic NPs also display quantum size effects in their electrical nature in addition to an increase in surface area and heterogeneity of atomic structure. Nanoscale pores additionally exhibit distinctive electronic confinement effects. Therefore, there are several potential for the advancement of catalysis provided by the union of nanoscience and nanotechnology.[190] However, the growth of nanoscience has raised awareness of the fact that catalytic NPs also display quantum size effects in their electrical nature in addition to an increase in surface area and heterogeneity of atomic structure. Nanoscale pores additionally exhibit distinctive electronic confinement effects. Therefore, there are several potentials for the advancement of catalysis provided by the union of nanoscience and nanotechnology. Alternatively, one can maximize the catalytic activity of active components by shrinking catalytic NPs to the size of a single atom or a "pseudo-single" atom.[191][192]

These investigations have expanded our knowledge of catalytic mechanisms in related processes as well as nano effects in catalysis, where the conversion of carbon monoxide, syngas, and methane uses nanoscale molecular sieves, nano-carbon materials, and nano oxide materials. A systematic investigation of the relationship between the structures/electronic states and the catalytic properties of nano catalytic systems, including nano-sized molecular sieves, nano-carbon materials, and nano oxide materials will be much needed. In such constrained catalytic systems, the electronic structure and consequently the catalytic capabilities are tuned in part by the nano effects. [193]–[195]

Take into account that based on their structure and degree of electron movement, nanomaterials are classified as zero-dimensional (0D), one-dimensional (1D), two-dimensional (2D), and three-dimensional (3D). [99] Graphene-like two-dimensional materials have recently received a lot of attention. This is because to their distinct geometric and electronic properties, which may be tweaked by forming aligned or twisted stacks of the same material or vertical heterostructures of several materials. [196]

Many materials with outstanding electrochemical activity have been synthesized in recent decades, including hexagonal boron nitride (h-BN), transition metal dichalcogenides (TMDs),[197] transition metal phosphorus trichalcogenides (MPX3),[198] and transition metal hydroxides (TMHs). [199] Controlled growth (to optimize active sites), defect engineering,[200] and other procedures have been used to generate Earth abundant electrocatalysts. Edge engineering, phase engineering, heterostructurring, and so on are all examples of nanostructure enhancements.[201] These techniques are thought to play a key role in increasing catalyst intrinsic activity and thereby maximizing the free energy of intermediate adsorption/desorption.

1.12 Strategies for enhancing electrolysis reaction:

For the development of effective low-Pt precious metal (LPM) and NPM (non-precious metal (NPM) electrochemical water splitting catalysts, effective manipulation of geometric and electronic structure, in addition to material type, is a key strategy. Specific surface area (SSA) and porous microstructure of nano catalysts are the most fundamental geometric features. Have been regarded as essential factors in improving electrocatalytic performance. For instance, mass-transfer rates and active-site density have significantly increased in high 3D super structures, 2D ultrathin nanosheets, 1D ultrafine nanowires, and other SSA materials like 0D nanoclusters, as well. Despite these efforts, adjusting geometric techniques often only offer a few opportunities to greatly improve EWS performance. But there are still more ways to enhance EWS catalytic performance by adjusting the electronic structure of electrocatalysts. We list recent developments in LPM and NPM nanomaterials' electronic structure control in this review. Specifically, we go over a number of methods for modifying electrical structure, including as alloying, doping, integrating, adding oxygen vacancies, and edge-defect engineering. We will provide some insight into the approaches that can be used to create LPM or NPM catalysts that are more effective for use in future fuel cells and electrochemical water splitting devices. [202]–[205]

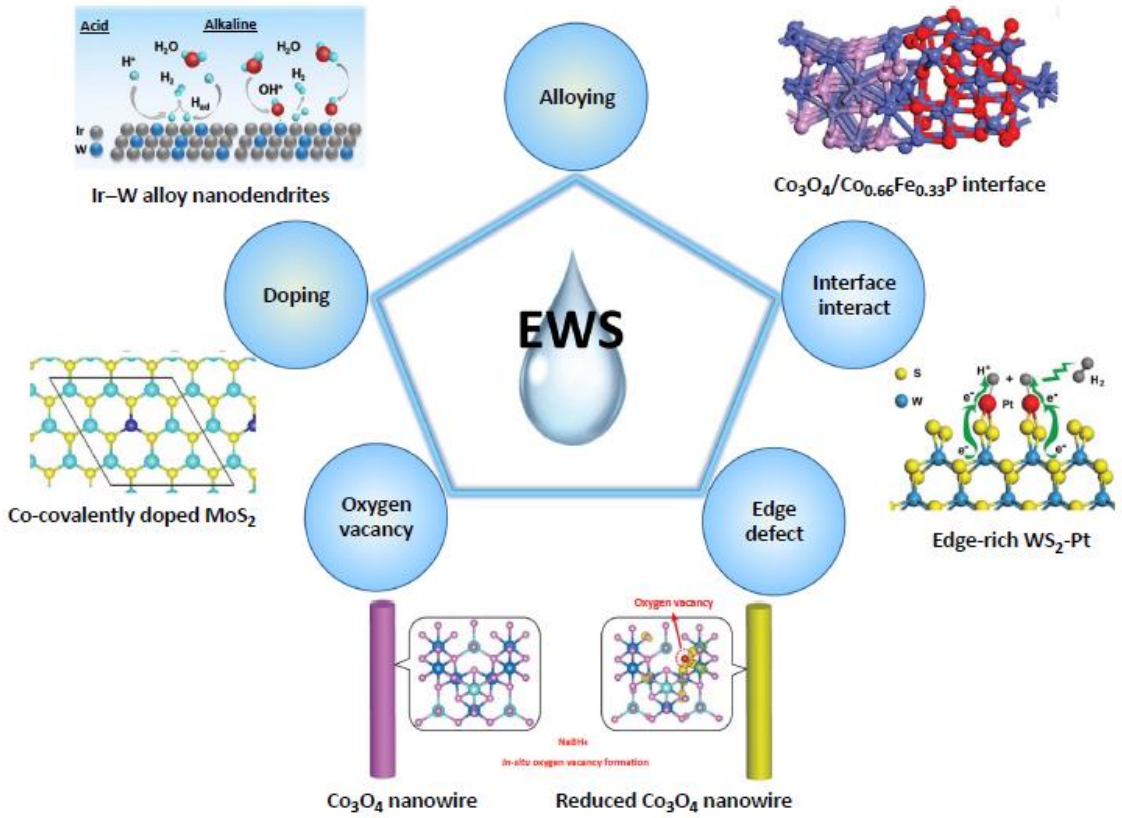

Figure 9: An illustration of the key controls for modifying the electronic structure of nano catalysts and encouraging electrochemical water splitting (EWS) [206]–[210]

1.12.1 Alloying:

The electrical structure of electrochemical water splitting nano catalysts is highly correlated with their activity. An effective method for creating more complex electrocatalysts for the HER, OER, and oxygen reduction process (ORR) with increased activity is controlled synthesis of alloying nanocrystals. LPM hybrids have been reported as effective electrochemical water splitting catalysts thus far, including Pt-Mn concave nanocube/Ni(OH)2 materials, IrCo nanoalloys, and rhombic dodecahedral MNi (M = Ir and Pt) nanoframes. By alloying Ir with 3d TMs, the oxygen adsorption energy may be efficiently controlled according to d-band center theory. By combining Ir and M, the ligand effect allows Ir to have its d-band center moved far from its initial Fermi level, making IrM's adsorption energy weaker than that of pure Ir and lowering the activation energy of the rate-determining step. For effective electrochemical water splitting devices, NPM alloy catalysts are particularly of interest because high-valent metals can stabilize other alloyed metals in low-valence states, creating a synergistic effect that results in high activity and high stability, rendering them effective electrochemical water splitting catalysts. [211]–[213]

1.12.2 Doping:

Doping is a useful strategy for increasing catalytic activity in host nanomaterials by purposefully adding trace amounts of foreign metal ions or heteroatoms. Zhang and colleagues have created single-atom Au-doped NiFe LDH catalysts in the field of LPM catalysts. Compared to LDH, these catalysts improved OER activity by a factor of six. Dopant Au atoms triggered charge redistribution in the system by transferring electrons to the LDH, which leads to better catalytic performance.[214][215]

In metal-oxide, hydroxide, and LDH catalysts, a number of TM elements, including Fe, Co, Ni, and Cu, have been successfully doped. These catalysts effectively encourage the creation of an active O radical intermediate and subsequent O-O coupling during the OER process. Recently, it was shown that Co and Fe doping have an electronic push-pull effect on the HER and OER performance of Ni-based hybrids. Fe dopants pull partial electrons from nearby Ni/Co sites, increasing their electron affinity and making it easier for OHadsorption and a faster charge transfer for the OER. In contrast, Co dopants increased the amount of lattice O2 groups and drove partial electrons to nearby Ni sites, which improved the HER's ability to adsorb H+ and transmit charge. further emphasizing how crucial it is to control the local electrical structure in order to boost OER activity. [216][205]

1.12.3 Oxygen-Vacancy Engineering:

By activating nearby atoms to increase the density of states close to the Fermi level and the reactivity of the active site, oxygen-vacancy engineering has recently been investigated as a potent method to induce electrochemical water splitting. These combined effects result in an increased rate of electron transfer, increased metal-oxygen bond instability, a quicker

intermediate exchange effect, and improved HER/OER performance. For increased conductivity, two electrons that already present on the oxygen vacancy can be easily stimulated into the conduction band. A typical LPM catalyst is a hollow porous polyhedron made of RuO2 doped with Cu. Rich O vacancies are created here close to Cu, which causes unsaturated Ru to arise, reduces the positive charge on the surrounding Ru atom, and moves the p-band center of nearby O atoms closer to the Fermi level to increase OER activity. Therefore, from the following perspectives, oxygen-vacancy engineering is a potentially effective method for enhancing the activity of the EWS catalysts: the improvement of conductivity, the activation of nearby atoms, and the energy efficiency barrier to the HER/OER reaction intermediates' production.[210][115][217]

1.12.4 Interfacial-Site Engineering:

It has been shown that interactions between distinct areas at interfaces can speed up electrochemical reaction rates and increase charge-transfer rates. For the oxidation of primary alcohols, for instance, Au/CeO2 single-atom catalysts with maximum interfacial sites exhibit improved catalytic activity. Similar ideas have been demonstrated for the preparation of Pd-Ni-Pt sandwich nanoparticles, PtPb/Pt core/shell nano-plates, and PtPd-Fe3O4 interface nanoparticles for improving the detection of H2O2, which is attributed to the abundance of active interfacial sites and coordinatively unsaturated atomic sites. [218]–[221]

Pt3Ni/NiS nanowire heterostructures created by directly sulfuring highly composition-segregated Pt-Ni nanowires are a typical illustration of LPM catalysts. In potassium hydroxide (KOH) solution, DFT simulations showed that the synergistic impact of NiS and Pt3Ni increases HER activity. NiS stimulated the initial water dissociation, while Pt3Ni effectively transferred H+ to H2. It has also been noted that carbon nanotubes, hollow carbon spheres, and reduced graphene oxide (rGO) are ideal substrates for creating interfacial catalysts. According to their highly hybridized projected density of state, Xiong and colleagues reported a Pd/Pt-rGO structure as effective HER catalysts, revealing that graphene substrates had strong electronic coupling with Pd and Pt, resulting in an interconnected and resistanceless network for effective HER catalysis.[222]

Enhancing the interface of the TM oxides, phosphides, nitrides, and chalcogenides on NPM catalysts may increase electrochemical water splitting activity. As an OER catalyst, a high-energy interfacial CoO/hi-Mn3O4 structure was developed. In this instance, MnIII-O pairs of high-Mn3O4 served as electron acceptors to pull electrons from CoO. This resulted in the formation of the Mn-O-Co interface and a highly oxidized state of CoO, which favors charge transfer and increases intrinsic OER activity. Interestingly, a class of CuS/NiS2 interface nanocrystal catalysts that can bind fresh chemical intermediates to advance the OER was also created. Furthermore, in MoS2/NiO/Ni3S2 heterostructures, interfacial engineering was successfully used to enable the simultaneous chemisorption of hydrogen- and oxygen-based intermediates independently, improving the overall electrochemical water splitting characteristics.[94], [221], [223], [224]

The following techniques might effectively optimize electron transport in heterojunctions and enhance the performance of the electrochemical water splitting: (1) lowering interfacial resistance and the absolute value of hydrogen- and oxygen-based adsorption energy, (2)

pulling electrons and creating metal-O-metal interfaces, and (3) synergistic effects between compositions encouraging various essential chemical stages. [225]–[227]

1.12.5 Edge-Defect Engineering:

Edge-defect engineering has just just come to light as a practical method for modifying the electrical structure of nanomaterials, leading to increased electrocatalytic activity. Guo and colleagues proposed ultrathin PtPdM (M = Co, Ni, Fe) nanorings as superior LPM catalysts because the atoms at the edge steps are inherently extremely active. Importantly, the large proportion of step atoms, effective atom consumption, and robust ligand impact from M to Pt were attributed to good OER activities. In another work, numerous edge-terminated active sites in winged Au@MoS2 nanostructures demonstrated significantly increased HER electrocatalytic activity, which was due to the optimized proton-adsorption procedure.[228]–[230]

The oxygenated species at the ends of the nanotubes were discovered to dominate the electrochemical characteristics of CNTs for NPM catalysts. It was also demonstrated that the graphene edge had two times the reactivity of the bulk atoms. The edge sites with unpaired electrons and carboxylic groups were shown to be capable of acting as active sites in electrocatalysis by Loh and colleagues. For the purpose of enhancing HER, 3D graphene with a high density of sharp edge sites was created. The numerous sharp edge defect sites of the 3D frameworks, which effectively enhance the adsorption and reduction of protons, were shown to be the primary cause of their exceptional HER performance, according to DFT analyses. Furthermore, 2D layered materials, such as LDH, CoSe2, MoS2, MoS2, WSe2, and 2H-WS2, frequently reveal basal planes with little roughness and dangling bonds ending the surface, but the edge surface has many dangling bonds that are chemically active in controlling electrocatalysis. It has been observed that MoS2 nanosheet/carbon macro-porous hybrid catalysts with a lot of tailored unsaturated sulfur edges can improve HER catalysis. The increased exposure of unsaturated sulfur edges might optimize DGH and considerably increase the intrinsic HER catalytic activity, according to DFT calculations. Edge-defect engineering, therefore, serves as a key method for creating highly effective EWS catalysts from two main perspectives: (1) edges serve as electrocatalytically active sites that can maximize hydrogen adsorption energy, and (2) edges serve as anchoring points for the doping of other active species.[230]–[234]

1.13 Nano particles synthesis:

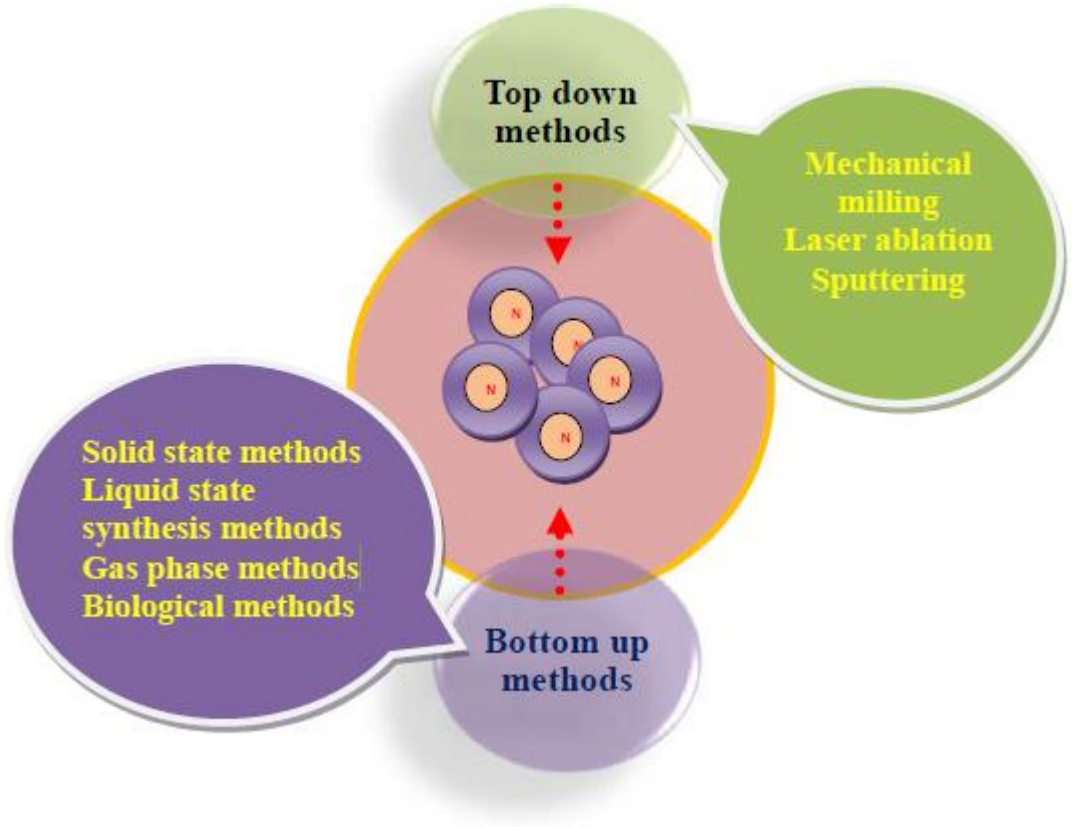

Figure 10: Synthesis process of nanoparticles.[235]

For the creation and stabilization of nanoparticles, a variety of physical and chemical techniques, including electrochemical modifications, chemical reduction, and photochemical reduction, are frequently used. The choice of a nanoparticle preparation technique is crucial because processes used in nanoparticle synthesis, such as the kinetics of metal ions' interactions with reducing agents, the adsorption of stabilizing agents onto metal nanoparticles, and various experimental techniques, have a significant impact on the stability, morphology (structure and size), and physicochemical properties of the finished product.[236][237] There are two primary categories of procedures used to create metallic nanoparticles: bottom up methods and top down methods. The primary distinction between the two approaches is the raw material used to prepare the nanoparticles. While atoms or molecules are the starting materials in bottom-up approaches, top-down methods start with bulk material and use various physical, chemical, and mechanical processes to reduce particle size to nanoparticles.[238]

1.13.1 Top-down methods:

It covers techniques including thermal, laser, and mechanical milling. Although top-down approaches are simple to use, they are not appropriate for creating irregularly shaped and

very small particles. Changes in the surface chemistry and physicochemical characteristics of nanoparticles are the method's main drawback.[239]

1.13.1.1 Mechanical milling:

1.13.1.1.1 Ball milling:

Mechanical milling's basic principle is the decrease of particle size by the use of high-energy ball milling. Process variables and the characteristics of the milling powder have an impact on how well mechanical milling works. There are two types of milling that depend on induced mechanical energy to turn a mixture into powder: low energy and high energy milling. For the synthesis of intermetallic nanoparticles, this approach is generally favored. In this technique, a container is filled with bulk powder and numerous large balls. With the aid of a high speed spinning ball, high mechanical energy is imparted to bulk powder material.[240]

1.13.1.1.2 Mechanochemical synthesis:

The repeated deformation, welding, and fracture of the reactant mixture is the foundation of the mechanochemical synthesis technique. During the milling process, many chemical changes are created at the interface of nano-sized particles. The raw components for the mechanochemical technique of synthesis are combined stoichiometrically and then grounded. The reactants are deformed, fractionated, and welded during the milling process. The surface interaction between substrate and reagent generates a number of chemical reactions.[241]

1.13.1.2 Laser ablation:

The laser irradiation employed in the laser ablation method causes the particle size to be reduced to the nano scale. After being covered by a thin layer, the solid target material is exposed to pulsed laser irradiation. The most common lasers employed are copper vapor lasers, neodymium-doped yttrium aluminium garnet (Nd:YAG) lasers, Ti:Sapphire (Titanium-doped sapphire) lasers, and Nd:YAG lasers with 106 μm output and its harmonic. When a material is exposed to laser energy, it fragments into nanoparticles, which remain in the liquid surrounding the target and create colloidal solution. [242] The proportionate quantity of ablated atoms and particles generated depends on the laser pulse duration and energy.

1.13.1.3 Ion sputtering:

Ion sputtering involves vaporizing a solid by sputtering with a beam of ions from an inert gas. Recently, employing magnetron sputtering of metal targets, this technique was used to create nanoparticles from a variety of metals. By using this technique, vast amounts of nanostructured films are deposited on silicon substrates in the form of collimated nanoparticle beams. Low pressures are used during the entire procedure. Sputter deposition is carried out in an evacuated vacuum chamber where working pressure is kept constant while sputtering gas is supplied. Along order to ionize the gas, a very high voltage is applied to the target

(cathode) and free electrons are pushed in a spiral path by means of a magnetic system. Here, they collide with the atoms of the sputtering gas (argon). This ongoing process generates a plasma glow discharge that can ignite. The positively charged gas ions were drawn to the target, where they kept hitting it.[243]

1.13.2 Bottom-up methods:

Bottom-up nanoparticle synthesis relies on combining of atoms, molecules, or tiny particles to create nanoparticles from larger molecules. By using this technique, the nanoparticle's building components are first generated and then put together to create the finished nanoparticle**.**

1.13.2.1 Solid state methods:

1.13.2.1.1 Physical vapor deposition method:

Material is placed on a surface using the physical deposition method as either a thin film or as nanoparticles. Material is vaporized by highly controlled vacuum techniques like thermal evaporation and sputtering deposition before being further condensed on a substrate. Typically, lanthanum strontium cobalt thin films are prepared using physical vapor deposition techniques like pulsed vapor deposition. For pulsed laser deposition, a solid target is subjected to laser ablation, which results in the generation of plasma of ablated species. These ablated species are then deposited on a substrate to create a film.[244][245]

1.13.2.1.2 Chemical vapor deposition method:

First documented and patented in the late 19th century, chemical vapor deposition was used to create carbon fiber filaments and carbon powder color pigments for electric lamps[246]. This type of deposition involves the chemical reaction of gaseous molecules containing atoms necessary for film formation, which deposit a thin film of the target material on a surface. A thin film is created through a sequence of chemical interactions involving the precursor fragment, the substrate surface, and the target material, which is released as a volatile molecule and functions as a precursor. In this approach, the surface chemical reaction often results in the production of atomic layer deposition (ALD) thin films.[246][247]

Thermally active chemical vapor deposition (TACVD), plasma enhanced chemical vapor deposition (PECVD), and photo initiated chemical vapor deposition (PICVD) are three methods for depositing the target material. The temperature-sensitive substrates, such as polymers, are not appropriate for thermally activated chemical vapor deposition. Because of operating conditions, the scaling up of the plasma accelerated chemical vapor deposition technology is problematic due to its instability to both aging and humidity and its equipment high costs as well as its time consumption, low energy processing and a broad spectrum of potential variation are involved in photo-initiated technologies such as chemical vapor deposition. Additionally, at ambient temperatures and pressure levels, photoinitiated operation doesn't require specialist equipment.[248][249]

1.13.2.2 Liquid state synthesis methods:

1.13.2.2.1 Sol gel method:

For the first time, Livage et al. (1988) reviewed this method for transition metal oxide sol gel chemistry. The sol-gel method of synthesis of nanoparticles involves one of three methods: a) direct mixing of metal and metal oxide or nanoparticles within a prehydrolyzed silica sol, b) direct mixing of metal and metal nanoparticles within a sol containing the matrix-forming species, or c) complexation of metal with silone and reduction of metal prior to hydrolysis. Gelatin and colloidal suspension (sol) are used in this technique to create a network in a continuous liquid phase (gel). Colloids are created using the ions of metal alkoxides and aloxysilanes as a precursor. The two silanes that are used to create silica gel most frequently are tetramethoxysilane (TMS) and traethoxysilane. Metal alkoxides are water-immiscible organo-metallic precursors for numerous metals, including titanium, silica, aluminum, and many others. There are four main processes in the production of a sol-gel: particle growth, particle aggregation, and hydrolysis.[250][251]

1.13.2.2.2 Chemical reduction method:

In the chemical reduction process, several reducing agents are used to reduce ionic salt in a suitable medium when surfactant is present. Metal nanoparticles are made by reducing a substance in an aqueous solution, such as sodium borohydride. Sodium lauryl sulphate (SLS) or trisodium citrate (TSC) are used to cap formed metal nanoparticles (SLS). Occasionally, reducing agent and stabilizing agent are combined.[252]

1.13.2.2.3 Hydrothermal method:

The term "hydrothermal synthesis" describes the heterogeneous processes used to create inorganic compounds in aqueous fluids at temperatures and pressures above ambient. In this instance, an aqueous combination of precursors is heated in a stainless-steel autoclave that is tightly sealed above the boiling point of water, substantially raising the pressure within the autoclave for the reaction over atmospheric pressure. High temperature and pressure work together synergistically to form highly crystalline materials in a single step without the use of post annealing procedures. A variety of nanomaterials have been created using hydrothermal methods as well. The products are significantly impacted by the reaction parameters, which include the type and concentration of the precursors, the solvent, the stabilizing agents, and the reaction temperature and duration.

Due to its high-temperature and high-pressure reaction conditions, hydrothermal synthesis might yield nanomaterials with extremely high crystallinity as opposed to "low-temperature" processes, which often result in poorly crystalline nanoparticles. Contrary to coprecipitation procedures, hydrothermal treatments have a relatively low product yield.[253]

It has been suggested also that nucleating or "seeding" with may be able to regulate the development of several transition metal oxides. In fact, using the seeding effect to regulate the growth of a chosen phase during the hydrothermal process and improve transformation kinetics.[254]–[256]

Additionally, the inclusion of a surfactant reduces the optical band gap overall by increasing the aspect ratio of nanoparticles (the ratio of their surface area to their volume). [257]

1.13.2.2.4 Solvothermal method:

In the presence of water or other organic solvents including methanol, ethanol, and polyol, the solvothermal process is employed to prepare nanophase. A pressure vessel that permits the solvents (water and alcohol) to heat above their boiling points produces the reaction. By using microwave-assisted processes, the kinetics of crystallization (crystal formation) can be enhanced by one to two orders of magnitude (microwave solvothermal). [258]

1.13.2.3 Gas phase methods:

1.13.2.3.1 Spray pyrolysis:

The heated reactor receives vaporized nanoparticle precursors when using the spray pyrolysis method. A nebulizer is used to inject precursor directly into the heated reactor in the form of tiny, imperceptible droplets. Metal precursors are frequently supplied in the form of acetate, nitrate, and chloride. Ultrasound is used to create atomized droplets from the precursor solution in the improved method known as ultrasonic spray pyrolysis. The formed aerosol droplets are then transported from the atomizer to the reactor furnace by the carrier gas for the formation of nanoparticles, which are subsequently collected by collection system. [259]

1.13.2.3.2 Laser pyrolysis:

The creation of nanoparticles by laser pyrolysis requires the use of laser energy. In this technique, homogenous nucleation processes are induced by allowing the precursor to absorb laser energy. Unlike heating the gas in a furnace, this results in extremely localized heating and cooling. The most popular type of laser energy for heating is the infrared CO2 laser, whose energy is absorbed by the inert photosensitizer sulfur hexafluoride. As soon as a significant level of super saturation of the condensable product is obtained in the vapor phase, nanoparticle production in CO2 pyrolysis starts.[243]

1.13.2.3.3 Flame pyrolysis:

The fundamental idea behind the flame pyrolysis method is the direct spraying of a liquid precursor into the flame to produce nanostructures. Precursors that don't have a high enough vapor pressure can nevertheless be delivered using this technique in the form of vapor. The precursor is exposed to the flame and permitted to create nanoparticles using vapor-fed aerosol flame synthesis, flame-assisted spray pyrolysis, and flame spray pyrolysis, respectively.[260][261]

1.13.2.4 Biological method / Biomimetic method / Green synthesis method

An emerging trend in nanotechnology is the creation of nanoparticles utilizing green synthesis techniques. These methods have been developed to address issues with the safety, high cost, and reaction-related challenges of traditional approaches. In order to lessen the risk to human health and the environment, new methods for chemical synthesis and a variety of chemical applications were combined into green chemistry approaches. These methods mostly fall under the following headings: 1) Clean chemistry, 2) Atom economy, 3) Environmentally benign chemistry, and 4) Benign by design chemistry.

The biological processes for making nanoparticles use a variety of microorganisms, their enzymes, and plant products like isolates and extracts. There are two types of naturally

occurring biogenic metallic nanoparticle production. 1) Bioreduction: Using microorganisms and their enzymes, metal ions are chemically reduced into the biologically stable state in this approach. The produced metallic nanostructures are safe to separate from contaminated sample since they are stable and inert in nature. 2) Biosorption: This novel technique for creating nanoparticles involves allowing metal cations to contact with organism cell walls in aqueous environments. This causes stable nanoparticles to form as a result of cell wall or peptide interaction.[262] [263]

1.13.2.4.1 Nanoparticle synthesis using bacteria

The desire to effectively use naturally available resources, such microorganisms, for the synthesis of nanoparticles is growing around the world. Prokaryotes have drawn interest as a method of synthesising metallic nanoparticles due to their abundance in the environment and capacity to adapt to harsh conditions. Bacteria are advantageous in that they multiply quickly and are simple to grow and control. By adjusting factors like oxygenation, temperature, and incubation period, the growth can be controlled. [263]

Bacteria	Nanoparticle	Size (nm)	Morphology	References
Bacillus cereus	Silver	20–40	Spherical	[264]
Bacillus megatherium D01	Gold	1.9 ± 0.8	Spherical	[265]
Klebsiella aerogenes	Cadmium sulfide	20–200	Crystalline	[266]
Lactobacillus strains	Silver-gold alloys	100–300	Crystalline and cluster	[267]

TABLE: Green biosynthesis of NPs using bacteria[268]

1.13.2.4.2 Nanoparticle synthesis using fungi

As a reducing agent, the enzyme and protein released by fungi can be employed to create metal nanoparticles from metal salt. Due to electrostatic contact, metals like Ag have the capacity to bind to cytoplasmic membranes and decrease, resulting in the formation of silver nuclei and the accumulation of silver nuclei and nanoparticles.[269]

Fungi	Nanoparticle	Size (nm)	Morphology	References
R. stolonifer	Ag	5–50	Spherical	[270]
P. glomerata	Ag	60–80	Spherical	[271]
F. oxysporum	CdS	5–20	Spherical	[272]
F. oxysporum	Ti	5–15	Quasi-Spherical	[273]

TABLE: Green biosynthesis of NPs using fungi [274]

1.13.2.4.3 Nanoparticle synthesis using plant and plant products:

Recent years have seen a surge in interest in plant-mediated nanoparticle production. Extracts from various plants are used to prepare a range of metallic nanoparticles, including gold, silver, copper, and zinc. The secondary plant metabolites such phenolic acid, flavonoids, terpenoids, and alkaloids that preferentially decrease metallic ions and result in the creation of bulk metallic nanoparticles are abundant in the crude extracts. Plant metabolic

pathways' redox reactions frequently involve the primary and secondary metabolites of plants. These characteristics are used as reducing and capping agents, which results in the creation of environmentally beneficial nanoparticles.[275] [276]

Plant Origin	Nanoparticle	Size (nm)	Morphology	References
Acalypha indica	silver	20–30	spherical	[277]
Bryophyllum sp.	silver	2–5	fcc unit cell structure	[278]
Hibiscus rosa sinensis	gold & silver	14	spherical, prism	[279]
Pear fruit extract	gold	200–500	triangular, hexagonal	[280]

TABLE: Green biosynthesis of NPs using plants [281]

1.14 Our catalysts:

Precious metals and their alloys and compounds make up the typical catalysts for HER and OER, but their high price and inherent scarcity prevent their wider use. In order to meet the low overpotential demand, cobalt-based compounds have been researched as homogenous molecular catalysts for HER and OER. Cobalt-based compounds are intriguing alternatives because they are abundant on earth and have a not so complicated chemistry that allows them to build molecules with various valence states.

However, difficulties with synthetic processes have limited the use of cobalt-based complexes, and at the same time, the intrinsic electronic structure and small number of surface active sites of common cobalt-based compounds prevent them from having good catalytic capabilities. [282]

As a homogenous molecular catalyst for HER and OER, cobalt-based complexes such as a variety of cobaloxime and diimine-dioxime compounds have drawn a lot of interest in order to meet the low overpotential requirement. Due to the high electrocatalytic activity in water splitting, cobalt-based compounds are intriguing non-noble metal alternatives. Nevertheless, difficulties with synthetics have prevented widespread application of the molecular catalysts. Given their wide range of potential uses in the sectors of energy and the environment, inorganic cobalt oxides like CoO and Co3O4 are regarded as stable in the Co-O system and one of the types of versatile materials among transition metal oxides. Because of their natural abundance, low cost, and ability to produce compounds with different valence states, cobalt-based compounds, such as metallic cobalt, oxides, hydroxides, carbides, nitrides, phosphides, sulfides, selenides, and tellurides, have been investigated as alternative catalysts for electrochemical water splitting. [283]–[285]

Because the charge transfer efficiency during electrolysis affects the reaction kinetics, cobalt-based compounds, especially oxides and hydroxides, typically don't have enough electrical conductivity to meet the high demand. Additionally, more exposed active sites typically result in increased activity because electrocatalysis typically takes place at active centers on the catalyst surface. In order to maximize the catalytic activity in water splitting, cobalt-based catalysts must be designed with a large active surface area and high

conductivity. Cobalt-based electrocatalysts can be loaded onto conductive substrates or grown in situ on conductive materials to improve charge transfer and reaction kinetics. As an example and Due to their increased specific surface area, high conductivity of reduced graphene oxide, and synergistic chemical effects, Co_3O_4 nanocrystals produced on reduced graphene oxide make effective OER catalysts in an alkaline solution.[286]

To methodically improve the extrinsic catalytic performance of cobalt-based electrocatalysts, numerous variables should be taken into account in addition to the morphology and electrode structure. First, the rapid release of gas bubbles during HER and OER affects the usage of active sites and the catalytic efficiency. Second, because HER and OER are frequently carried out in acidic or alkaline media, excellent chemical/electrochemical stability and corrosion resistance are required of the electrocatalysts and related equipment in order to minimize catalyst poisoning and deactivation. Thirdly, the effectiveness and cost of the entire water splitting system depend on the anode, cathode, and electrolyte being properly matched.

Since the morphology, electrode structure, substrate, gas release, corrosion resistance, charge transport, as well as matched anode and cathode, can all be controlled to maximize the extrinsic activity of cobalt-based catalysts, techniques involving the formation of surface defects, heteroatom doping, new hetero-structures, etc. have recently attracted a lot of attention.[287][288][289]

Following the initial electrochemical conversion of hydroxyl to (oxy) hydroxyl, cobalt-based electrocatalysts in OER are subjected to oxidation via a number of intermediary stages. In particular, solitary oxo sites $Co^{IV}=O$ undergo surface proton/electron hopping to form the $Co^{IV}(=O)\text{-}O\text{-}Co^{IV}=O$ pair, which is nucleophilically attacked by water molecules to form the $Co^{III}\text{-}OOH$ hydroperoxide. In the end, the addition and deprotonation of fresh water molecules restarts the electrocatalytic cycle by creating hydroxyl $Co^{III}\text{-}OH$ at the active center. Combination with another oxo creates a superoxo $Co^{III}\text{-}OO^-$ releases the oxygen molecules.[290][291] As a result, the catalysts as-prepared only function as pre-catalysts and not as actual catalytic centers. While the highly conductive core of cobalt-based carbides, nitrides, phosphides, sulfides, etc. can speed up charge transport and the OER kinetics, cobalt-based (oxy)hydroxides formed from metallic cobalt or cobalt-based compounds can increase the active surface centers to enhance the OER activity.

1.14.1 Role of heterostructurring between sulfide and oxide:

Unfortunately, the poor conductivity of TMO materials is one of their biggest drawbacks. Traditionally, this problem has been solved by adding carbon nanostructures to the composite.

Additionally, even though TMO-based catalysts have outstanding OER performance, their HER activities fall far short of realistic standards, making it difficult to build a bifunctional electrode. To speed up the splitting of water molecules, it is essential to simultaneously lower the energy of hydrogen and oxygen intermediate production. Sulfides, particularly cobalt sulfides, have recently been shown to possess very effective HER activities thanks to their intrinsically improved electrical transmission capabilities and innovative surface design. It has also been acknowledged that the fabrication of heterostructures based on transition metals is advantageous for improving catalytic performance due to increased active sites, altered

electronic structures, improved electrical conductivity, and optimum chemisorption strength for reactants.[292]–[294]

2. Objectives of this thesis and outline:

The theme of this research is the recreation of cobalt (II) Oxide electrochemical catalysts known to have good activity toward oxygen evolution reaction (OER) with an objective of introducing a heterostructure of cobalt sulfides (CoSx) through a hydrothermal reaction process, as well as investigating this new heterostructure of different concentrations using Cyclic voltammetry, sweep voltammetry, SEM and XRD measurements.

3. Experimental section & Methods:

3.1 Material:

Cobalt (II) chloride hexahydrate CoCl2·6H2O (≥97%, Sigma-Aldrich), thiourea SC(NH2)2 (97%, Sigma-Aldrich), Urea NH_2CONH_2 (99%, Sigma-Aldrich), absolute ethanol (99%, Sigma-Aldrich), acetone (99%, Sigma-Aldrich), ultrapure water and deionized water (with conductivity < 20μS/cm) were used for the preparation of the samples.

3.1.1 Preparation of the electrocatalyst:

3.1.1.1 CoOH Scheme:

Carbon fibers (CF) were ultra-sonically washed by acetone, ethanol and ultrapure water in sequence and then dried at 60 °C subsequently. Then in a 100 ml beaker a 40 ml of ethanol were added and then a 1.90 g of CoCl2·6H2O and NH_2CONH_2 were dissolved within it for 10 minutes, followed by seed layer formation using a calcination process at 450 °C for 4h under an argon flow using the CVD Device. Then in a 150 ml Teflon-lined stainless-steel autoclave, the seeded CFs were immersed in a solution of ultrapure water with 5.7 g of cobalt CoCl2·6H2O and 7.272 g of NH_2CONH_2, the autoclave was then heated for 4h in an electrical oven at 90 °C. After cooling down to room temperature the obtained Co(OH)2 Nanowires where washed with water and ethanol then dried at 60 °C for future use.[201]

3.1.1.2 CoSx Scheme:

This step includes the preparation of CoSx on pre-grown CoOH/CF. where the initial seeded CF was cut into 4 pieces with equal dimensions, were 1 was left as a pure cobalt oxide sample and the rest were autoclaved separately at different concentrations of material used, the first piece was immersed in a 150 ml Teflon autoclave with 120 ml of distilled water dissolved in it 0.087g of CoCl2·6H2O and 0.228g of SC(NH2)2 then the second sample with 0.357g of CoCl2·6H2O of and 1.14g of SC(NH2)2 then the third sample with 0.534g of CoCl2·6H2O of and 1.71g of SC(NH2)2, all heated in an electrical oven for 12h at 60 °C. [295]

Sample	Cobalt (II) chloride hexahydrate	Urea	thiourea
Pure	5.7 g	7.272g	-
Sample 1	0.087g	-	0.228g

Sample 2	0.357g	-	1.14g
Sample 3	0.534g	-	1.71g

3.2 Material characterization:

Field emission scanning electron microscopy (FE-SEM) using a ZEISS SUPRA 40 and an X-ray diffractometer utilizing Cu Ka radiation in the range 2 between 10° and 80° were used to determine the crystal structure and morphology of the produced samples, respectively. The FE-SEM equipment on an energy dispersive X-ray spectrometer (EDXS) was used to produce the elemental mapping images.

3.2.1 X-ray diffraction spectroscopy:

A ZEISS SUPRA 40 X-ray diffractometer set on the 2-scan with CuK-1 (=1.5406) radiation was used to analyze the structures of the produced materials. The radiation was generated at a current of 30 mA and a voltage of 40 kV. 0.2 mm of slits were employed as the detector and source. The sample was rotated across the angle range of 2 = 10°–80° while the X-ray radiations were shining directly on it. The diffracted radiations were collected and recorded.

To obtain the geometry, the X-ray detector was designed so that the angle between the detector and the atomic planes was 2θ as shown in **Figure 10**.

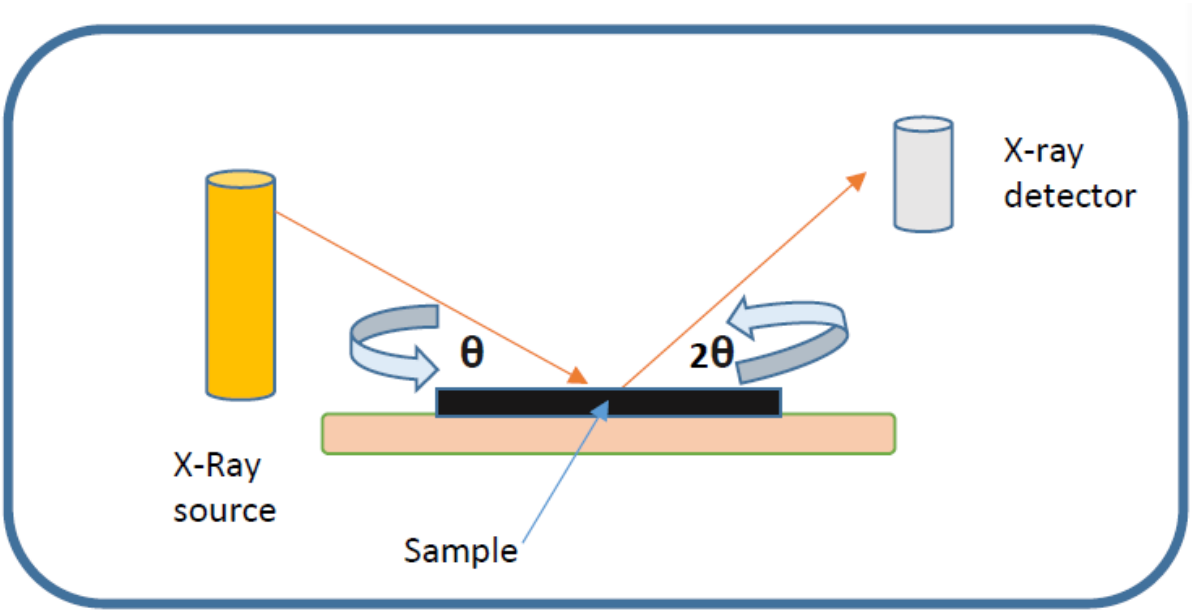

Figure 10: Schematic diagram of an X-ray diffractometer

3.2.2 Scanning electron microscopy:

SEM was used to analyze the morphology and physical image surface of the produced material using a topographic approach. The benefit of SEM is that it may be used to show how materials that are produced in highly crucial range sizes such as micrometers and

nanometers form (nm). This made it easier to clearly see and characterize each sample when observing and analyzing it.

3.3 Electrochemical measurements of cobalt-based material for water splitting:

At an electrochemical station, all the electrochemical measurements were carried out using a standard three-electrode electrochemical cell setup in 1 M KOH aqueous solution (pH=14). The working electrode was CoOH/CoS2 that had been developed as-is on CF, while the reference and counter electrodes were Ag/AgCl (3 M KCl) and platinum wire, respectively as shown in **Figure 11**.

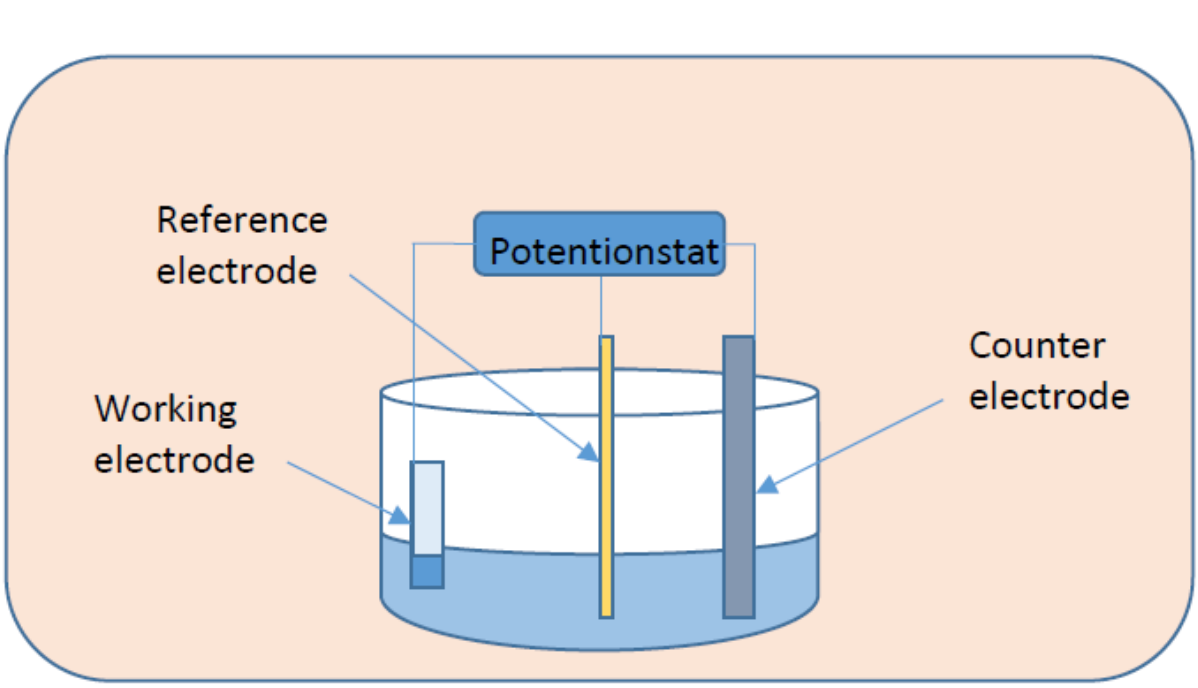

Figure 11: Three cell electrochemical measurement system.

The reference electrode's recorded potentials were transformed into a reversible hydrogen electrode (RHE) using the Nernst equation:

$$ERHE = EAg/AgCl + 0.059 * pH + 0.1976$$

To avoid O2 contaminants in the air, the OER activities were assessed in a 1 M N2-saturated KOH solution. With a scan rate of 5 mV s-1, linear sweep voltammetry (LSV) scans were taken in the potential range of -0.3 V to 0.9 V (vs RHE). To measure the double-layer capacitance, cyclic voltammetry (CV) scans were performed at a scan rate ranging from 10 mVs-1 to 200 mVs-1, from -0.04 to 0 V vs. RHE with various scan rates (20,40,60,80,100,120,140,160,180,200 mV s-1) (Cdl). The CV curves were swept for 300 cycles at a scan rate of 2 mV s-1 between -0.125 and 0.125 V (versus RHE) in order to determine durability. Next, it was determined how the anodic scan LSVs before and after the stability test compared.

4.Results & Discussion:

4.1 SEM Data:

Field-emission scanning electron microscopy was used to evaluate the morphologies of the as-prepared samples (FE-SEM).

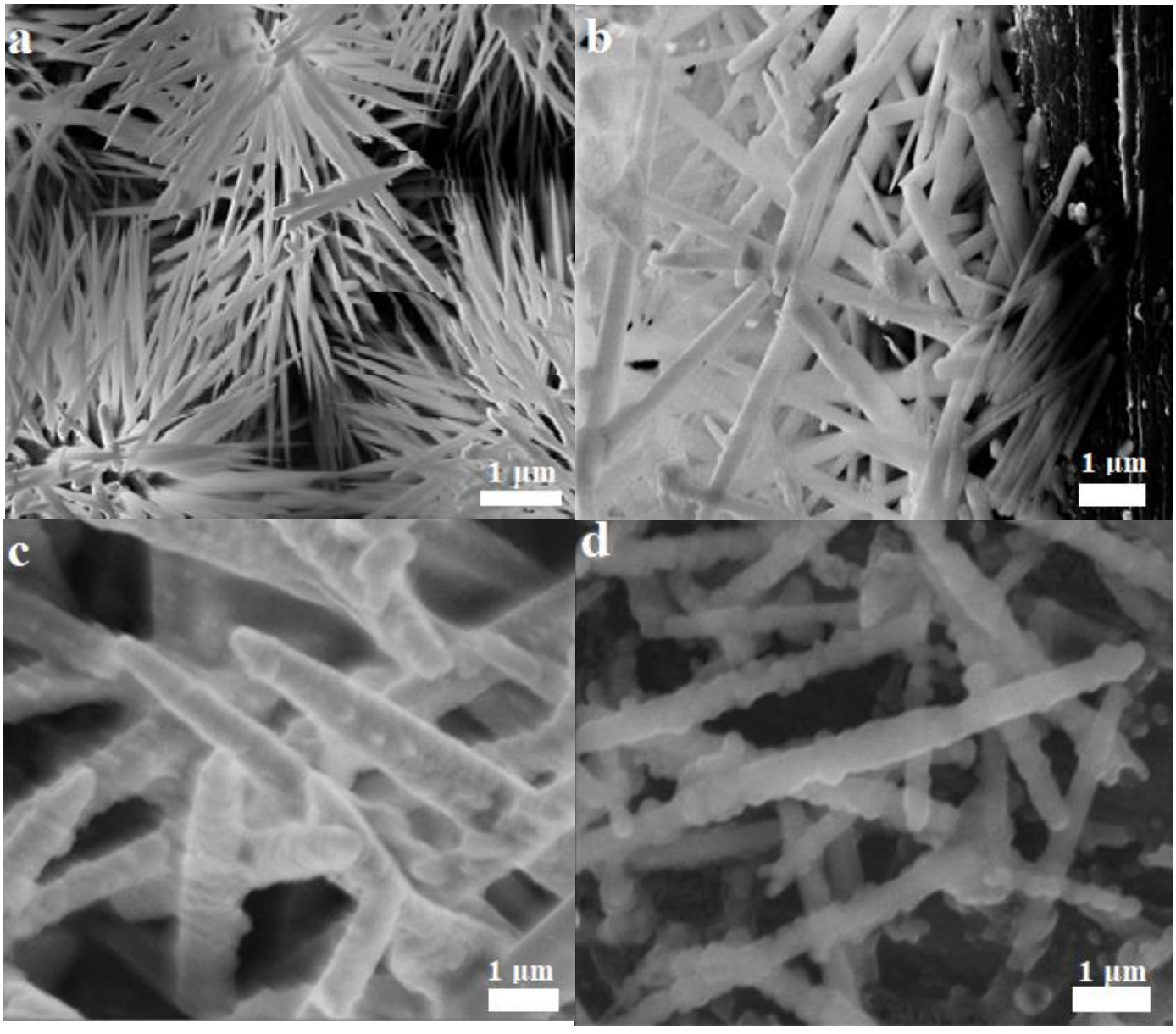

Figure 12: FE-SEM Images, a) pure CoOH, b) Sample 1 of CoSx, c) Sample 2 of CoSx and d) Sample 3 of CoSx.

Where we find that the pure sample in **Figure-12a** shows a smooth surface of cobalt oxide nanowires formed neatly on our carbon fiber sheet base, while **Figure-12b** shows an increased roughness on the said nanowires due to cobalt sulfer composites nucleation from added thiourea in the second synthesis step on top of the wires in sample 1, the roughness tends to increase significantly in size with increased thiourea concentrations added as in **Figure-12c** and **Figure-12d**.

The judicious modulations made to the carbon skeleton at hand and the smoothly formed carbon oxide nanowires are all but needed modifications to improve both the conductivity and offer this enhanced stable and corrosive resistant substance a more active surface area for an improved electrochemical activity. These advances are but increased exponentially with the incorporation of a cobalt sulfer composites, where more and more reaction sites are developed on the nanowire surface for OER activity due to the increased surface roughness, and where synergism between the cobalt oxide wires and the sulfer growth enhances both the inherent activity resulting in reduced turnover frequency as well as enabling excellent mechanical adhesion.

4.2 Elemental composition analysis:

Energy-dispersive X-ray spectroscopy (EDX) was used to determine the types of elements and their distribution in the sample matrix. Showing element traces of our materials used to fabricate the nanowires.

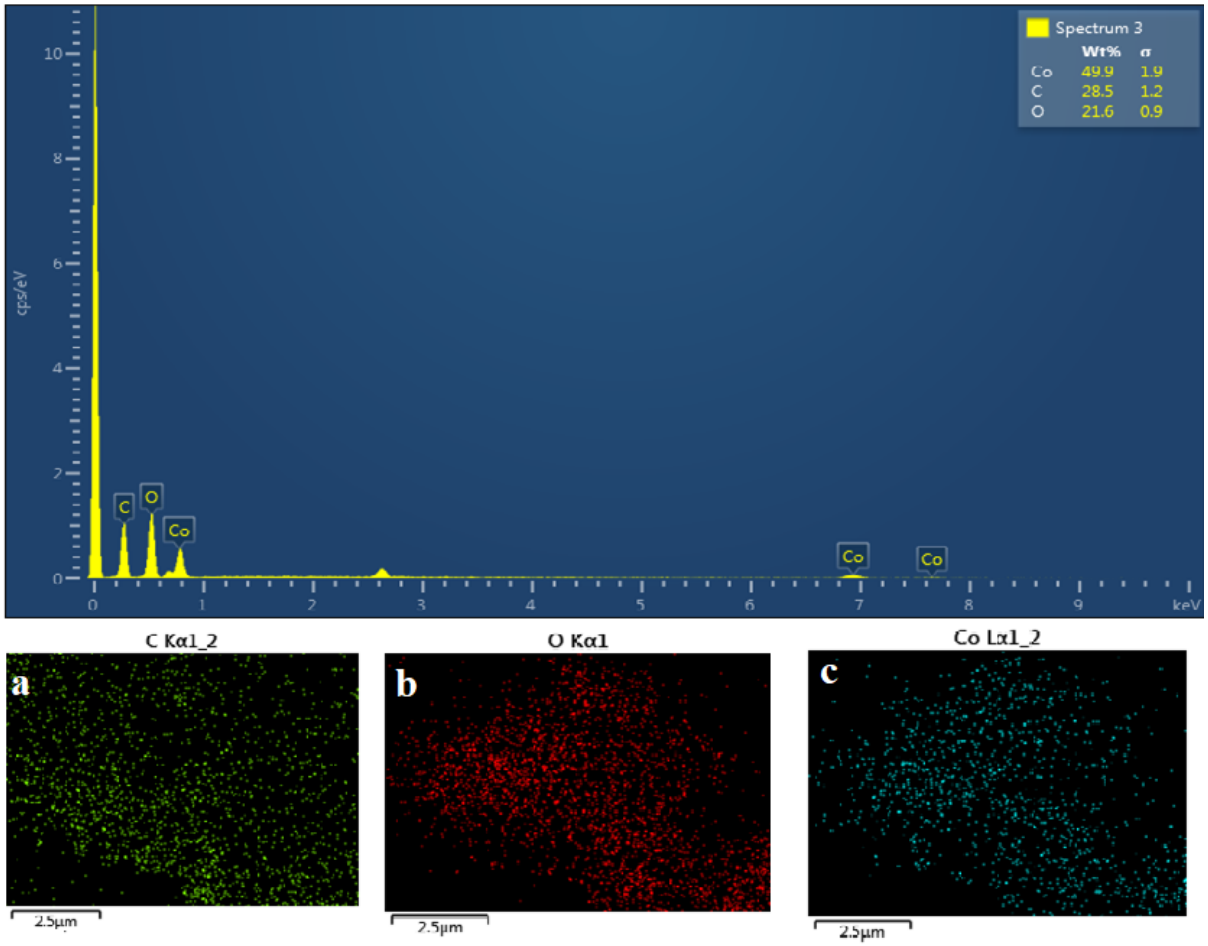

Figure 13: EDX and graph elemental mapping of CoOH on CF: a) Carbon, b) Oxygen and c) Cobalt

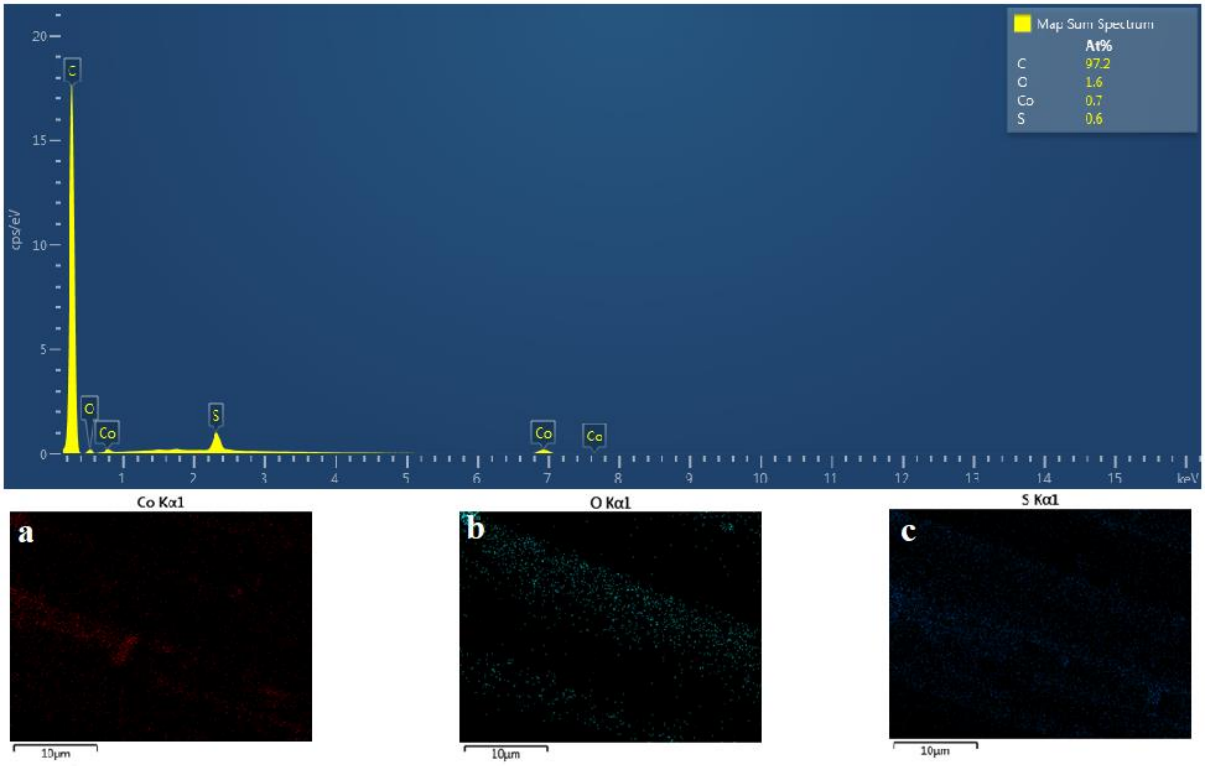

Figure 14: EDX and graph elemental mapping of CoOH/CoSx in sample 1 on CF: a) Cobalt, b) Oxygen and c) Sulfer

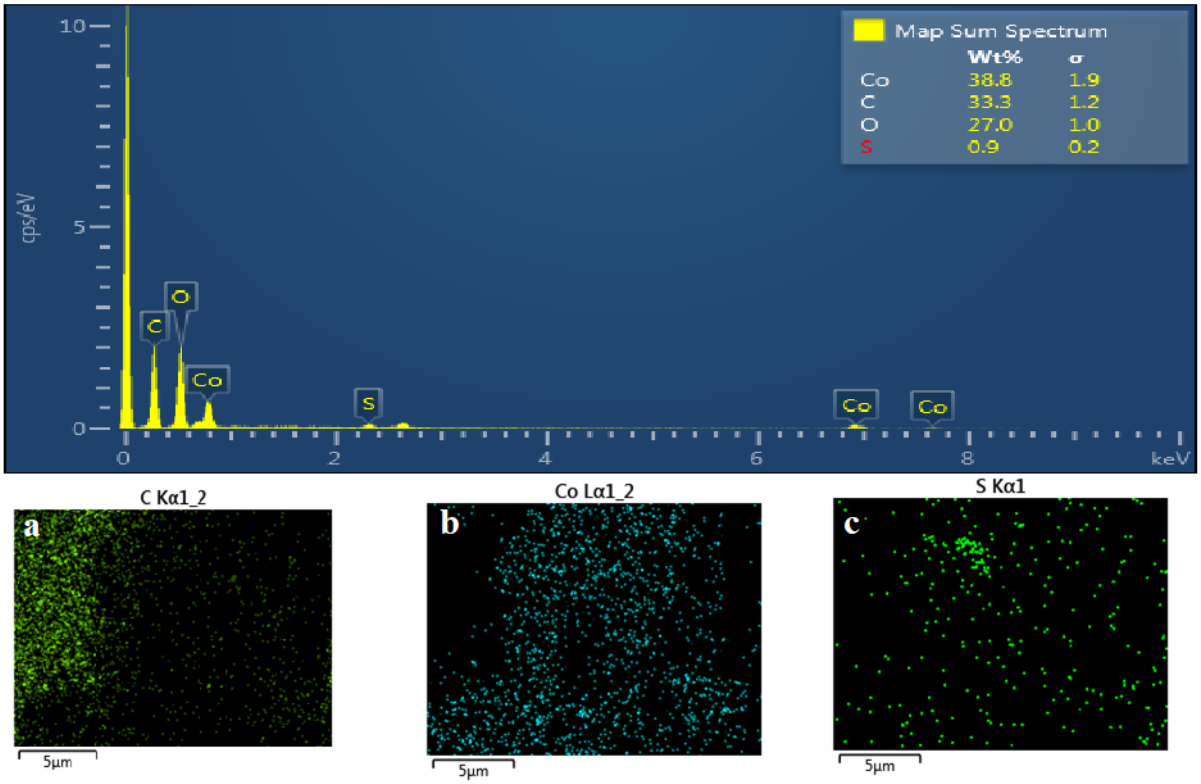

Figure 15: EDX and graph elemental mapping of CoOH/CoSx in sample 2 on CF: a) Carbon, b) Cobalt and c) Sulfer.

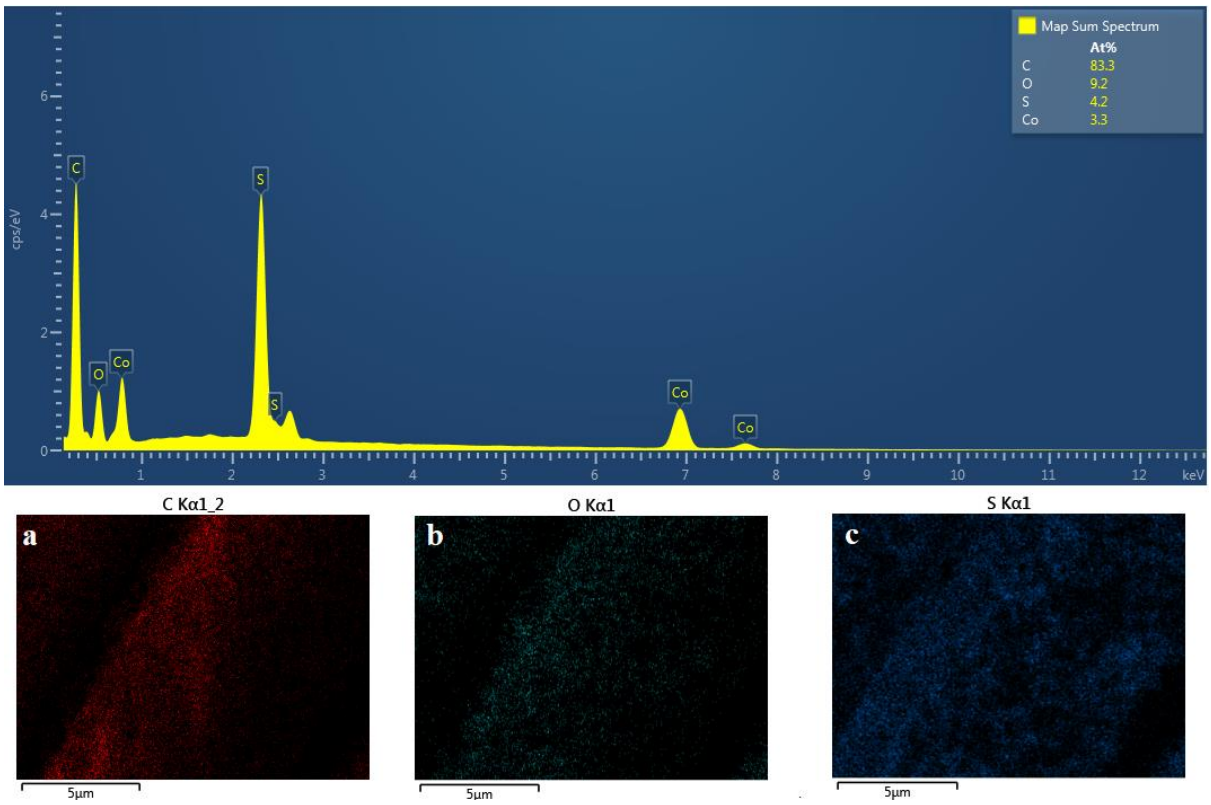

Figure 16: EDX and graph elemental mapping of CoOH/CoSx in sample 3 on CF: a) Carbon, b) Oxygen and c) Sulfer.

The previous figures clearly showing the presence of sulfer, oxygen, cobalt, and carbon atoms within our samples, we can see also an evident spike in concentration of Sulfur as the heterostructure concentration increases in our samples.

Note that as we move chronologically though the samples, we have an indication of a more porous fixation of sulfur on the surface of the cobalt oxide nanowires formed, these images also indicate random fixations on the surface of the nanowires but more concentrated toward the stem of the smooth nanowires rather than the bases.

4.3 X-Ray diffraction analysis:

Using Cu K radiation in the range 2 between 10° and 80°, the crystal structure of CoOH and CoOH/CoSx on CFs was investigated using an X-ray diffractometer.

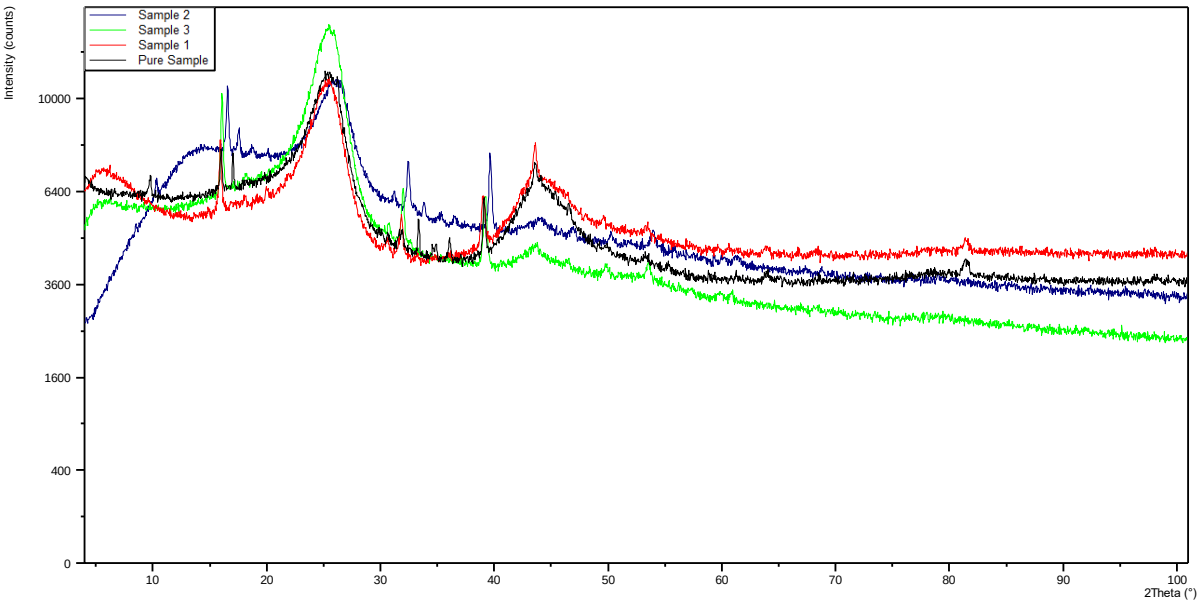

Figure 17: XRD patterns of CoOH shown in black and samples 1-3 of CoOH/CoSx heterostructure shown in Red, Blue, and Green respectively.

It doesn't escape the eye the noise noticed between the angle 20 and 30 for that represents the XRD pattern of our CF, but as shown within the figure w

e start to notice a strong patterns representing the Metallic cobalt present in our samples especially the Cobalt II Oxide CoO notably seen at the peak between 40,50,36 and 42 where the cobalt was found to be cubic in crystallinity and presumed to be face centred cubic. While Cobalt Hydroxide CoOH2 was most notably seen at the peaks between 10 and 20 degrees. The samples with added thiourea during the synthesis step show and a very strong peak resemblance to Linnaeite Co3S4 with a cubic crystalline structure at peaks between 30 and 40 and Alpha sulfer α-S with an orthorhombic crystalline structure conforming with the peaks at 20 and 25.

As we added more thiourea to the hydrothermal reaction mix and as we acquired higher concentrations of sulfer in our samples, we noticed that sulfer takes the shape of a stable polymorph of sulfer (α-S or S-I phase) consisting of 16 crown like with member ring molecules forming an orthorhombic crystalline structure, and the added activity of this addition is but an enhancement to the Oxide amorphous high activity offered by higher specific surface area in a synergistic manner as those crystalline structures offer a high exchange current density.

4.4 Tafel slopes:

Furthermore, comparable Tafel plots taken from the LSV curves were used to explore the kinetics of cobalt oxide cobalt sulfur heterostructures CFs under OER conditions.

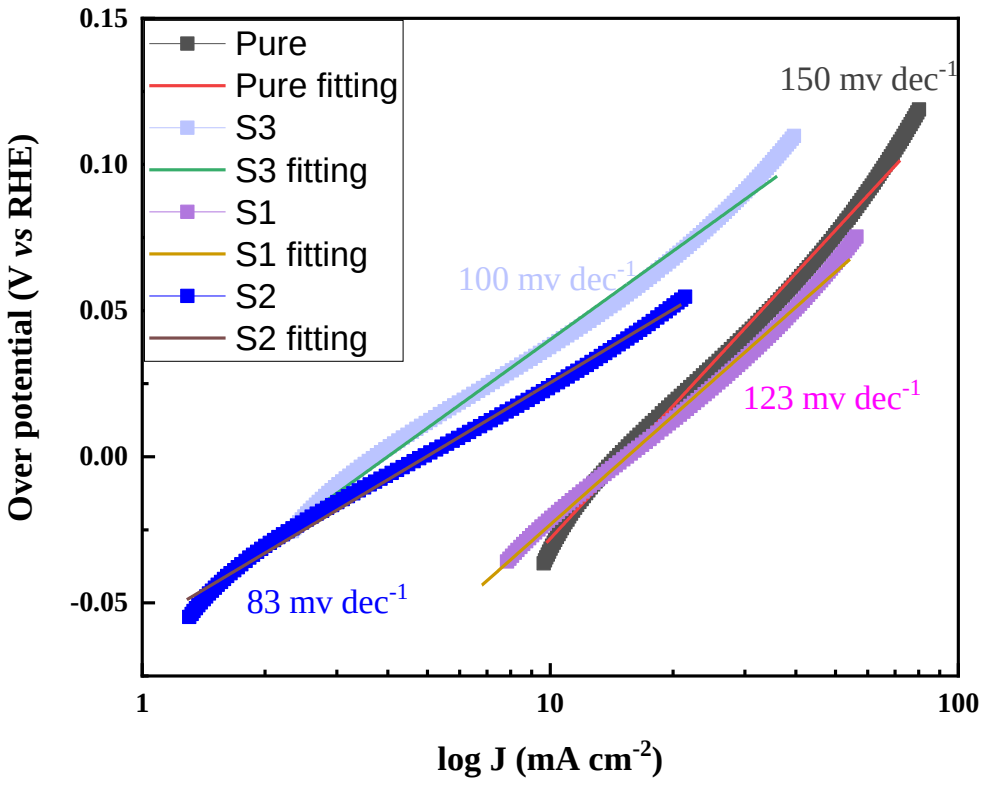

Figure 18: Tafel slopes plot

we were provided with the smallest Tafel slope was of 83 mV dec-1 provided by sample 2 while pure sample had a Tafel slope of 150 mV dec-1, sample 1 of 123 mV dec-1 and sample 3 of 100 mV dec-1.

These Tafel slopes clearly show the synergistic effects of the added heterostructure with the cobalt oxides, where a better activity towards OER electrocatalysis is present within all samples of the heterostructure. But most notably seen is the pattern that represents itself where only a specific concentration of the heterostructure shows a much higher activity than the rest in sample 2 but this activity tends to decline with higher concentrations of the heterostructure, presumed to be the cause of the capping of the heterostructure system where such high levels of CoSx give a blocking effect of the metallic cobalt active sites rendering the synergistic activity quite ineffective. Table showing comparisons of state of art Cobalt based electrochemical catalysts and our work.

Sample name	η10 (mV)	Tafel slope (mV dec-1)	Reference
P.S. CoOH		150	This work
S.1 CoOH/CoSx		123	This work
S.2 CoOH/CoSx		83	This work
S.3 CoOH/CoSx		100	This work
RuO2	380	65	[296]
CPP	200	83	[297]
NCPP	180	82	[297]
Co3O4 NCs	320	116	[298]
Co-P	350	47	[299]
Co@N-C	420	108	[300]

Table 2: Comparison of selected state-of-the-art Co-based OER bifunctional electrocatalysts tested in alkaline media and our work.

4.5 Linear sweep voltammetry measurements:

Catalytic activity toward OER was studied with three-electrode setup by performing an LSV scan shown in figure:

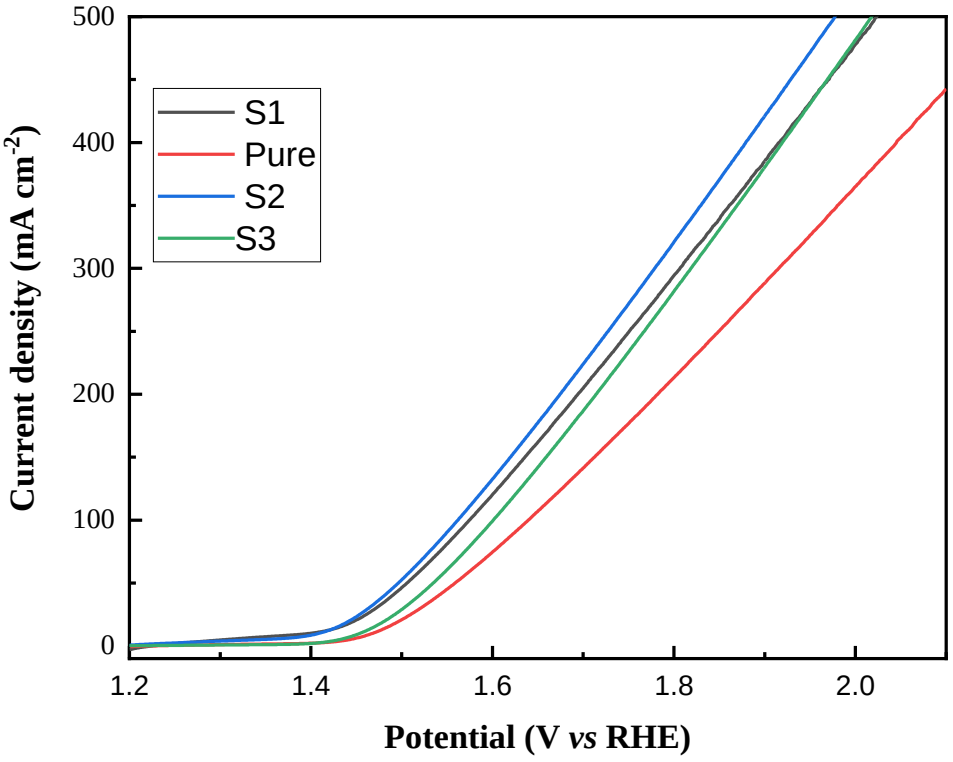

Figure 19: Linear sweep voltammetry measurements

Pure cobalt oxide shows the highest over potential(mV) refereeing to the poor catalytic activity of cobalt oxide based catalysts, but as the heterostructure starts to increase the overpotentials start to be lower showing best activity at Sample 2 (mV), while sample 1 gives an overpotential of(mV) and sample 3 giving an over potential of(mV), this but emphasizes the importance of the heterostructures and how it facilitates an enhanced activity of the electrocatalyst at hand with reaching a maximum value when concentrations are between sample 1 and 3.

4.6 stability test (to be updated)

5. Conclusions

All in all, Cobalt oxide CoOH smooth Nanowires arrays were successfully fabricated on carbon fibers via a calcination process followed by a hydrothermal process, where a cobalt precursor namely cobalt chloride hexahydride and urea were added together and calcinated at 450 °C to form a seed layer then this seed layer was immersed in a Teflon-lined stainless-steel autoclave to form an array of nanowires at 90 °C. the formed Cobalt oxide catalyst showed good electrochemical activity according to our measurements in alkaline conditions for OER catalysis, furthermore we optimized our Cobalt oxide catalyst by forming a heterostructure of cobalt sulfide CoSx with different concentrations of Sulfer by substituting Urea with Thiourea as a precursor for sulfer where only the hydrothermal step was calibrated to a 60 °C. Grown heterostructures showed a rough form on the smooth cobalt oxide nanowires and offered an enhanced synergistic effect towards OER activity by lowering both Tafel slope and overpotential of the pure cobalt oxide nanowires, interestingly, our 3 created heterostructure samples showed a pattern where an optimum value of synergy where reached at sample 2 contrary to lower values at both a lower concentration as well as a high one than sample 2, in detail Sample 2 which carried medium levels of surface roughness heterostructure nanowires based on a CF gave us a Tafel slope of (mV dec-1) and an overpotential of (mV) showing that these heterostructure of earth abundant material offer a promising substitute to noble metal catalysts.

6.Acknowledgments

7.References

[1] N. S. Lewis and D. G. Nocera, “Powering the planet: Chemical challenges in solar energy utilization,” *Proc. Natl. Acad. Sci. U. S. A.*, vol. 103, no. 43, pp. 15729–15735, 2006.

[2] J. Barber, “Photosynthetic energy conversion: Natural and artificial,” *Chem. Soc. Rev.*, vol. 38, no. 1, pp. 185–196, 2009.

[3] S. Dunn, “Hydrogen futures: Toward a sustainable energy system,” *Int. J. Hydrogen Energy*, vol. 27, no. 3, pp. 235–264, 2002.

[4] B. Lim *et al.*, “Pd-Pt bimetallic nanodendrites with high activity for oxygen reduction,” *Science (80-.).*, vol. 324, no. 5932, pp. 1302–1305, 2009.

[5] R. F. de Souza, J. C. Padilha, R. S. Gonçalves, M. O. de Souza, and J. Rault-Berthelot, “Electrochemical hydrogen production from water electrolysis using ionic liquid as electrolytes: Towards the best device,” *J. Power Sources*, vol. 164, no. 2, pp. 792–798, 2007.

[6] D. L. Stojić, M. P. Marčeta, S. P. Sovilj, and Š. S. Miljanić, “Hydrogen generation from water electrolysis - Possibilities of energy saving,” *J. Power Sources*, vol. 118, no. 1–2, pp. 315–319, 2003.

[7] K. Zeng and D. Zhang, “Recent progress in alkaline water electrolysis for hydrogen production and applications,” *Prog. Energy Combust. Sci.*, vol. 36, no. 3, pp. 307–326, 2010.

[8] “1 . 1 Historical Context and Relationship Between Energy.”

[9] J. P. Buchet, A. Denis, J. Desesquelles, and M. Dufay, “Doubly excited states of lithium,” *Phys. Lett. A*, vol. 28, no. 7, pp. 529–530, 1969.

[10] I. Roger, M. A. Shipman, and M. D. Symes, “Earth-abundant catalysts for electrochemical and photoelectrochemical water splitting,” *Nat. Rev. Chem.*, vol. 1, 2017.

[11] K. S. Joya, Y. F. Joya, K. Ocakoglu, and R. Van De Krol, “Water-splitting catalysis and solar fuel devices: Artificial leaves on the move,” *Angew. Chemie - Int. Ed.*, vol. 52, no. 40, pp. 10426–10437, 2013.

[12] E. B. Agyekum, C. Nutakor, A. M. Agwa, and S. Kamel, “A Critical Review of Renewable Hydrogen Production Methods: Factors Affecting Their Scale-Up and Its Role in Future Energy Generation,” *Membranes (Basel).*, vol. 12, no. 2, 2022.

[13] J. D. Holladay, J. Hu, D. L. King, and Y. Wang, “An overview of hydrogen production technologies,” *Catal. Today*, vol. 139, no. 4, pp. 244–260, 2009.

[14] P. Nikolaidis and A. Poullikkas, “A comparative overview of hydrogen production

processes," *Renew. Sustain. Energy Rev.*, vol. 67, pp. 597–611, 2017.

[15] C. Song, "Fuel processing for low-temperature and high-temperature fuel cells: Challenges, and opportunities for sustainable development in the 21st century," *Catal. Today*, vol. 77, no. 1–2, pp. 17–49, 2002.

[16] R. Farrauto *et al.*, "New Material Needs for Hydrocarbon Fuel Processing: Generating Hydrogen for the PEM Fuel Cell," *Annu. Rev. Mater. Res.*, vol. 33, pp. 1–27, 2003.

[17] R. M. Navarro, M. A. Peña, and J. L. G. Fierro, "Hydrogen production reactions from carbon feedstocks: Fossil fuels and biomass," *Chem. Rev.*, vol. 107, no. 10, pp. 3952–3991, 2007.

[18] R. Wilhelm, DJ; Simbeck, DR; Karp, AD; Dickenson, "Syngas production for gas-to-liquids applications: technologies, issues and outlook," in *Syngas production for gas-to-liquids applications: technologies, issues and outlook*, 2001, pp. 139–148.

[19] E. Holladay, J; Jones, E; Palo, DR; Phelps, M; Chin, YH; Dagle, R; Hu, JL; Wang, Y; Baker, "MATERIALS RESEARCH SOCIETY SYMPOSIUM PROCEEDINGS," in *Miniature fuel processors for portable fuel cell power supplies*, 2003, pp. 429–434.

[20] N. Muradov, "Emission-free fuel reformers for mobile and portable fuel cell applications," *J. Power Sources*, vol. 118, no. 1–2, pp. 320–324, 2003.

[21] A. Demirbaş, "Hydrocarbons from pyrolysis and hydrolysis processes of biomass," *Energy Sources*, vol. 25, no. 1, pp. 67–75, 2003.

[22] A. Demirbaş, "Recovery of chemicals and gasoline-range fuels from plastic wastes via pyrolysis," *Energy Sources*, vol. 27, no. 14, pp. 1313–1319, 2005.

[23] T. Hammer, T. Kappes, and M. Baldauf, "Plasma catalytic hybrid processes: Gas discharge initiation and plasma activation of catalytic processes," *Catal. Today*, vol. 89, no. 1–2, pp. 5–14, 2004.

[24] D. Buddhi, R. Kothari, and R. L. Sawhney, "An experimental study on the effect of electrolytic concentration on the rate of hydrogen production," *Int. J. Green Energy*, vol. 3, no. 4, pp. 381–395, 2006.

[25] B. Urban, Y. Shirazi, B. Maddi, S. Viamajala, and S. Varanasi, "Flash Pyrolysis of Oleaginous Biomass in a Fluidized-Bed Reactor," *Energy and Fuels*, vol. 31, no. 8, pp. 8326–8334, 2017.

[26] L. Bromberg, D. R. Cohn, A. Rabinovich, and N. Alexeev, "Plasma catalytic reforming of methane," *Int. J. Hydrogen Energy*, vol. 24, no. 12, pp. 1131–1137, 1999.

[27] T. Paulmier and L. Fulcheri, "Use of non-thermal plasma for hydrocarbon reforming," *Chem. Eng. J.*, vol. 106, no. 1, pp. 59–71, 2005.

[28] R. B. Biniwale, A. Mizuno, and M. Ichikawa, "Hydrogen production by reforming of iso-octane using spray-pulsed injection and effect of non-thermal plasma," *Appl. Catal. A Gen.*, vol. 276, no. 1–2, pp. 169–177, 2004.

[29] N. Boukis, V. Diem, U. Galla, and E. Dinjus, "Methanol reforming in supercritical water for hydrogen production," *Combust. Sci. Technol.*, vol. 178, no. 1–3, pp. 467–485, 2006.

[30] R. R. Davda, J. W. Shabaker, G. W. Huber, R. D. Cortright, and J. A. Dumesic,

"Aqueous-phase reforming of ethylene glycol on silica-supported metal catalysts," *Appl. Catal. B Environ.*, vol. 43, no. 1, pp. 13–26, 2003.

[31] B. Rozmiarek, "2008 DOE Hydrogen Program Hydrogen Generation from Biomass-Derived Carbohydrates via Aqueous-Phase Reforming Process," 2008.

[32] G. W. Huber and J. A. Dumesic, "An overview of aqueous-phase catalytic processes for production of hydrogen and alkanes in a biorefinery," *Catal. Today*, vol. 111, no. 1–2, pp. 119–132, 2006.

[33] T. V Choudhary and D. W. Goodman, "CO-free fuel processing for fuel cell applications Choudhary, T. V. and Goodman, D. W. Catalysis Today, 2002, 77, (1–2), 65–78," *Fuel Energy Abstr.*, vol. 44, no. 4, p. 224, 2003.

[34] A. Wojcik, H. Middleton, I. Damopoulos, and J. Van Herle, "Ammonia as a fuel in solid oxide fuel cells," *J. Power Sources*, vol. 118, no. 1–2, pp. 342–348, 2003.

[35] H. L. Chum and R. P. Overend, "Biomass and renewable fuels," *Fuel Process. Technol.*, vol. 71, no. 1–3, pp. 187–195, 2001.

[36] H. Jacobsen, "'Heterogreeneous' chemistry: Catalysts for hydrogen production from biomass," *Angew. Chemie - Int. Ed.*, vol. 43, no. 15, pp. 1912–1914, 2004.

[37] A. Demirbas, "Combustion characteristics of different biomass fuels," *Prog. Energy Combust. Sci.*, vol. 30, no. 2, pp. 219–230, 2004.

[38] M. F. Demirbas, "Hydrogen from various biomass species via pyrolysis and steam gasification processes," *Energy Sources, Part A Recover. Util. Environ. Eff.*, vol. 28, no. 3, pp. 245–252, 2006.

[39] A. M. HAPIPI, M. A. UDDIN, and Y. KATO, "Carbonization of Sugarcane Bagasse and Heat Transfer Property by Pyrolysis in Superheated Steam and Nitrogen Atmosphere," *J. Japan Inst. Energy*, vol. 97, no. 2, pp. 31–39, 2018.

[40] M. Asadullah, S. I. Ito, K. Kunimori, M. Yamada, and K. Tomishige, "Energy efficient production of hydrogen and syngas from biomass: Development of low-temperature catalytic process for cellulose gasification," *Environ. Sci. Technol.*, vol. 36, no. 20, pp. 4476–4481, 2002.

[41] B. Bálint, Z. Bagi, A. Tóth, G. Rákhely, K. Perei, and K. L. Kovács, "Utilization of keratin-containing biowaste to produce biohydrogen," *Appl. Microbiol. Biotechnol.*, vol. 69, no. 4, pp. 404–410, 2005.

[42] M. D. Redwood and L. E. Macaskie, "A two-stage, two-organism process for biohydrogen from glucose," *Int. J. Hydrogen Energy*, vol. 31, no. 11, pp. 1514–1521, 2006.

[43] J. Sarkar and S. Bhattacharyya, "Application of graphene and graphene-based materials in clean energy-related devices Minghui," *Arch. Thermodyn.*, vol. 33, no. 4, pp. 23–40, 2012.

[44] K. L. Kovács, G. Maróti, and G. Rákhely, "A novel approach for biohydrogen production," *Int. J. Hydrogen Energy*, vol. 31, no. 11, pp. 1460–1468, 2006.

[45] E. Touloupakis and G. Torzillo, *Photobiological hydrogen production*. Elsevier Inc., 2019.

[46] D. B. Levin, L. Pitt, and M. Love, “Biohydrogen production: Prospects and limitations to practical application,” *Int. J. Hydrogen Energy*, vol. 29, no. 2, pp. 173–185, 2004.

[47] D. B. Levin, H. Zhu, M. Beland, N. Cicek, and B. E. Holbein, “Potential for hydrogen and methane production from biomass residues in Canada,” *Bioresour. Technol.*, vol. 98, no. 3, pp. 654–660, 2007.

[48] I. K. Kapdan and F. Kargi, “Bio-hydrogen production from waste materials,” *Enzyme Microb. Technol.*, vol. 38, no. 5, pp. 569–582, 2006.

[49] D. Call and B. E. Logan, “Hydrogen production in a single chamber microbial electrolysis cell lacking a membrane,” *Environ. Sci. Technol.*, vol. 42, no. 9, pp. 3401–3406, 2008.

[50] J. Ditzig, H. Liu, and B. E. Logan, “Production of hydrogen from domestic wastewater using a bioelectrochemically assisted microbial reactor (BEAMR),” *Int. J. Hydrogen Energy*, vol. 32, no. 13, pp. 2296–2304, 2007.

[51] N. S. F. Zina Deretsky, “Microbial Electrolysis Cell,” 2010. [Online]. Available: https://www.nsf.gov/news/mmg/mmg_disp.jsp?med_id=66454.

[52] J. E. Funk, “Thermochemical hydrogen production: Past and present,” *Int. J. Hydrogen Energy*, vol. 26, no. 3, pp. 185–190, 2001.

[53] A. Steinfeld, “Solar thermochemical production of hydrogen - A review,” *Sol. Energy*, vol. 78, no. 5, pp. 603–615, 2005.

[54] D. O. E. Hydrogen, F. Cells, I. Technologies, and J. A. Turner, “Photoelectrochemical Water Systems for H 2 Production,” pp. 250–255, 2005.

[55] J. Akikusa and S. U. M. Khan, “Photoelectrolysis of water to hydrogen in p-SiC/Pt and p-SiC/n-TiO2 cells,” *Int. J. Hydrogen Energy*, vol. 27, no. 9, pp. 863–870, 2002.

[56] V. M. Aroutiounian, V. M. Arakelyan, and G. E. Shahnazaryan, “Metal oxide photoelectrodes for hydrogen generation using solar radiation-driven water splitting,” *Sol. Energy*, vol. 78, no. 5, pp. 581–592, 2005.

[57] G. Hodes, “Quantized nanocrystalline photoelectrodes: A review,” *Sol. Energy Mater. Sol. Cells*, vol. 32, no. 3, p. 323, 1994.

[58] M. Franques, “a P H O T O E L E C T R O D E a R R a Y System for H Y D R O G E N,” no. 4, pp. 243–247, 1991.

[59] M. Grätzel, “Perspectives for dye-sensitized nanocrystalline solar cells,” *Prog. Photovoltaics Res. Appl.*, vol. 8, no. 1, pp. 171–185, 2000.

[60] K. W. Harrison, R. Remick, and G. D. Martin, “Stability Enhancement of Power System With Facts Based Damping Controller Using Bfoa,” *Natl. Renew. Energy Lab.*, vol. 2, no. 1, pp. 6–11, 2014.

[61] J. Pettersson, B. Ramsey, and D. Harrison, “A review of the latest developments in electrodes for unitised regenerative polymer electrolyte fuel cells,” *J. Power Sources*, vol. 157, no. 1, pp. 28–34, 2006.

[62] P. J. Howard and I. Szkoda, “Corrosion resistance of sofc and soec glass-ceramic seal materials in high temperature steam/hydrogen,” *J. Fuel Cell Sci. Technol.*, vol. 9, no. 4, pp. 1–4, 2012.

[63] J. Pan, J. Yang, D. Yan, J. Pu, B. Chi, and J. Li, “Effect of thermal cycling on durability of a solid oxide fuel cell stack with external manifold structure,” *Int. J. Hydrogen Energy*, vol. 45, no. 35, pp. 17927–17934, 2020.

[64] S. Kim *et al.*, “Enhanced reliability of planar-type solid oxide fuel cell stack incorporating leakage gas induction channels,” *Int. J. Hydrogen Energy*, vol. 45, no. 20, pp. 11834–11841, 2020.

[65] H. Janssen, J. C. Bringmann, B. Emonts, and V. Schroeder, “Safety-related studies on hydrogen production in high-pressure electrolysers,” *Int. J. Hydrogen Energy*, vol. 29, no. 7, pp. 759–770, 2004.

[66] C. Koroneos, A. Dompros, G. Roumbas, and N. Moussiopoulos, “Life cycle assessment of hydrogen fuel production processes,” *Int. J. Hydrogen Energy*, vol. 29, no. 14, pp. 1443–1450, 2004.

[67] S. Shiva Kumar and V. Himabindu, “Hydrogen production by PEM water electrolysis – A review,” *Mater. Sci. Energy Technol.*, vol. 2, no. 3, pp. 442–454, 2019.

[68] R. Hino, K. Haga, H. Aita, and K. Sekita, “38. R&D on hydrogen production by high-temperature electrolysis of steam,” *Nucl. Eng. Des.*, vol. 233, no. 1–3, pp. 363–375, 2004.

[69] V. Utgikar and T. Thiesen, “Life cycle assessment of high temperature electrolysis for hydrogen production via nuclear energy,” *Int. J. Hydrogen Energy*, vol. 31, no. 7, pp. 939–944, 2006.

[70] T. R. Ayodele and J. L. Munda, “The potential role of green hydrogen production in the South Africa energy mix,” *J. Renew. Sustain. Energy*, vol. 11, no. 4, 2019.

[71] S. Licht, “Solar water splitting to generate hydrogen fuel - A photothermal electrochemical analysis,” *Int. J. Hydrogen Energy*, vol. 30, no. 5, pp. 459–470, 2005.

[72] G. Tao and M. Homel, “Development of a Novel Efficient Solid-Oxide Hybrid for Co-generation of Hydrogen and Electricity Using Nearby Resources for Local Application,” *US DOE Hydrog. program, FY 2007 Annu. Prog. Rep.*, pp. 82–86, 2007.

[73] W. Yue *et al.*, “Enhancing coking resistance of Ni/YSZ electrodes: In situ characterization, mechanism research, and surface engineering,” *Nano Energy*, vol. 62, no. May, pp. 64–78, 2019.

[74] Y. Naimi and A. Antar, “Hydrogen Generation by Water Electrolysis,” *Adv. Hydrog. Gener. Technol.*, pp. 1–18, 2018.

[75] S. Ardo *et al.*, “Pathways to electrochemical solar-hydrogen technologies,” *Energy Environ. Sci.*, vol. 11, no. 10, pp. 2768–2783, 2018.

[76] X. Zheng *et al.*, “Managing grains and interfaces via ligand anchoring enables 22.3%-efficiency inverted perovskite solar cells,” *Nat. Energy*, vol. 5, no. 2, pp. 131–140, 2020.

[77] B. You and Y. Sun, “Innovative Strategies for Electrocatalytic Water Splitting,” *Acc. Chem. Res.*, vol. 51, no. 7, pp. 1571–1580, 2018.

[78] H. Dau, C. Limberg, T. Reier, M. Risch, S. Roggan, and P. Strasser, “The Mechanism of Water Oxidation: From Electrolysis via Homogeneous to Biological Catalysis,”

ChemCatChem, vol. 2, no. 7, pp. 724–761, 2010.

[79] M. Bekmezci, E. E. Altuner, V. Erduran, R. Bayat, I. Isik, and F. Şen, *Fundamentals of electrochemistry*. 2021.

[80] F. G. Becker *et al.*, *No 主観的健康感を中心とした在宅高齢者における健康関連指標に関する共分散構造分析Title*, vol. 7, no. 1. 2015.

[81] and F. H. T. F. O'Brien, T. V. Bommaraju, *Handbook of Chlor- Alkali Technology*. New York: Springer, 2005.

[82] A. C. de B. V. Dias, "Chlor-Alkali Membrane Cell Process," *Univ. Porto*, pp. 1–213, 2010.

[83] F. Song *et al.*, "An Unconventional Iron Nickel Catalyst for the Oxygen Evolution Reaction," *ACS Cent. Sci.*, vol. 5, no. 3, pp. 558–568, 2019.

[84] A. J. Medford *et al.*, "From the Sabatier principle to a predictive theory of transition-metal heterogeneous catalysis," *J. Catal.*, vol. 328, pp. 36–42, 2015.

[85] C. N. Brodsky *et al.*, "In situ characterization of cofacial Co(IV) centers in Co4O4 cubane: Modeling the high-valent active site in oxygen-evolving catalysts," *Proc. Natl. Acad. Sci. U. S. A.*, vol. 114, no. 15, pp. 3855–3860, 2017.

[86] G. T. Burstein, "A hundred years of Tafel's Equation: 1905-2005," *Corros. Sci.*, vol. 47, no. 12, pp. 2858–2870, 2005.

[87] B. Hinnemann *et al.*, "Ja0504690-1.Pdf," *J. Am. Chem. Soc.*, vol. 127, pp. 5308–5309, 2005.

[88] W. I. Choi, B. C. Wood, E. Schwegler, and T. Ogitsu, "Site-dependent free energy barrier for proton reduction on MoS2 edges," *J. Phys. Chem. C*, vol. 117, no. 42, pp. 21772–21777, 2013.

[89] C. C. L. McCrory, S. Jung, I. M. Ferrer, S. M. Chatman, J. C. Peters, and T. F. Jaramillo, "Benchmarking Hydrogen Evolving Reaction and Oxygen Evolving Reaction Electrocatalysts for Solar Water Splitting Devices," *J. Am. Chem. Soc.*, vol. 137, no. 13, pp. 4347–4357, 2015.

[90] S. Anantharaj *et al.*, "Precision and correctness in the evaluation of electrocatalytic water splitting: Revisiting activity parameters with a critical assessment," *Energy Environ. Sci.*, vol. 11, no. 4, pp. 744–771, 2018.

[91] M. R. Gao *et al.*, "An efficient molybdenum disulfide/cobalt diselenide hybrid catalyst for electrochemical hydrogen generation," *Nat. Commun.*, vol. 6, 2015.

[92] X. Lu and C. Zhao, "Electrodeposition of hierarchically structured three-dimensional nickel-iron electrodes for efficient oxygen evolution at high current densities," *Nat. Commun.*, vol. 6, 2015.

[93] Z. Lu *et al.*, "Three-dimensional NiFe layered double hydroxide film for high-efficiency oxygen evolution reaction," *Chem. Commun.*, vol. 50, no. 49, pp. 6479–6482, 2014.

[94] R. D. L. Smith *et al.*, "Photochemical route for accessing amorphous metal oxide materials for water oxidation catalysis," *Science (80-.).*, vol. 340, no. 6128, pp. 60–63,

2013.

[95] H. Deng *et al.*, "Evolution Reaction Catalysts," *J. Mater. Chem. A Mater. energy Sustain.*, vol. 4, no. 6303, pp. 6824–6830, 2016.

[96] P. Zhang *et al.*, "Dendritic core-shell nickel-iron-copper metal/metal oxide electrode for efficient electrocatalytic water oxidation," *Nat. Commun.*, vol. 9, no. 1, pp. 1–10, 2018.

[97] Y. Jiao, Y. Zheng, M. Jaroniec, and S. Z. Qiao, "Design of electrocatalysts for oxygen- and hydrogen-involving energy conversion reactions," *Chem. Soc. Rev.*, vol. 44, no. 8, pp. 2060–2086, 2015.

[98] J. Masa *et al.*, "Amorphous Cobalt Boride (Co 2 B) as a Highly Efficient Nonprecious Catalyst for Electrochemical Water Splitting: Oxygen and Hydrogen Evolution," *Adv. Energy Mater.*, vol. 6, no. 6, pp. 1–10, 2016.

[99] M. Tahir *et al.*, "Electrocatalytic oxygen evolution reaction for energy conversion and storage: A comprehensive review," *Nano Energy*, vol. 37, pp. 136–157, 2017.

[100] Y. Lee, J. Suntivich, K. J. May, E. E. Perry, and Y. Shao-Horn, "Synthesis and activities of rutile IrO 2 and RuO 2 nanoparticles for oxygen evolution in acid and alkaline solutions," *J. Phys. Chem. Lett.*, vol. 3, no. 3, pp. 399–404, 2012.

[101] T. Reier, M. Oezaslan, and P. Strasser, "Electrocatalytic oxygen evolution reaction (OER) on Ru, Ir, and pt catalysts: A comparative study of nanoparticles and bulk materials," *ACS Catal.*, vol. 2, no. 8, pp. 1765–1772, 2012.

[102] M. Oezaslan, F. Hasché, and P. Strasser, "Pt-based core-shell catalyst architectures for oxygen fuel cell electrodes," *J. Phys. Chem. Lett.*, vol. 4, no. 19, pp. 3273–3291, 2013.

[103] S. Chen and S. Z. Qiao, "Hierarchically porous nitrogen-doped graphene-NiCo2O4 Hybrid Paper as an advanced electrocatalytic water-splitting material," *ACS Nano*, vol. 7, no. 11, pp. 10190–10196, 2013.

[104] E. Detsi *et al.*, "Mesoporous Ni60Fe30Mn10-alloy based metal/metal oxide composite thick films as highly active and robust oxygen evolution catalysts," *Energy Environ. Sci.*, vol. 9, no. 2, pp. 540–549, 2016.

[105] X. Huang, S. Chang, W. S. V. Lee, J. Ding, and J. M. Xue, "Three-dimensional printed cellular stainless steel as a high-activity catalytic electrode for oxygen evolution," *J. Mater. Chem. A*, vol. 5, no. 34, pp. 18176–18182, 2017.

[106] S. Chang *et al.*, "High loading accessible active sites: Via designable 3D-printed metal architecture towards promoting electrocatalytic performance," *J. Mater. Chem. A*, vol. 7, no. 31, pp. 18338–18347, 2019.

[107] W. Chen *et al.*, "In Situ Electrochemically Derived Nanoporous Oxides from Transition Metal Dichalcogenides for Active Oxygen Evolution Catalysts," *Nano Lett.*, vol. 16, no. 12, pp. 7588–7596, 2016.

[108] S. H. Ye, Z. X. Shi, J. X. Feng, Y. X. Tong, and G. R. Li, "Activating CoOOH Porous Nanosheet Arrays by Partial Iron Substitution for Efficient Oxygen Evolution Reaction," *Angew. Chemie - Int. Ed.*, vol. 57, no. 10, pp. 2672–2676, 2018.

[109] J. Zhao *et al.*, "Ultra-thin wrinkled NiOOH-NiCr2O4 nanosheets on Ni foam: an

advanced catalytic electrode for oxygen evolution reaction," *Chem. Commun.*, vol. 54, no. 39, pp. 4987–4990, 2018.

[110] X. Shang, B. Dong, Y. M. Chai, and C. G. Liu, "In-situ electrochemical activation designed hybrid electrocatalysts for water electrolysis," *Sci. Bull.*, vol. 63, no. 13, pp. 853–876, 2018.

[111] Y. Pi, N. Zhang, S. Guo, J. Guo, and X. Huang, "Ultrathin laminar Ir superstructure as highly efficient oxygen evolution electrocatalyst in broad pH range," *Nano Lett.*, vol. 16, no. 7, pp. 4424–4430, 2016.

[112] L. Yuan, Z. Yan, L. Jiang, E. Wang, S. Wang, and G. Sun, "Gold-iridium bifunctional electrocatalyst for oxygen reduction and oxygen evolution reactions," *J. Energy Chem.*, vol. 25, no. 5, pp. 805–810, 2016.

[113] R. Frydendal *et al.*, "Benchmarking the Stability of Oxygen Evolution Reaction Catalysts: The Importance of Monitoring Mass Losses," *ChemElectroChem*, vol. 1, no. 12, pp. 2075–2081, 2014.

[114] S. Cherevko *et al.*, "Oxygen and hydrogen evolution reactions on Ru, RuO2, Ir, and IrO2 thin film electrodes in acidic and alkaline electrolytes: A comparative study on activity and stability," *Catal. Today*, vol. 262, pp. 170–180, 2016.

[115] L. Xu *et al.*, "Plasma-Engraved Co3O4 Nanosheets with Oxygen Vacancies and High Surface Area for the Oxygen Evolution Reaction," *Angew. Chemie - Int. Ed.*, vol. 55, no. 17, pp. 5277–5281, 2016.

[116] A. Mendoza-Garcia *et al.*, "Controlled Anisotropic Growth of Co-Fe-P from Co-Fe-O Nanoparticles," *Angew. Chemie - Int. Ed.*, vol. 54, no. 33, pp. 9642–9645, 2015.

[117] H. Y. Wang, Y. Y. Hsu, R. Chen, T. S. Chan, H. M. Chen, and B. Liu, "Ni3+-induced formation of active NiOOH on the spinel Ni-Co oxide surface for efficient oxygen evolution reaction," *Adv. Energy Mater.*, vol. 5, no. 10, pp. 1–8, 2015.

[118] M. Gong *et al.*, "An advanced Ni-Fe layered double hydroxide electrocatalyst for water oxidation," *J. Am. Chem. Soc.*, vol. 135, no. 23, pp. 8452–8455, 2013.

[119] L. Trotochaud, S. L. Young, J. K. Ranney, and S. W. Boettcher, "Nickel-Iron oxyhydroxide oxygen-evolution electrocatalysts: The role of intentional and incidental iron incorporation," *J. Am. Chem. Soc.*, vol. 136, no. 18, pp. 6744–6753, 2014.

[120] Y. Surendranath, M. W. Kanan, and D. G. Nocera, "Mechanistic studies of the oxygen evolution reaction by a cobalt-phosphate catalyst at neutral pH," *J. Am. Chem. Soc.*, vol. 132, no. 46, pp. 16501–16509, 2010.

[121] M. Serhan *et al.*, "Total iron measurement in human serum with a smartphone," *AIChE Annu. Meet. Conf. Proc.*, vol. 2019-Novem, 2019.

[122] W. Zhou *et al.*, "Ni3S2 nanorods/Ni foam composite electrode with low overpotential for electrocatalytic oxygen evolution," *Energy Environ. Sci.*, vol. 6, no. 10, pp. 2921–2924, 2013.

[123] C. Tang, N. Cheng, Z. Pu, W. Xing, and X. Sun, "NiSe Nanowire Film Supported on Nickel Foam: An Efficient and Stable 3D Bifunctional Electrode for Full Water Splitting," *Angew. Chemie - Int. Ed.*, vol. 54, no. 32, pp. 9351–9355, 2015.

[124] J. A. Haber, C. Xiang, D. Guevarra, S. Jung, J. Jin, and J. M. Gregoire, "High-Throughput Mapping of the Electrochemical Properties of (Ni-Fe-Co-Ce)Ox Oxygen-Evolution Catalysts," *ChemElectroChem*, vol. 1, no. 3, pp. 524–528, 2014.

[125] R. D. L. Smith, M. S. Prévot, R. D. Fagan, S. Trudel, and C. P. Berlinguette, "Water oxidation catalysis: Electrocatalytic response to metal stoichiometry in amorphous metal oxide films containing iron, cobalt, and nickel," *J. Am. Chem. Soc.*, vol. 135, no. 31, pp. 11580–11586, 2013.

[126] S. Enthaler, K. Junge, and M. Beller, "Sustainable metal catalysis with iron: From rust to a rising star?," *Angew. Chemie - Int. Ed.*, vol. 47, no. 18, pp. 3317–3321, 2008.

[127] Y. Wu *et al.*, "Fast and simple preparation of iron-based thin films as highly efficient water-oxidation catalysts in neutral aqueous solution," *Angew. Chemie - Int. Ed.*, vol. 54, no. 16, pp. 4870–4875, 2015.

[128] X. Xu, X. Tian, Z. Zhong, L. Kang, and J. Yao, "In-situ growth of iron/nickel phosphides hybrid on nickel foam as bifunctional electrocatalyst for overall water splitting," *J. Power Sources*, vol. 424, no. March, pp. 42–51, 2019.

[129] Z. Xu, H. Pan, Y. Lin, Z. Yang, J. Wang, and Y. Gong, "Constructing a hexagonal copper-coin-shaped NiCoSe2@NiO@CoNi2S4@CoS2 hybrid nanoarray on nickel foam as a robust oxygen evolution reaction electrocatalyst," *J. Mater. Chem. A*, vol. 6, no. 38, pp. 18641–18648, 2018.

[130] X. Zheng *et al.*, "In Situ Fabrication of Heterostructure on Nickel Foam with Tuned Composition for Enhancing Water-Splitting Performance," *Small*, vol. 14, no. 50, pp. 1–10, 2018.

[131] W. Chen *et al.*, "In situ electrochemical oxidation tuning of transition metal disulfides to oxides for enhanced water oxidation," *ACS Cent. Sci.*, vol. 1, no. 5, pp. 244–251, 2015.

[132] J. B. Gerken, S. E. Shaner, R. C. Massé, N. J. Porubsky, and S. S. Stahl, "A survey of diverse earth abundant oxygen evolution electrocatalysts showing enhanced activity from Ni-Fe oxides containing a third metal," *Energy Environ. Sci.*, vol. 7, no. 7, pp. 2376–2382, 2014.

[133] J. G. Mcalpin *et al.*, "Ja1013344.Pdf," *J. Am. Chem. Soc.*, vol. 4, no. Iv, pp. 6882–6883, 2010.

[134] L. Wang, Y. Jiao, S. Yao, P. Li, R. Wang, and G. Chen, "MOF-derived NiO/Ni architecture encapsulated into N-doped carbon nanotubes for advanced asymmetric supercapacitors," *Inorg. Chem. Front.*, vol. 6, no. 6, pp. 1553–1560, 2019.

[135] T. A. Shifa *et al.*, "In Situ-Generated Oxide in Sn-Doped Nickel Phosphide Enables Ultrafast Oxygen Evolution," *ACS Catal.*, vol. 11, no. 8, pp. 4520–4529, 2021.

[136] J. Huang *et al.*, "CoOOH Nanosheets with High Mass Activity for Water Oxidation," *Angew. Chemie - Int. Ed.*, vol. 54, no. 30, pp. 8722–8727, 2015.

[137] W. Yuan, M. Zhao, J. Yuan, and C. M. Li, "Ni foam supported three-dimensional vertically aligned and networked layered CoO nanosheet/graphene hybrid array as a high-performance oxygen evolution electrode," *J. Power Sources*, vol. 319, pp. 159–167, 2016.

[138] L. Yang, H. Xu, H. Liu, D. Cheng, and D. Cao, “Active Site Identification and Evaluation Criteria of In Situ Grown CoTe and NiTe Nanoarrays for Hydrogen Evolution and Oxygen Evolution Reactions,” *Small Methods*, vol. 3, no. 5, pp. 1–11, 2019.

[139] C. Huang *et al.*, “Recent progress and perspective of cobalt-based catalysts for water splitting: design and nanoarchitectonics,” *Mater. Today Energy*, vol. 23, p. 100911, 2022.

[140] H. Maros and S. Juniar, “済無No Title No Title No Title,” vol. 17, pp. 1–23, 2016.

[141] X. Wen, X. Yang, M. Li, L. Bai, and J. Guan, “Co/CoOx nanoparticles inlaid onto nitrogen-doped carbon-graphene as a trifunctional electrocatalyst,” *Electrochim. Acta*, vol. 296, pp. 830–841, 2019.

[142] D. T. Tran, H. T. Le, T. L. Luyen Doan, N. H. Kim, and J. H. Lee, “Pt nanodots monolayer modified mesoporous Cu@Cu x O nanowires for improved overall water splitting reactivity,” *Nano Energy*, vol. 59, pp. 216–228, 2019.

[143] G. Shi *et al.*, “Stabilization of cobalt clusters with graphdiyne enabling efficient overall water splitting,” *Nano Energy*, vol. 74, p. 104852, 2020.

[144] G. M. Pereira, T. S. P. Cellet, R. H. Gonçalves, A. F. Rubira, and R. Silva, “Trapped metallic cobalt nanoparticles in doped porous graphite: An electrocatalyst that gets better over reaction time,” *Appl. Catal. B Environ.*, vol. 217, pp. 144–153, 2017.

[145] H. Guo *et al.*, “Cobalt nanoparticle-embedded nitrogen-doped carbon/carbon nanotube frameworks derived from a metal-organic framework for tri-functional ORR, OER and HER electrocatalysis,” *J. Mater. Chem. A*, vol. 7, no. 8, pp. 3664–3672, 2019.

[146] J. Omran, B. Firwana, A. Al-Dadah, and M. Alpert, “Relation of Obesity To Ventricular Repolarization: a Meta-Analysis of Clinical Studies,” *J. Am. Coll. Cardiol.*, vol. 65, no. 10, p. A337, 2015.

[147] P. Ball, “Single-atom catalysis: a new field that learns from tradition,” *Natl. Sci. Rev.*, vol. 5, no. 5, pp. 690–693, 2018.

[148] D. Zhao *et al.*, “Atomic site electrocatalysts for water splitting, oxygen reduction and selective oxidation,” *Chem. Soc. Rev.*, vol. 49, no. 7, pp. 2215–2264, 2020.

[149] N. Li *et al.*, “Phase-mediated robust interfacial electron-coupling over core-shell Co@carbon towards superior overall water splitting,” *Appl. Catal. B Environ.*, vol. 266, 2020.

[150] F. Niu, D. Wang, F. Li, Y. Liu, S. Shen, and T. J. Meyer, “Hybrid Photoelectrochemical Water Splitting Systems: From Interface Design to System Assembly,” *Adv. Energy Mater.*, vol. 10, no. 11, pp. 1–24, 2020.

[151] K. N. Dinh *et al.*, “Nanostructured metallic transition metal carbides, nitrides, phosphides, and borides for energy storage and conversion,” *Nano Today*, vol. 25, pp. 99–121, 2019.

[152] B. Liu *et al.*, “In situ nitridated porous nanosheet networked Co 3 O 4 -Co 4 N heteronanostructures supported on hydrophilic carbon cloth for highly efficient electrochemical hydrogen evolution,” *J. Mater. Chem. A*, vol. 7, no. 2, pp. 775–782,

2019.

[153] J. Mohammed-Ibrahim and S. Xiaoming, “Recent progress on earth abundant electrocatalysts for hydrogen evolution reaction (HER) in alkaline medium to achieve efficient water splitting – A review,” *J. Energy Chem.*, vol. 34, pp. 111–160, 2019.

[154] M. Zhao *et al.*, “Electrochemical Phase Evolution of Metal-Based Pre-Catalysts for High-Rate Polysulfide Conversion,” *Adv. Mater.*, vol. 59, no. 23, pp. 9096–9102, 2020.

[155] Y. Pan *et al.*, “Core-Shell ZIF-8@ZIF-67-Derived CoP Nanoparticle-Embedded N-Doped Carbon Nanotube Hollow Polyhedron for Efficient Overall Water Splitting,” *J. Am. Chem. Soc.*, vol. 140, no. 7, pp. 2610–2618, 2018.

[156] P. Xiao, W. Chen, and X. Wang, “A Review of Phosphide-Based Materials for Electrocatalytic Hydrogen Evolution,” *Adv. Energy Mater.*, vol. 5, no. 24, pp. 1–13, 2015.

[157] W. Li *et al.*, “Encapsulating hollow (Co,Fe)P nanoframes into N,P-codoped graphene aerogel for highly efficient water splitting,” *J. Power Sources*, vol. 456, no. March, 2020.

[158] N. K. Oh *et al.*, “In-situ local phase-transitioned MoSe 2 in La 0.5 Sr 0.5 CoO 3-δ heterostructure and stable overall water electrolysis over 1000 hours,” *Nat. Commun.*, vol. 10, no. 1, pp. 1–12, 2019.

[159] D. Chen *et al.*, “Ru-doped 3D flower-like bimetallic phosphide with a climbing effect on overall water splitting,” *Appl. Catal. B Environ.*, vol. 279, no. August, p. 119396, 2020.

[160] J. Wu *et al.*, “Controllable Heteroatom Doping Effects of Cr xCo2-xP Nanoparticles: A Robust Electrocatalyst for Overall Water Splitting in Alkaline Solutions,” *ACS Appl. Mater. Interfaces*, vol. 12, no. 42, pp. 47397–47407, 2020.

[161] Y. Li *et al.*, “Bifunctional Porous Cobalt Phosphide Foam for High-Current-Density Alkaline Water Electrolysis with 4000-h Long Stability,” *ACS Sustain. Chem. Eng.*, vol. 8, no. 27, pp. 10193–10200, 2020.

[162] Y. Tong, Q. Sun, P. Chen, L. Chen, Z. Fei, and P. J. Dyson, “Nitrogen-Incorporated Cobalt Sulfide/Graphene Hybrid Catalysts for Overall Water Splitting,” *ChemSusChem*, vol. 13, no. 18, pp. 5112–5118, 2020.

[163] H. Lu, Y. Zhang, Y. Huang, C. Zhang, and T. Liu, “Reaction Packaging CoSe 2 Nanoparticles in N-Doped Carbon Polyhedra with Bifunctionality for Overall Water Splitting,” *ACS Appl. Mater. Interfaces*, vol. 11, no. 3, pp. 3372–3381, 2019.

[164] X. Wu *et al.*, “Metal Organic Framework Derived Fe-Doped CoSe2 Incorporated in Nitrogen-Doped Carbon Hybrid for Efficient Hydrogen Evolution,” *ACS Sustain. Chem. Eng.*, vol. 6, no. 7, pp. 8672–8678, 2018.

[165] C. Tomon *et al.*, “Enhancing bifunctional electrocatalysts of hollow Co3O4 nanorods with oxygen vacancies towards ORR and OER for Li–O2 batteries,” *Electrochim. Acta*, vol. 367, p. 137490, 2021.

[166] K. K. Hazarika, Y. Yamada, E. V. Matus, M. Kerzhentsev, and P. Bharali, “Enhancing the electrocatalytic activity via hybridization of Cu(I/II) oxides with Co3O4 towards

oxygen electrode reactions," *J. Power Sources*, vol. 490, no. October 2020, p. 229511, 2021.

[167] Y. Pan, H. Ren, R. Chen, Y. Wu, and D. Chu, "Enhanced electrocatalytic oxygen evolution by manipulation of electron transfer through cobalt-phosphorous bridging," *Chem. Eng. J.*, vol. 398, p. 125660, 2020.

[168] Z. Liu *et al.*, "Charge redistribution of Ru nanoclusters on Co3O4 porous nanowire via the oxygen regulation for enhanced hydrogen evolution reaction," *Nano Energy*, vol. 85, no. March, p. 105940, 2021.

[169] J. Hao, W. Wu, Q. Wang, D. Yan, G. Liu, and S. Peng, "Effect of grain size on electrochemical performance and kinetics of Co3O4 electrode materials," *J. Mater. Chem. A*, vol. 8, no. 15, pp. 7192–7196, 2020.

[170] Y. Yan *et al.*, "Substitutionally Dispersed High-Oxidation CoOx Clusters in the Lattice of Rutile TiO2 Triggering Efficient Co-Ti Cooperative Catalytic Centers for Oxygen Evolution Reactions," *Adv. Funct. Mater.*, vol. 31, no. 9, pp. 1–13, 2021.

[171] J. Wang *et al.*, "Earth-abundant transition-metal-based bifunctional catalysts for overall electrochemical water splitting: A review," *J. Alloys Compd.*, vol. 819, p. 153346, 2020.

[172] Z. J. Wang, M. X. Jin, L. Zhang, A. J. Wang, and J. J. Feng, "Amorphous 3D pomegranate-like NiCoFe nanoassemblies derived by bi-component cyanogel reduction for outstanding oxygen evolution reaction," *J. Energy Chem.*, vol. 53, pp. 260–267, 2020.

[173] H. Sun, J. Dai, W. Zhou, and Z. Shao, "Emerging Strategies for Developing High-Performance Perovskite-Based Materials for Electrochemical Water Splitting," *Energy and Fuels*, vol. 34, no. 9, pp. 10547–10567, 2020.

[174] P. Rekha, S. Yadav, and L. Singh, "A review on cobalt phosphate-based materials as emerging catalysts for water splitting," *Ceram. Int.*, vol. 47, no. 12, pp. 16385–16401, 2021.

[175] W. Li, Y. Chen, B. Yu, Y. Hu, X. Wang, and D. Yang, "3D hollow Co-Fe-P nanoframes immobilized on N,P-doped CNT as an efficient electrocatalyst for overall water splitting," *Nanoscale*, vol. 11, no. 36, pp. 17031–17040, 2019.

[176] H. Xie, F. Chen, A. Nie, T. Pu, M. Rehwoldt, and D. Yu, "Carbothermal shock synthesis of high-entropy-alloy nanoparticles[J]. 2018, 1494(March): 1489–1494.ermal shock synthesis of high-entropy-alloy nanoparticles," vol. 1494, no. March, pp. 1489–1494, 2018.

[177] H. J. Qiu *et al.*, "Nanoporous high-entropy alloys for highly stable and efficient catalysts," *J. Mater. Chem. A*, vol. 7, no. 11, pp. 6499–6506, 2019.

[178] T. A. A. Batchelor, J. K. Pedersen, S. H. Winther, I. E. Castelli, K. W. Jacobsen, and J. Rossmeisl, "High-Entropy Alloys as a Discovery Platform for Electrocatalysis," *Joule*, vol. 3, no. 3, pp. 834–845, 2019.

[179] H. Liu *et al.*, "Free-standing nanoporous NiMnFeMo alloy: An efficient non-precious metal electrocatalyst for water splitting," *Chem. Eng. J.*, vol. 404, p. 126530, 2021.

[180] Z. Jin *et al.*, "Nanoporous Al-Ni-Co-Ir-Mo High-Entropy Alloy for Record-High

Water Splitting Activity in Acidic Environments," *Small*, vol. 15, no. 47, pp. 1–7, 2019.

[181] Y. Xin *et al.*, "High-Entropy Alloys as a Platform for Catalysis: Progress, Challenges, and Opportunities," *ACS Catal.*, vol. 10, no. 19, pp. 11280–11306, 2020.

[182] Y. K. Lee, "Density functional theory (Dft) calculations and catalysis," *Catalysts*, vol. 11, no. 4, pp. 10–12, 2021.

[183] N. J. Nilsson A, Pettersson LG, *Chemical bonding at surfaces and interfaces.* Amsterdam: Elsevier, 2008.

[184] B. M. Anderson JR, *Catalysis science and technology.* New York: Springer, 1987.

[185] G. Ertl, "Surface Science and Catalysis—Studies on the Mechanism of Ammonia Synthesis: The P. H. Emmett Award Address," *Catal. Rev.*, vol. 21, no. 2, pp. 201–223, 1980.

[186] J. Greeley, J. K. Nørskov, and M. Mavrikakis, "Electronic structure and catalysis on metal surfaces," *Annu. Rev. Phys. Chem.*, vol. 53, pp. 319–348, 2002.

[187] R. Schlögl and S. B. Abd Hamid, "Nanocatalysis: Mature science revisited of something really new?," *Angew. Chemie - Int. Ed.*, vol. 43, no. 13, pp. 1628–1637, 2004.

[188] S. Vajda *et al.*, "Subnanometre platinum clusters as highly active and selective catalysts for the oxidative dehydrogenation of propane," *Nat. Mater.*, vol. 8, no. 3, pp. 213–216, 2009.

[189] K. Yamamoto *et al.*, "Size-specific catalytic activity of platinum clusters enhances oxygen reduction reactions," *Nat. Chem.*, vol. 1, no. 5, pp. 397–402, 2009.

[190] M. Valden, X. Lai, and D. W. Goodman, "Onset of catalytic activity of gold clusters on titania with the appearance of nonmetallic properties," *Science (80-.).*, vol. 281, no. 5383, pp. 1647–1650, 1998.

[191] X. Xie, Y. Li, Z. Q. Liu, M. Haruta, and W. Shen, "Low-temperature oxidation of CO catalysed by Co 3 O 4 nanorods," *Nature*, vol. 458, no. 7239, pp. 746–749, 2009.

[192] H. Wei *et al.*, "FeO x -supported platinum single-atom and pseudo-single-atom catalysts for chemoselective hydrogenation of functionalized nitroarenes," *Nat. Commun.*, vol. 5, no. 457, pp. 1–8, 2014.

[193] S. Matar, M. J. Mirbach, and H. A. Tayim, "Catalytic Oxidation Reactions," *Catal. Petrochemical Process.*, vol. XXX, no. Xx, pp. 84–108, 1989.

[194] X. Pan and X. Bao, "The effects of confinement inside carbon nanotubes on catalysis," *Acc. Chem. Res.*, vol. 44, no. 8, pp. 553–562, 2011.

[195] J. Sun *et al.*, "Toward monodispersed silver nanoparticles with unusual thermal stability," *J. Am. Chem. Soc.*, vol. 128, no. 49, pp. 15756–15764, 2006.

[196] J. Yu *et al.*, "Designing the Bending Stiffness of 2D Material Heterostructures," *Adv. Mater.*, vol. 33, no. 9, pp. 1–8, 2021.

[197] Y. Wang, J. Mao, X. Meng, L. Yu, D. Deng, and X. Bao, "Catalysis with Two-Dimensional Materials Confining Single Atoms: Concept, Design, and Applications,"

Chem. Rev., vol. 119, no. 3, pp. 1806–1854, 2019.

[198] P. Yu *et al.*, "Earth abundant materials beyond transition metal dichalcogenides: A focus on electrocatalyzing hydrogen evolution reaction," *Nano Energy*, vol. 58, no. December 2018, pp. 244–276, 2019.

[199] B. Zhang *et al.*, "Defect-Rich 2D Material Networks for Advanced Oxygen Evolution Catalysts," *ACS Energy Lett.*, vol. 4, no. 1, pp. 328–336, 2019.

[200] Q. Wang, Y. Lei, D. Wang, and Y. Li, "Defect engineering in earth-abundant electrocatalysts for CO2 and N2 reduction," *Energy Environ. Sci.*, vol. 12, no. 6, pp. 1730–1750, 2019.

[201] S. Shit *et al.*, "Cobalt Sulfide/Nickel Sulfide Heterostructure Directly Grown on Nickel Foam: An Efficient and Durable Electrocatalyst for Overall Water Splitting Application," *ACS Appl. Mater. Interfaces*, vol. 10, no. 33, pp. 27712–27722, 2018.

[202] G. Fu *et al.*, "Boosting Bifunctional Oxygen Electrocatalysis with 3D Graphene Aerogel-Supported Ni/MnO Particles," *Adv. Mater.*, vol. 30, no. 5, pp. 1–10, 2018.

[203] Y. Yang *et al.*, "A Universal Strategy for Intimately Coupled Carbon Nanosheets/MoM Nanocrystals (M = P, S, C, and O) Hierarchical Hollow Nanospheres for Hydrogen Evolution Catalysis and Sodium-Ion Storage," *Adv. Mater.*, vol. 30, no. 18, pp. 1–8, 2018.

[204] Q. Hu *et al.*, "Crafting MoC2-doped bimetallic alloy nanoparticles encapsulated within N-doped graphene as roust bifunctional electrocatalysts for overall water splitting," *Nano Energy*, vol. 50, pp. 212–219, 2018.

[205] Q. Zhao *et al.*, "Tuning Electronic Push/Pull of Ni-Based Hydroxides to Enhance Hydrogen and Oxygen Evolution Reactions for Water Splitting," *ACS Catal.*, vol. 8, no. 6, pp. 5621–5629, 2018.

[206] Q. Xiong *et al.*, "Cobalt Covalent Doping in MoS2 to Induce Bifunctionality of Overall Water Splitting," *Adv. Mater.*, vol. 30, no. 29, pp. 1–7, 2018.

[207] X. Zhang *et al.*, "Co3O4/Fe0.33Co0.66P Interface Nanowire for Enhancing Water Oxidation Catalysis at High Current Density," *Adv. Mater.*, vol. 30, no. 45, pp. 1–8, 2018.

[208] F. Lv *et al.*, "Iridium-Tungsten Alloy Nanodendrites as pH-Universal Water-Splitting Electrocatalysts," *ACS Cent. Sci.*, vol. 4, no. 9, pp. 1244–1252, 2018.

[209] K. Tang, X. Wang, Q. Li, and C. Yan, "High Edge Selectivity of In Situ Electrochemical Pt Deposition on Edge-Rich Layered WS2 Nanosheets," *Adv. Mater.*, vol. 30, no. 7, pp. 1–7, 2018.

[210] Y. Wang *et al.*, "Reduced mesoporous Co3O4 nanowires as efficient water oxidation electrocatalysts and supercapacitor electrodes," *Adv. Energy Mater.*, vol. 4, no. 16, pp. 1–7, 2014.

[211] W. Wang, B. Lei, and S. Guo, "Engineering Multimetallic Nanocrystals for Highly Efficient Oxygen Reduction Catalysts," *Adv. Energy Mater.*, vol. 6, no. 17, 2016.

[212] Y. Wang *et al., Synergistic effect between undercoordinated platinum atoms and defective nickel hydroxide on enhanced hydrogen evolution reaction in alkaline*

solution, vol. 48. Elsevier Ltd, 2018.

[213] H. Jin *et al.*, "Lanthanide metal-assisted synthesis of rhombic dodecahedral MNi (M = Ir and Pt) nanoframes toward efficient oxygen evolution catalysis," *Nano Energy*, vol. 42, pp. 17–25, 2017.

[214] G. Zhang *et al.*, "Enhanced Catalysis of Electrochemical Overall Water Splitting in Alkaline Media by Fe Doping in Ni3S2 Nanosheet Arrays," *ACS Catal.*, vol. 8, no. 6, pp. 5431–5441, 2018.

[215] J. Zhang *et al.*, "Single-Atom Au/NiFe Layered Double Hydroxide Electrocatalyst: Probing the Origin of Activity for Oxygen Evolution Reaction," *J. Am. Chem. Soc.*, vol. 140, no. 11, pp. 3876–3879, 2018.

[216] H. Xiao, H. Shin, and W. A. Goddard, "Synergy between Fe and Ni in the optimal performance of (Ni,Fe)OOH catalysts for the oxygen evolution reaction," *Proc. Natl. Acad. Sci. U. S. A.*, vol. 115, no. 23, pp. 5872–5877, 2018.

[217] J. Sun *et al.*, "A Facile Strategy to Construct Amorphous Spinel-Based Electrocatalysts with Massive Oxygen Vacancies Using Ionic Liquid Dopant," *Adv. Energy Mater.*, vol. 8, no. 27, pp. 1–13, 2018.

[218] Z. Zhuang *et al.*, "MoB/g-C3N4 Interface Materials as a Schottky Catalyst to Boost Hydrogen Evolution," *Angew. Chemie - Int. Ed.*, vol. 57, no. 2, pp. 496–500, 2018.

[219] I. Ro, J. Resasco, and P. Christopher, "Approaches for Understanding and Controlling Interfacial Effects in Oxide-Supported Metal Catalysts," *ACS Catal.*, vol. 8, no. 8, pp. 7368–7387, 2018.

[220] W. Zhang *et al.*, "Single-Walled Carbon Nanotube Induced Optimized Electron Polarization of Rhodium Nanocrystals to Develop an Interface Catalyst for Highly Efficient Electrocatalysis," *ACS Catal.*, vol. 8, no. 9, pp. 8092–8099, 2018.

[221] Y. Wu *et al.*, "Coupling Interface Constructions of MoS2/Fe5Ni4S8 Heterostructures for Efficient Electrochemical Water Splitting," *Adv. Mater.*, vol. 30, no. 38, pp. 1–8, 2018.

[222] S. Bai *et al.*, "Surface Polarization Matters: Enhancing the Hydrogen-Evolution Reaction by Shrinking Pt Shells in Pt-Pd-Graphene Stack Structures," *Angew. Chemie - Int. Ed.*, vol. 53, no. 45, pp. 12120–12124, 2014.

[223] X. Liu *et al.*, "Metal (Ni, Co)-Metal Oxides/Graphene Nanocomposites as Multifunctional Electrocatalysts," *Adv. Funct. Mater.*, vol. 25, no. 36, pp. 5799–5808, 2015.

[224] L. An *et al.*, "Atomic-Level Coupled Interfaces and Lattice Distortion on CuS/NiS2 Nanocrystals Boost Oxygen Catalysis for Flexible Zn-Air Batteries," *Adv. Funct. Mater.*, vol. 27, no. 42, pp. 1–9, 2017.

[225] T. Li *et al.*, "Atomic-scale insights into surface species of electrocatalysts in three dimensions," *Nat. Catal.*, vol. 1, no. 4, pp. 300–305, 2018.

[226] K. Rui *et al.*, "Hybrid 2D Dual-Metal–Organic Frameworks for Enhanced Water Oxidation Catalysis," *Adv. Funct. Mater.*, vol. 28, no. 26, pp. 1–9, 2018.

[227] T. Liu, A. Li, C. Wang, W. Zhou, S. Liu, and L. Guo, "Interfacial Electron Transfer of

Ni2P–NiP2 Polymorphs Inducing Enhanced Electrochemical Properties," *Adv. Mater.*, vol. 30, no. 46, pp. 1–9, 2018.

[228] R. Sharma, J. H. Baik, C. J. Perera, and M. S. Strano, "Anomalously large reactivity of single graphene layers and edges toward electron transfer chemistries," *Nano Lett.*, vol. 10, no. 2, pp. 398–405, 2010.

[229] Y. Zhang *et al.*, "Rational Design of MXene/1T-2H MoS2-C Nanohybrids for High-Performance Lithium–Sulfur Batteries," *Adv. Funct. Mater.*, vol. 28, no. 38, pp. 1–9, 2018.

[230] C. Su *et al.*, "Probing the catalytic activity of porous graphene oxide and the origin of this behaviour," *Nat. Commun.*, vol. 3, pp. 1298–1299, 2012.

[231] H. Wang *et al.*, "Three-Dimensional Graphene Networks with Abundant Sharp Edge Sites for Efficient Electrocatalytic Hydrogen Evolution," *Angew. Chemie - Int. Ed.*, vol. 57, no. 1, pp. 192–197, 2018.

[232] Q. Xu, Y. Liu, H. Jiang, Y. Hu, H. Liu, and C. Li, "Unsaturated Sulfur Edge Engineering of Strongly Coupled MoS2 Nanosheet–Carbon Macroporous Hybrid Catalyst for Enhanced Hydrogen Generation," *Adv. Energy Mater.*, vol. 9, no. 2, pp. 1–8, 2019.

[233] Y. Wang, C. Xie, Z. Zhang, D. Liu, R. Chen, and S. Wang, "In Situ Exfoliated, N-Doped, and Edge-Rich Ultrathin Layered Double Hydroxides Nanosheets for Oxygen Evolution Reaction," *Adv. Funct. Mater.*, vol. 28, no. 4, pp. 1–6, 2018.

[234] H. Jiang *et al.*, "Defect-rich and ultrathin N doped carbon nanosheets as advanced trifunctional metal-free electrocatalysts for the ORR, OER and HER," *Energy Environ. Sci.*, vol. 12, no. 1, pp. 322–333, 2019.

[235] P. G. Jamkhande, N. W. Ghule, A. H. Bamer, and M. G. Kalaskar, "Metal nanoparticles synthesis: An overview on methods of preparation, advantages and disadvantages, and applications," *J. Drug Deliv. Sci. Technol.*, vol. 53, p. 101174, 2019.

[236] W. Chen, W. Cai, L. Zhang, G. Wang, and L. Zhang, "Sonochemical processes and formation of gold nanoparticles within pores of mesoporous silica," *J. Colloid Interface Sci.*, vol. 238, no. 2, pp. 291–295, 2001.

[237] M. Vijayakumar, K. Priya, F. T. Nancy, A. Noorlidah, and A. B. A. Ahmed, "Biosynthesis, characterisation and anti-bacterial effect of plant-mediated silver nanoparticles using Artemisia nilagirica," *Ind. Crops Prod.*, vol. 41, no. 1, pp. 235–240, 2013.

[238] N. L. Pacioni, C. D. Borsarelli, V. Rey, and A. V. Veglia, *Synthetic Routes for the Preparation of Silver Nanoparticles: A Mechanistic Perspective*. 2015.

[239] M. N. Nadagouda, T. F. Speth, and R. S. Varma, "Microwave-assisted green synthesis of silver nanostructures," *Acc. Chem. Res.*, vol. 44, no. 7, pp. 469–478, 2011.

[240] M. Ullah, M. E. Ali, and S. B. A. Hamid, "Surfactant-assisted ball milling: A novel route to novel materials with controlled nanostructure-A review," *Rev. Adv. Mater. Sci.*, vol. 37, no. 1–2, pp. 1–14, 2014.

[241] T. Tsuzuki and P. G. McCormick, "Mechanochemical synthesis of nanoparticles," *J.*

Mater. Sci., vol. 39, no. 16–17, pp. 5143–5146, 2004.

[242] A. V. Simakin, V. V. Voronov, N. A. Kirichenko, and G. A. Shafeev, "Nanoparticles produced by laser ablation of solids in liquid environment," *Appl. Phys. A Mater. Sci. Process.*, vol. 79, no. 4–6, pp. 1127–1132, 2004.

[243] M. T. Swihart, "Vapor-phase synthesis of nanoparticles," vol. 8, pp. 127–133, 2003.

[244] P. A. Pandey *et al.*, "Physical vapor deposition of metal nanoparticles on chemically modified graphene: Observations on metal-graphene interactions," *Small*, vol. 7, no. 22, pp. 3202–3210, 2011.

[245] J. S. Park, W. H. Chung, H. S. Kim, and Y. B. Kim, "Rapid fabrication of chemical-solution-deposited La0.6Sr0.4CoO3−δthin films via flashlight sintering," *J. Alloys Compd.*, vol. 696, pp. 102–108, 2017.

[246] H. Pedersen and S. D. Elliott, "Studying chemical vapor deposition processes with theoretical chemistry," *Theor. Chem. Acc.*, vol. 133, no. 5, pp. 1–10, 2014.

[247] S. M. George, "Atomic layer deposition: An overview," *Chem. Rev.*, vol. 110, no. 1, pp. 111–131, 2010.

[248] A. Reina *et al.*, "Cvd法制备石墨烯," pp. 1–6, 2008.

[249] G. L. Doll, B. A. Mensah, H. Mohseni, and T. W. Scharf, "Chemical vapor deposition and atomic layer deposition of coatings for mechanical applications," *J. Therm. Spray Technol.*, vol. 19, no. 1–2, pp. 510–516, 2010.

[250] B. L. Cushing, V. L. Kolesnichenko, and C. J. O'Connor, "Recent advances in the liquid-phase syntheses of inorganic nanoparticles," *Chem. Rev.*, vol. 104, no. 9, pp. 3893–3946, 2004.

[251] N. Rajput, "Methods of preparation of nanoparticles-A review," *Int. J. Adv. Eng. Technol. 7*, vol. 6, no. 1806, 2015.

[252] J. D. S. G. Maribel G. Guzmán, "AgNPs prepared by hydrazine hydrate," *World Acad. Sci. Eng. Technol.* , pp. 357–364, 2008.

[253] G. Huang, C. H. Lu, and H. H. Yang, *Magnetic Nanomaterials for Magnetic Bioanalysis*. Elsevier Inc., 2018.

[254] M. D. Kass and D. M. Cecala, "Enhanced sinterability of alumina particles by pretreating in liquid ammonia," *Mater. Lett.*, vol. 32, no. 2–3, pp. 55–58, 1997.

[255] M. A. Dar, S. K. Kulkarni, Z. A. Ansari, S. G. Ansari, and H. S. Shin, "Preparation and characterization of α-FeOOH and α-Fe 2O3 by sol-gel method," *J. Mater. Sci.*, vol. 40, no. 11, pp. 3031–3034, 2005.

[256] G. B. McGarvey and D. G. Owen, "Copper (II) oxide as a morphology directing agent in the hydrothermal crystallization of magnetite," *J. Mater. Sci.*, vol. 31, no. 1, pp. 49–53, 1996.

[257] L. Kumari *et al.*, "Effect of Surfactants on the Structure and Morphology of Magnesium Borate Hydroxide Nanowhiskers Synthesized by Hydrothermal Route," *Nanoscale Res. Lett.*, vol. 5, no. 1, pp. 149–157, 2010.

[258] Y. Yang, S. Matsubara, L. Xiong, T. Hayakawa, and M. Nogami, "Solvothermal

synthesis of multiple shapes of silver nanoparticles and their SERS properties," *J. Phys. Chem. C*, vol. 111, no. 26, pp. 9095–9104, 2007.

[259] K. Okuyama and W. W. Lenggoro, "Preparation of nanoparticles via spray route," *Chem. Eng. Sci.*, vol. 58, no. 3–6, pp. 537–547, 2003.

[260] L. Mädler, H. K. Kammler, R. Mueller, and S. E. Pratsinis, "Controlled synthesis of nanostructured particles by flame spray pyrolysis," *J. Aerosol Sci.*, vol. 33, no. 2, pp. 369–389, 2002.

[261] R. Wallace, A. P. Brown, R. Brydson, K. Wegner, and S. J. Milne, "Synthesis of ZnO nanoparticles by flame spray pyrolysis and characterisation protocol," *J. Mater. Sci.*, vol. 48, no. 18, pp. 6393–6403, 2013.

[262] P. Yong, N. A. Rowson, J. P. G. Farr, I. R. Harris, and L. E. Macaskie, "Bioreduction and biocrystallization of palladium by Desulfovibrio desulfuricans NCIMB 8307," *Biotechnol. Bioeng.*, vol. 80, no. 4, pp. 369–379, 2002.

[263] N. Pantidos, "Biological Synthesis of Metallic Nanoparticles by Bacteria, Fungi and Plants," *J. Nanomed. Nanotechnol.*, vol. 05, no. 05, 2014.

[264] S. Sunkar and C. V. Nachiyar, "Biogenesis of antibacterial silver nanoparticles using the endophytic bacterium Bacillus cereus isolated from Garcinia xanthochymus," *Asian Pac. J. Trop. Biomed.*, vol. 2, no. 12, pp. 953–959, 2012.

[265] L. Wen *et al.*, "Extracellular biosynthesis of monodispersed gold nanoparticles by a SAM capping route," *J. Nanoparticle Res.*, vol. 11, no. 2, pp. 279–288, 2009.

[266] J. D. Holmes, P. R. Smith, R. Evans-Gowing, D. J. Richardson, D. A. Russell, and J. R. Sodeau, "Energy-dispersive X-ray analysis of the extracellular cadmium sulfide crystallites of Klebsiella aerogenes," *Arch. Microbiol.*, vol. 163, no. 2, pp. 143–147, 1995.

[267] B. Nair and T. Pradeep, "Coalescence of Nanoclusters and Formation of Submicron Crystallites Assisted by Lactobacillus Strains," *Cryst. Growth Des.*, vol. 2, no. 4, pp. 293–298, 2002.

[268] S. Iravani, "Bacteria in Nanoparticle Synthesis: Current Status and Future Prospects," *Int. Sch. Res. Not.*, vol. 2014, pp. 1–18, 2014.

[269] A. Ahmad *et al.*, "Extracellular biosynthesis of silver nanoparticles using the fungus Fusarium oxysporum," *Colloids Surfaces B Biointerfaces*, vol. 28, no. 4, pp. 313–318, 2003.

[270] R. E. Afreen, Rathod V, "Synthesis of monodispersed silver nanoparticles by Rhizopus Stolonifer and its antibacterial activity against MDR strains of Pseudomonas Aeruginosa from burnt patients," *Int. J. Environ. Sci.*, vol. 1, no. 7, pp. 1838–1848, 2011.

[271] S. S. Birla, V. V. Tiwari, A. K. Gade, A. P. Ingle, A. P. Yadav, and M. K. Rai, "Fabrication of silver nanoparticles by Phoma glomerata and its combined effect against Escherichia coli, Pseudomonas aeruginosa and Staphylococcus aureus," *Lett. Appl. Microbiol.*, vol. 48, no. 2, pp. 173–179, 2009.

[272] A. Ahmad *et al.*, "Enzyme mediated extracellular synthesis of CdS nanoparticles by the fungus, Fusarium oxysporum," *J. Am. Chem. Soc.*, vol. 124, no. 41, pp. 12108–

12109, 2002.

[273] V. Bansal *et al.*, "Fungus-mediated biosynthesis of silica and titania particles," *J. Mater. Chem.*, vol. 15, no. 26, pp. 2583–2589, 2005.

[274] J. Saxena *et al.*, "Emerging Role of Fungi in Nanoparticle Synthesis and," *World J. Pharm. Pharm. Sci.*, vol. 3, no. 9, pp. 1586–1613, 2014.

[275] P. Kuppusamy, M. M. Yusoff, G. P. Maniam, and N. Govindan, "Biosynthesis of metallic nanoparticles using plant derivatives and their new avenues in pharmacological applications – An updated report," *Saudi Pharm. J.*, vol. 24, no. 4, pp. 473–484, 2016.

[276] T. C. Prathna, N. Chandrasekaran, A. M. Raichur, and A. Mukherjee, "Biomimetic synthesis of silver nanoparticles by Citrus limon (lemon) aqueous extract and theoretical prediction of particle size," *Colloids Surfaces B Biointerfaces*, vol. 82, no. 1, pp. 152–159, 2011.

[277] R. G. Haverkamp and A. T. Marshall, "The mechanism of metal nanoparticle formation in plants: Limits on accumulation," *J. Nanoparticle Res.*, vol. 11, no. 6, pp. 1453–1463, 2009.

[278] A. K. Jha, K. Prasad, K. Prasad, and A. R. Kulkarni, "Plant system: Nature's nanofactory," *Colloids Surfaces B Biointerfaces*, vol. 73, no. 2, pp. 219–223, 2009.

[279] D. Philip, "Green synthesis of gold and silver nanoparticles using Hibiscus rosa sinensis," *Phys. E Low-Dimensional Syst. Nanostructures*, vol. 42, no. 5, pp. 1417–1424, 2010.

[280] G. S. Ghodake, N. G. Deshpande, Y. P. Lee, and E. S. Jin, "Pear fruit extract-assisted room-temperature biosynthesis of gold nanoplates," *Colloids Surfaces B Biointerfaces*, vol. 75, no. 2, pp. 584–589, 2010.

[281] S. Iravani, "Green synthesis of metal nanoparticles using plants," *Green Chem.*, vol. 13, no. 10, pp. 2638–2650, 2011.

[282] X. Peng, X. Jin, B. Gao, Z. Liu, and P. K. Chu, "Strategies to improve cobalt-based electrocatalysts for electrochemical water splitting," *J. Catal.*, vol. 398, pp. 54–66, 2021.

[283] P. Jacques, V. Artero, and J. Pécaut, "Cobalt and nickel diimine-dioxime complexes as molecular electrocatalysts for …," *Proc. Natl. Acad. Sci.*, vol. 106, no. 49, pp. 20627–20632, 2009.

[284] G. Huang *et al.*, "Co2P/CoP hybrid as a reversible electrocatalyst for hydrogen oxidation/evolution reactions in alkaline medium," *J. Catal.*, vol. 390, pp. 23–29, 2020.

[285] X. Peng, C. Pi, X. Zhang, S. Li, K. Huo, and P. K. Chu, "Recent progress of transition metal nitrides for efficient electrocatalytic water splitting," *Sustain. Energy Fuels*, vol. 3, no. 2, pp. 366–381, 2019.

[286] Y. Liang *et al.*, "Co3O4 nanocrystals on graphene as a synergistic catalyst for oxygen reduction reaction," *Nat. Mater.*, vol. 10, no. 10, pp. 780–786, 2011.

[287] J. Wang, W. Cui, Q. Liu, Z. Xing, A. M. Asiri, and X. Sun, "Recent Progress in

Cobalt-Based Heterogeneous Catalysts for Electrochemical Water Splitting," *Adv. Mater.*, vol. 28, no. 2, pp. 215–230, 2016.

[288] X. Zhang, X. Zhang, H. Xu, Z. Wu, H. Wang, and Y. Liang, "Iron-Doped Cobalt Monophosphide Nanosheet/Carbon Nanotube Hybrids as Active and Stable Electrocatalysts for Water Splitting," *Adv. Funct. Mater.*, vol. 27, no. 24, pp. 1–12, 2017.

[289] R. Zhang *et al.*, "Engineering Cobalt Defects in Cobalt Oxide for Highly Efficient Electrocatalytic Oxygen Evolution," *ACS Catal.*, vol. 8, no. 5, pp. 3803–3811, 2018.

[290] A. Bergmann *et al.*, "Reversible amorphization and the catalytically active state of crystalline Co3O4 during oxygen evolution," *Nat. Commun.*, vol. 6, 2015.

[291] H. H. Pham, M. J. Cheng, H. Frei, and L. W. Wang, "Surface Proton Hopping and Fast-Kinetics Pathway of Water Oxidation on Co3O4 (001) Surface," *ACS Catal.*, vol. 6, no. 8, pp. 5610–5617, 2016.

[292] M. S. Faber, R. Dziedzic, M. A. Lukowski, N. S. Kaiser, Q. Ding, and S. Jin, "High-performance electrocatalysis using metallic cobalt pyrite (CoS 2) micro- and nanostructures," *J. Am. Chem. Soc.*, vol. 136, no. 28, pp. 10053–10061, 2014.

[293] M. Cabán-Acevedo *et al.*, "Efficient hydrogen evolution catalysis using ternary pyrite-type cobalt phosphosulphide," *Nat. Mater.*, vol. 14, no. 12, pp. 1245–1251, 2015.

[294] C. Li, X. Han, F. Cheng, Y. Hu, C. Chen, and J. Chen, "Phase and composition controllable synthesis of cobalt manganese spinel nanoparticles towards efficient oxygen electrocatalysis," *Nat. Commun.*, vol. 6, pp. 1–8, 2015.

[295] K. Liu *et al.*, "An efficient ternary CoP2:XSe2(1- x) nanowire array for overall water splitting," *Nanoscale*, vol. 9, no. 11, pp. 3995–4001, 2017.

[296] S. Jung, C. C. L. McCrory, I. M. Ferrer, J. C. Peters, and T. F. Jaramillo, "Benchmarking nanoparticulate metal oxide electrocatalysts for the alkaline water oxidation reaction," *J. Mater. Chem. A*, vol. 4, no. 8, pp. 3068–3076, 2016.

[297] J. A. Vigil, T. N. Lambert, and B. T. Christensen, "Cobalt phosphide-based nanoparticles as bifunctional electrocatalysts for alkaline water splitting," *J. Mater. Chem. A*, vol. 4, no. 20, pp. 7549–7554, 2016.

[298] F. Paquin, J. Rivnay, A. Salleo, N. Stingelin, and C. Silva, "Multi-phase semicrystalline microstructures drive exciton dissociation in neat plastic semiconductors," *J. Mater. Chem. C*, vol. 3, pp. 10715–10722, 2015.

[299] N. Jiang, B. You, M. Sheng, and Y. Sun, "Electrodeposited Cobalt-Phosphorous-Derived Films as Competent Bifunctional Catalysts for Overall Water Splitting," *Angew. Chemie*, vol. 127, no. 21, pp. 6349–6352, 2015.

[300] J. Wang *et al.*, "Cobalt nanoparticles encapsulated in nitrogen-doped carbon as a bifunctional catalyst for water electrolysis," *J. Mater. Chem. A*, vol. 2, no. 47, pp. 20067–20074, 2014.

7.Appendices